Dissertation

submitted to the

Combined Faculty of Natural Sciences and Mathematics

of the Ruperto Carola University Heidelberg, Germany

for the degree of

Doctor of Natural Sciences

Presented by

M. Sc. Vasileios Kampanis

born in Villingen-Schwenningen, Germany

Oral Examination: 23.02.2021

# Novel candidate intrinsic and extrinsic regulators of regeneration after axonal injury

Referees:         Jun.-Prof. Dr. Daniela Mauceri

Dr. Radhika Puttagunta

to my mother…

**Abstract**

Injured neurons in the peripheral nervous system (PNS) can regenerate long-distances and re-establish function, while in the central nervous system (CNS) they do not. Anatomical and cellular signaling discrepancies set up different post-traumatic landscapes between the PNS and CNS, therefore residing neurons respond distinctively to axonal injury. A clear example is when the lesioned peripheral branches of dorsal root ganglia (DRG) regenerate spontaneously, while the lesioned central branches do not. Understanding why such differences occur is the underlying theme of the work presented here.

The regenerative capacity of the lesioned PNS is known to be transcription dependent. Recently, the histone acetyl-transferase p300/CBP-associated factor (PCAF) was discovered to enhance the axonal regenerative program of the DRG as well as prime growth of injured central DRG axons. Although PCAF was found to be an essential player in the transcriptional regulation of a handful of key regeneration-associated genes (RAGs), the precise mechanism of how PCAF enhances axonal regeneration remained elusive. We identified PCAF-dependent RAGs (PCAF-RAGs) through analysis of the DRG transcriptome (RNA-seq) from wildtype and PCAF knockout mice after a peripheral regenerative lesion. Transcription factor binding site analysis predicted potential co-regulators, Specificity protein 1 (Sp1) and myc-associated zinc finger protein (MAZ). Knockdown and overexpression experiments showed that Sp1 and MAZ can enhance neurite outgrowth *in vitro,* dependent upon the presence of PCAF. More importantly, pharmaceutical activation of PCAF allowed for enhanced neurite outgrowth of cultured DRG and systemic administration of the PCAF activator promoted increased regeneration of the PNS.

Anatomically, the periphery subjects its neurons to mechanical forces that may influence its repair outcome. These mechanical cues are missing from the CNS. Therefore, we explored if and how sensory neurons can respond regeneratively to mechanical stimulation. An in-house built bioreactor applied cyclic mechanical tension to PNS- or CNS-located DRG-nerve explants. Neurite length analysis showed that stretch can induce outgrowth of medium to large diameter DRG, partially through the expression of activating transcription factor 3 (ATF3).

Our work shows that either a regenerative injury or mechanical stimulation regulate specific outgrowth-related transcriptional machinery. Better understanding of such mechanisms will allow recapitulation of regenerative programs in non-regenerating neuronal populations, in hopes of promoting functional regeneration and recovery.

## Zusammenfassung

Während Neurone des peripheren Nervensystems (PNS) nach Verletzungen über weite Distanzen hinweg regenerieren und dadurch verlorene neurologische Funktionen wiederherstellen können, sind Neurone des zentralen Nervensystems (ZNS) dazu nicht in der Lage. Diese Diskrepanz ist durch Unterschiede der Anatomie sowie zellulärer Signalwege zwischen PNS und ZNS bedingt, wodurch ein unterschiedliches molekulares Milieu erzeugt wird, welches zu differenten Wachstumsreaktionen von Neuronen des PNS und ZNS führt. Als ideales Beispiel hierfür dienen Neurone der dorsalen Wurzelganglien (dorsal root ganglion, DRG): während das periphere DRG-Axon nach Verletzung regeneriert, ist das zentrale Axon des gleichen Neurons dazu nicht in der Lage. Das Regenerationsverhalten von Neuronen der DRG ist bedingt durch deren Gentranskription. Die Histon-Acetyltransferase PCAF (p300/CBP-associated factor) wurde hierbei als wichtiger molekularer Schalter für die Regenerationsfähigkeit von DRG-Neuronen identifiziert. Mit Hilfe von PCAF wird ein genetisches Regenerationsprogramm reguliert, welches regeneratives Wachstum des peripheren DRG-Axons initiiert und das zentrale DRG-Axon zum Wachstum befähigt. Weiterhin ist das PNS aufgrund seiner Anatomie äußeren mechanischen Kräften ausgesetzt, welche dessen Wachstumsfähigkeit beeinflussen. Im Gegensatz dazu sind Neurone des ZNS diesen mechanischen Kräften nicht ausgesetzt und es ist bisher unklar, ob das ZNS ebenfalls mit Wachstum auf mechanische Stimulation reagieren kann. Die Untersuchung der Reaktion des ZNS auf mechanische Stimulation sowie die Aufklärung der molekularen Grundlagen sind folglich von großem Interesse für die regenerative Medizin. Das Ziel der vorliegenden Arbeit ist daher, intrinsische Regeneration-assoziierte Unterschiede zwischen ZNS und PNS zu untersuchen.

Die Expression von Regenerations-assoziierten Genen (RAG) kann durch epigenetische Mechanismen reguliert und nach einer Verletzung zu axonaler Regeneration führen. Obwohl PCAF essentiell für die Expression einiger RAGs ist, sind der exakte molekulare Signalweg sowie die Frage, wie PCAF Axonwachstum beeinflusst bisher nur unvollständig untersucht. Mit Hilfe von Transkriptionsanalysen (RNAseq) an Wildtyp- sowie transgenen PCAF-knock out-Mäusen wurden RAGs identifiziert, welche spezifisch von PCAF nach einer Verletzung des peripheren DRG-Axons reguliert werden. Zusätzlich wurden potenzielle Transkriptionsfaktor Bindestellen spezifisch für Specificity protein 1 (Sp1) sowie myc-associated zinc finger protein (MAZ) in den PCAF-regulierten RAGs identifiziert. *In vitro*-Studien basierend auf Knock down sowie Überexpression von Sp1 oder MAZ zeigten, dass beide Faktoren im Zusammenspiel mit PCAF Neuritenwachstum in kultivierten DRG-

Neuronen verstärken können. Des Weiteren konnte dieses PCAF-abhängige Regenerationprogramm pharmakologisch ohne vorhergehende Verletzung des PNS oder virale Überexpression der einzelnen molekularen Komponenten nachgebildet werden.

Zudem wurde der Effekt von mechanischer Stimulation auf die Regenerationsfähigkeit von sensorischen Axonen untersucht. Mit Hilfe eines speziell angefertigten Bioreaktors konnten definierte mechanische Impulse in Form von zyklischer mechanischer Streckung an DRG-Nerven Explantate appliziert werden. Durch anschließende Analyse des Neuritenwachstums konnte nachgewiesen werden, dass die zyklische mechanische Streckung das Wachstum von DRG-Neuronen mit mittlerem und großen Zelldurchmesser verbessert, partiell durch die verstärkte Expression von Activating Transcription Factor 3 (ATF3) in diesen Neuronen. Das Verständnis der molekularen Mechanismen der intrinsischen Regenerationsfähigkeit des PNS kann folglich dazu dienen, die verminderte Regenerationsfähigkeit des ZNS zu beeinflussen, wodurch letztlich axonale Regeneration nach Verletzungen des ZNS erreicht werden kann.

# Acknowledgements

I would like to thank Prof. Dr. Norbert Weidner for allowing me to conduct my research in the Spinal Cord Injury Center at the University Hospital of Heidelberg. He was always very supportive and provided me with precious and constructive feedback. Also, I am very grateful to my direct supervisor Dr. Radhika Puttagunta, who believed in me since the first time we met in her class in Tübingen. Her passion for research inspired me to stay in the field of Regenerative Neuroscience. I have learned a lot next to her all these years and her critical point of view on research has made me a better scientist and a critical thinker. I would like to thank my Thesis Advisory Committee members, Dr. Daniela Mauceri, Dr. Ana Olivera and Prof. Gudrun Rappold for providing their expertise that helped me manage my projects better and for their helpful feedback which led to the successful completion of my studies. Also, I specially thank the Onassis Foundation, for trusting me all these years and granting me a scholarship (ID: F ZM 034-1/ 2016-2017) for completing my studies at the University of Heidelberg.

A special thank you goes to all our collaborators without whom I would not have been able to finish this thesis. I would like to thank Prof. Wiltrud Richter, for kindly offering her incubator, so that I could finish parts of my project and Prof. Simone Di Giovanni, for his support all these years and for kindly offering overexpression vectors. Also, I am grateful to Dr. Luming Zhou, for his constant support and for providing his expertise every time he was asked; Mr. Wolfgang Roth, for helping me build a bioreactor and horizontal ladder; Mr. Joachim Schweidler, for providing his expertise in computer science; Dr. Arnau Hervera, for always being willing to help me troubleshoot problems; Dr. Florence Bareyre and Dr. Julie Fourneau, for teaching me how to do stereotactic brain injections; everyone at the materials engineering department of the University of Heidelberg, for helping me find the best options for my nerve explant cultures and to Prof. Dr. Katrin Marcus and Dr. Katalin Barkovits at the Medical Proteome Center at the Ruhr University of Bochum for their help in our proteomics experiments. I, also, owe a special thank you to everyone at the nCounter core facility at the University of Heidelberg. More specifically, I would like to thank Dr. Beate Niesler and Mr. Ralph Roth, for helping me during my experiments and for the transcriptomics data analysis.

Of course, in this scientific journey I was not alone; I had with me everyone working in our lab and friends from other labs who all contributed to the success of my studies and made my Ph.D. an unforgettable experience. I would like to particularly thank Melanie Motsch for introducing me to the lab and always being a willing supporter in every challenge during these years. Beatrice Sandner made our lab a fun place and I will never forget our Halloween preparations among pumpkin flesh, carving tools and laughter. A special thank you goes to my

scientific brothers, Christopher Sliwinski and Thomas Schackel. Discussions about science and our latest results were mixed with dry ice bombs, unsuccessful attempts to teach them Greek and bad German Schlager music. They have not been just colleagues but also my friends. Furthermore, I would like to thank Xing Cheng for his support and for introducing me to the Asian culture; Naëmi Kühn, for our conversations while working in the cell culture room and her endless positive energy; Bahar Tolou, for helping me analyze my data and her support with my projects; Paul Ruf and Andrea Genthner for helping me with the animal breeding. Of course, I should not forget to thank my fellow colleagues in neighbouring labs who always were there for me. More specifically, I would like to thank Safak Chasan, Justyna Buchert, Matthias Gerstner, Tim Hammersen, Felicia Klampfleuthner, Ursula Kreuser and Janine Lücken for their help whenever needed. Also, a special thank you goes to all my students, Sonja Bergmann, Ann-Kristin Afflerbach, Annika Wagener and Larissa Diem for trusting me as their mentor and for helping me further my projects. I hope you enjoyed working with me and you have learned a lot!

I would not have been here today finishing my studies, if I did not have next to me good friends and my family, whose love and support were the fuels to keep going through every challenge all these years. The people who kept reminding me my goals and made this journey more pleasant. I owe a huge thank you to Ypsipili for being a patient listener and a great friend. Her support was always a source of courage and her accomplishments a constant reminder that we can achieve everything we can dream of. Also, I would like to thank Lora, Marc, Michael, Jason, James, Celine, my friends from TEDxHeidelberg and the German Brain Bee, everyone at my theatre group and my Swing family. Maybe they do not know it, but they all have made my years in Heidelberg the best of my life, always supporting me when things were not going smoothly and enjoying with me my greatest moments. I am grateful to every single one of them!

While writing the last sentences of my acknowledgments, I am trying to find the correct words to express my gratitude to the most important person during my studies and my life. I have concluded that probably there are no words to describe my appreciation for her unconditional support. My biggest thank you goes to my greatest ally and most honest friend, my mother. Her life is an inspiration for everything I am doing. She never stopped smiling, even in the darkest moments, with her wings always around me. And when I learned how to fly, we flew together above every obstacle. I dedicate this thesis to her and to everything she stands for. Thank you, mom!

(*Τελειώνοτας τις ευχαριστίες μου, προσπαθώ να βρω τις κατάλληλες λέξεις για να περιγράψω την ευγνωμοσύνη μου για τον πιο σημαντικό άνθρωπο κατά τη διάρκεια των σπουδών*

Vasileios Kampanis

# Table of Contents

**Abbreviations**

| | |
|---|---|
| 5hM | 5-hydroxymethlylation |
| 6330403A02Rik | Stum, Mechanosensory Transduction Mediator Homolog |
| Actb | Beta actin |
| Adam19 | ADAM Metallopeptidase Domain 19 |
| Adc | Antizyme Inhibitor 2 |
| Akt | Protein kinase B |
| APS | Ammonium persulfate solution |
| Arrb1 | Arrestin Beta 1 |
| ATF3 | Activating transcription factor 3 |
| BBB | Blood-brain barrier |
| Bcl9l | B-Cell CLL/Lymphoma 9 Protein- like |
| Bdnf | Brain derived neurotrophic factor |
| BS | Binding site |
| BSA | Bovine Serum Albumin |
| Cacna1b | Calcium voltage-gated channel subunit alpha1 |
| cAMP | Cyclin adenosine monophosphate |
| CBP | CREB binding protein |
| CGRP | Calcitonin gene-related peptide |
| Cic | Capicua Transcriptional Repressor |
| CL | Conditioning lesion |
| CNS | Central nervous system |
| Crmp1 | Collapsin Response Mediator Protein 1 |
| Crtac1 | Cartilage Acidic Protein 1 |
| CST | Corticospinal tract |
| CSPGs | Chondroitin sulfate proteoglycans |
| Cyfip2 | Cytoplasmic FMR1 Interacting Protein 2 |
| Cys | Cysteine |
| DAPI | 4',6-diamidino-2- phenylindole |
| DCA | Dorsal column axotomy |
| Dgkq | Diacylglycerol Kinase Theta |
| DH | Dorsal hemisection |
| DNA | Deoxyribonucleic acid |
| DNMT | DNA-methyltransferase |

| | |
|---|---|
| Dot1l | DOT1 Like Histone Lysine Methyltransferase |
| DPBS | Dulbecco's phosphate buffered saline |
| DRG | Dorsal root ganglion/ -a |
| GSP | Glucose-derived carbon nanospheres |
| EDTA | Ethylenediaminetetraacetic acid |
| ERK | Extracellular signal-regulated kinase |
| ESR1 | Estrogen receptor 1 |
| Evi5l | Ecotropic Viral Integration Site 5 Like |
| Exoc3 | Exocyst 3 |
| Fam171b | Family With Sequence Similarity 171 Member B |
| FBS | Foetal bovine serum |
| FDA | Food and Drug Administration |
| GAP-43 | Growth-associated protein-43 |
| GCN5 | General Control Of Amino Acid Synthesis Protein 5 |
| GNAT | Gcn5-related-acetyltransferase |
| GNG4 | G protein subunit gamma 4 |
| GPI | Glycosyl-phosphatidylinositol |
| Greb1l | Growth Regulating Estrogen Receptor Binding 1- like |
| Grid2 | Glutamate Ionotropic Receptor Delta Type Subunit 2 |
| H&E | Hematoxylin-Eosin |
| H1f0 | Histone 1 |
| H3 | Histone 3 |
| H3ac | Histone acetylation |
| H3K9ac | Histone 3 lysine 9 acetylation |
| H3K9K14ac | Histone 3 lysine 9 lysine 14 acetylation |
| H4 | Histone 4 |
| HAT | Histone acetyltransferase |
| HBSS | Hanks' balanced salt solution |
| HDAC5 | Histone deacetylase 5 |
| HeLa | Henrietta Lacks |
| His | Histidine |
| hSyn1 | human synapsin 1 |
| Hz | Herz |
| ICC | Immunocytochemistry |

| | |
|---|---|
| IHC | Immunohistochemistry |
| i.p. | Intraperitoneal |
| KAT | Lysine (K) acetyltransferase |
| Kat2b | Lysine (K) acetyltransferase 2h |
| KO | knockout |
| Lama1 | Laminin Subunit Alpha 1 |
| LB broth | Luria/Miller broth |
| Lmtk3 | Lemur Tyrosine Kinase 3 |
| LRR | Leucine rich repeat |
| MAG | Myelin-associated glycoprotein |
| MAIs | Myelin-associated inhibitors |
| MAZ | Myc-associated zinc finger protein |
| MAZOE | MAZ overexpression |
| Med25 | Mediator Complex Subunit 25 |
| Myt1l | Myelin Transcription Factor 1 Like |
| Ndst1 | N-Deacetylase And N-Sulfotransferase 1 |
| NF200 | Neurofilament 200 kDa |
| NGR1 | Nogo-66 receptor 1 |
| NMDA | N-methyl-D-aspartate |
| NT-3 | Neurotrophin 3 |
| Nos1 | Nitric Oxide Synthase 1 |
| OMgp | Oligodendrocyte myelin glycoprotein |
| PCAF | p300/CBP-associated factor |
| PCAF KO | PCAF knockout |
| Pcdhga8 | Protocadherin Gamma Subfamily A, 8 |
| PCR | Polymerase chain reaction |
| PEEK | Poly-ether-ether-ketone |
| Pen/Strep | Penicillin-streptomycin |
| Penk | Proenkephalin |
| PFA | Paraformaldehyde |
| Pfkfb3 | Kinase/Fructose-2,6-Biphosphatase 3 |
| PI3K | Phosphoinositide 3-kinase |
| Pik3cd | Phosphatidylinositol-4,5-Bisphosphate3-Kinase Catalytic Subunit $\Delta$ |
| PKA | Protein kinase A |

| | |
|---|---|
| Plekhh1 | Pleckstrin Homology, MyTH4 And FERM Domain Containing H1 |
| PLO | Poly-L-ornithine hydrobromide |
| PNS | Peripheral nervous system |
| Psd2 | Pleckstrin And Sec7 Domain Containing 2 |
| PTEN | Phosphatase and tensin homolog |
| PTM | Post-translational modifications |
| Ptpn1 | Protein Tyrosine Phosphatase Non-Receptor Type 1 |
| RAG | Regeneration-associated gene |
| RNA | Ribonucleic acid |
| RNAi | RNA interference |
| RNAseq | RNA-sequencing |
| ROCK | RhoA-associated kinase |
| RPL13a | Ribosomal Protein L13a |
| SCI | Spinal cord injury |
| SDS | Sodium Dodecyl Sulfate |
| SEM | Standard error of the mean |
| Serpina3m | Serpin Family A Member 3 |
| Shank2 | SH3 And Multiple Ankyrin Repeat Domains 2 |
| Sidt2 | SID1 Transmembrane Family Member 2 |
| Slc4a8 | Solute Carrier Family 4 Member 8 |
| Smad1 | SMAD family member 1 |
| SNC | Sciatic nerve crush |
| Sox11 | SRY-box containing gene 11 |
| Sp1 | Specificity protein 1 |
| Sp1OE | Sp1 overexpression |
| Sppr1 | Small proline-repeat protein 1A |
| SPV106 | Pentadecylidenemalonate 1b |
| Ssh1 | Slingshot Protein Phosphatase 1 |
| Stx1b | Syntaxin 1B |
| SV40 | Simian virus 40 |
| Syngap1 | Synaptic Ras GTPase Activating Protein 1 |
| Tacr1 | Tachykinin Receptor 1 |
| TAF | TAB-associated factors |
| TEMED | N, N, N', N'- Tetramethylethylenediamine |

| | |
|---|---|
| TF | Transcription factor |
| TFBS | Transcription factor binding site |
| TRAAK | TWIK-related arachidonic acid activated K+ |
| Tris-HCl | Tris-Hydrochloride |
| Trk-C | Neurotrophic Receptor Tyrosine Kinase 3 |
| Trpm3 | Transient Receptor Potential Cation Channel Subfamily M Member 3 |
| TRPV2 | Transient receptor potential cation channel subfamily V member 2 |
| Tuj1 | β-III tubulin |
| VEGF | Vascular endothelial growth factor |
| WT | Wild type |
| Xylt1 | Xylosyltransferase 1 |

**Chemical formulas**

| | |
|---|---|
| $C_4H_{11}NO_3$ | Tris(hydroxymethyl)aminomethane |
| $CH_3COOH$ | Glacial acetic acid |
| NaCl | Sodium Chloride |
| $NaH_2PO_4$ | Sodium Phosphate Monobasic Solution |
| NaOH | Sodium hydroxide |

**List of Figures**

**List of Tables**

# **Introduction**

# 1. Introduction

## 1.1. Background

### 1.1.1. Nervous system regeneration across species and neuronal damage

Perceiving the outside world and interacting with it is crucial for the survival and reproduction of all living organisms on the planet. From more simple mechanisms, such as photo-perception in planarian flatworms[1], to very complicated functions such as the flight-or-fight response and the formation of memories in invertebrates and vertebrates, the presence of an organized nervous system is required. It can detect external cues as well as process and initiate appropriate responses to them. Undoubtedly, humans have the most evolved and organized nervous systems, allowing for the most delicate and complicated processes, such as abstract thinking and problem-solving. Irrespective of how simple or elaborate a nervous system is, it still consists of neuronal cells that cluster together, making connections with other cells to elicit a specific response. Thus, damage to a neuronal cell can either temporarily or permanently interfere with its function.

Not all organisms that possess a nervous system have the same capacity to restore their injured neurons. Across species, it has been observed that the simpler the organism, the higher its regenerative capacity. For example, the planarian flatworm shows exceptional regeneration of its nervous system, able to restore it entirely even from small fragments of its body[2]. This impressive phenomenon is less prominent higher up in the evolutionary ladder, with higher mammals showing poor regeneration levels. Lower vertebrates, such as fish and urodele amphibians, might not restore their whole nervous system, but they can regain severed fins[3] and limbs[4], respectively. Mammals show dramatically lower levels of regeneration compared to other classes, and it is mostly limited to the regeneration of appendages, such as ear regeneration in mice and rabbits[5,6], antlers in deers[7] and amputated digit tips in humans and rodents[8–10].

In higher vertebrates, the peripheral nervous system (PNS) is more vulnerable to external insults due to its anatomy compared to the bone-protected central nervous system (CNS). However, upon injury, the neuronal axons in the PNS can achieve long-distance regeneration with a rate of around 2.5 cm per month[11]. This discrepancy between the two nervous systems suggests different response mechanisms to injuries between the CNS and PNS.

## 1.1.2. Challenges in regeneration of the CNS upon injury

The CNS consists of the brain and spinal cord enclosed in bony structures, the skull and spinal vertebrae, respectively. Although protected, the CNS is subjected to injuries either by external factors, e.g., falls, car accidents, violence, etc. or by pathological conditions such as an ischemic stroke. These conditions result in the loss of neurons or damage to neuronal axons leading in many cases to severe disruption of the physiology of the individual.

Upon an injury to the spinal cord, ascending sensory and descending cerebrospinal nerve fibers that support locomotion, bladder function and sexual activity are damaged. The primary injury causes bleeding, disruption of the blood-spinal cord barrier (BSB) and discontinuity of injured axons. Due to bleeding and the evoked immune response, the primary injury is followed by a secondary phase. Extensive bleeding leads to hypoxia, which can cause irreversible damage to the neurons[12]. Upon injury, the massive release of excitatory neurotransmitters and overactivation of neurons leads to further damage beyond the injury epicenter[13]. Calcium influx to the injured neurons can have detrimental effects and contribute to neuronal toxicity[14]. Lastly, following spinal cord injury (SCI), various cell types, including astrocytes, microglia, endothelial cells, macrophages and fibroblasts, are recruited to the lesion site to seal the wound and remove the cellular debris. This cellular infiltration leads to the formation of a fibro-glial scar, limiting the damage beyond the injury site and restoring the BSB, but also hindering the regeneration of injured neurons[15].

It is known that adult neurons cannot regrow after an insult to the spinal cord due to the presence of a hostile environment, which restrains them from growing through and beyond the lesion site. Myelin is a crucial component for the insulation of axons and the increase of the electrical conductance of neurons. However, upon injury, myelin debris factors called myelin-associated inhibitors (MAIs) can be detected by injured neurons inhibiting their outgrowth[16]. Nogo-A and the myelin-associated glycoprotein (MAG) are two members of the family of MAIs that are known to activate the RhoA/ROCK signaling pathway[17]. This signaling pathway leads to inhibition of tubulin polymerization and interferes with the lengthening of injured axons[18]. Furthermore, the fibro-glial scar contains chondroitin sulfate proteoglycans (CSPGs) that inhibit axonal regeneration of damaged neurons also through the RhoA/ROCK signaling pathway[19,20].

Given this, it would be plausible to assume that manipulating the extracellular environment would be sufficient to achieve long-distance regeneration and functional recovery in the CNS. Surprisingly, Tom and colleagues have showed that removing the CSPG-mediated

inhibitory signal by treatment with chondroitinase ABC, degrading CSPGs, supported sprouting of spared serotonergic fibers but failed to promote axonal regeneration of injured axons. Moreover, it did not promote functional recovery[21]. Nevertheless, earlier work from Bradbury and colleagues had shown that the removal of CSPGs following an SCI allowed for regeneration of ascending and descending spinal tracts and amelioration of locomotor and proprioceptive outcomes[22]. The modulation of the extracellular inhibitory SCI environment through chondroitinase ABC treatment has, undoubtedly, beneficial effects on neuronal regeneration and repair. Even today, it is used in combination with alternative methods to promote functional recovery[23,24].

Other approaches aiming to manipulate the CNS milieu upon injury have shown that it plays an important role in the plasticity of descending fibers. Nogo-66 receptor 1 (NgR1), a receptor for Nogo-A, MAG, oligodendrocyte myelin glycoprotein (OMgp) and glycosyl-phosphatidylinositol (GPI)-anchored member of the LRR (leucine-rich repeat) proteins[21,25–28], are part of the non-regenerating environment of the injured CNS. Blocking these factors results in acute sprouting of spared corticospinal fibers and some extent of functional recovery but not the regeneration of injured axons[29,30]. Notably, when a dorsal hemisection was applied on the cords of MRL/MpJ mice, which have reduced astrogliosis, the corticospinal tract (CST) was able to grow through and beyond the lesion site but showed only limited locomotor recovery[31,32]. Surprisingly, more recent work has proven that scar formation is crucial for the regeneration of damaged spinal tracts and it negatively impacts the response of neurons to growth-stimulating factors[33]. Altogether, these findings indicate that the extrinsic environment of CNS neurons has a vital role in their regeneration; however, it is not the only component in the process of recovery upon injury. Seminal studies in the 1980s have shown that when CNS neurons are exposed to PNS grafts, they can support outgrowth through this permissive environment, indicating that the CNS neurons retain the intrinsic capacity to initiate growth[34,35]. It is not clear, though, how the PNS grafts contribute to the growth of CNS axons. However, this regenerative capacity is limited since the PNS graft-supported growing neurons can only project into the CNS for a short distance[35]. Also, even when adult CNS neurons are injured without the formation of an inhibitory extracellular environment, they cannot support long-distance regeneration[36], although some neuronal populations retain their ability to grow into a scar-free CNS environment[36].

Other studies have focused on manipulating single intrinsic factors that might negatively regulate neuronal regeneration, but this also had limited effects. Retinal ganglion cells (RGC) are sensory neurons that convey visual information to the brain. As part of the

CNS, they fail to regrow their axons upon an injury. Specifically, phosphatase and tensin homolog (PTEN) deletion in adult RGC and activation of the mammalian target of rapamycin (mTOR) support RGCs survival and regeneration, but functional recovery was not reported[37]. Nevertheless, the silencing of PTEN in corticospinal neurons has been sufficient for axonal regeneration following SCI and was associated with forelimb motor functional recovery[38]. Activation of the Janus kinase/signal transducer and activator of transcription proteins (JAK/STAT) pathway through suppressor of cytokine signaling 3 (SOCS3) promotes axonal regeneration of RGCs, with the concomitant activation of the mTOR pathway having an additive effect on the regeneration of the optic nerve up to 3mm[39], but again no functional recovery was observed. In the spinal cord, SOCS3 deletion does not promote axonal regeneration of damaged axons, but it allows for enhanced sprouting of intact fibers and the double deletion of SOCS3 and PTEN allows for an improvement in skilled locomotion[40]. Other paradigms regarding injuries in the spinal cord indicate that manipulating intrinsic mechanisms has a beneficial but limited effect on CNS regeneration. Overexpression of the transcription factor cAMP Responsive Element Binding Protein 1 (CREB) in sensory neurons followed by injury of their central branches results in enhanced axonal regeneration through but not beyond the lesion site[41]. STAT3 is a transcription factor known for its role in the PNS regeneration[42], and its overexpression in lesioned corticospinal tracts allows for sprouting around the lesion site contributing to partial functional recovery[43]. However, STAT3 overexpressing neurons cannot grow through the lesion site[43]. Interestingly, the overexpression of the transcription factor Sox11 in the CNS enhances neuronal protection and regeneration, but it does not promote functional recovery[44].

CNS regeneration potential remains low and is by no means comparable to the regenerative capacity of the PNS. Some of the paradigms showed above have demonstrated that regeneration and sprouting might be possible in the CNS following injury, but it is not always accompanied by functional recovery. Regeneration might be one part of the equation, but correctly formed new connections are crucial for functional recovery, and the understanding of their contribution is vital. The PNS provides an interesting regenerative paradigm whose investigation can shed light on the intrinsic mechanisms contributing to axonal regeneration. Intrinsic regenerative genetics, epigenetics and mechanical properties of the permissive regenerative PNS offer a fruitful field to discover potential mechanisms whose activation after a CNS injury may enhance axonal regeneration.

## 1.1.3. PNS can support long-distance regeneration: The dorsal root ganglion regenerative paradox

Extrinsic and intrinsic mechanisms have been examined for the discrepancy between the CNS and PNS regenerative capacity. The PNS has structural as well as cellular composition differences with the CNS, which affects its recovery following injury. Trauma in the PNS initiates an immune response recruiting macrophage and Schwann cells, which efficiently clear myelin debris present in the PNS[45–48]. Although the consistency of the CNS and PNS myelin is different[49], the inhibitory effect of MAG exists in both, which is overridden by the presence of laminin in the PNS, strongly supporting axonal regeneration[50]. More importantly, Schwann cells facilitate regeneration upon a peripheral injury as they can undergo dedifferentiation and form physical bridges that support damaged neurons and enhance the elongation of lacerated axons[51–53].

Apart from differences in the extracellular environment and the cells surrounding PNS neurons post-insult, distinct cell-autonomous mechanisms are initiated in peripheral neurons that support long-distance regeneration. Genetic and epigenetic changes can set up different outcomes between the two nervous systems[54,55]. Investigating such changes provides mechanisms to target for the recapitulation of PNS regenerative processes in the lacking CNS.

Regeneration-associated genes (RAGs) are classified as genes upregulated in regenerative neuronal populations[56] but are modestly expressed upon an injury in the CNS[57,58]. Among them, activating transcription factor 3 (ATF3)[59], c-Jun[60], SRY-box containing gene 11 (Sox11)[61], small proline-repeat protein 1A (SPRR1A) [62], growth-associated protein-43 (GAP-43), brain abundant membrane attached signal protein 1 (BASP1 or CAP-23)[63] and superior cervical ganglion-10 (SCG-10)[64] are some of the genes whose expression is significantly increased within 24 hours post-injury[65] in the PNS and can contribute to regeneration. Most of these genes have come from investigating the regeneration of dorsal root ganglion cells (DRG). DRG are sensory neurons, with their somas clustered in the periphery. They are responsible for the perception of mechanical, noxious, or visceral stimuli by conveying this information to the CNS. Each DRG cell is considered pseudo-unipolar, as it projects one axon bifurcating into two branches; one branch is innervating the PNS and the other branch enters the CNS where it meets its targets. Notably, although these branches share the same soma, they respond differently to an injury, with the peripheral branch able to readily regenerate, unlike the central branch.

Given the particularity of the DRG neurons, it was found early on that although the two branches do not show the same regenerative capacities, the response of the PNS branches can influence the regenerative response of the CNS ones. Initially, it was revealed that an injury in peripheral branches prior to a second injury in the same branches can evoke a regenerative response and prime the subjected neurons to enhanced regeneration compared to peripheral fibers receiving only one injury[66]. The initial peripheral injury evoking a regenerative response is called a conditioning lesion (CL). This CL initiates an importin-dependent retrograde regenerative signal causing genetic and epigenetic changes in the soma of injured neurons[67–69]. However, the regenerative effect of this CL is not limited only to the PNS. In 1999, S. Neuman and C. J. Woolf investigated the efficacy of a CL in promoting neuronal regeneration of ascending sensory fibers. In this paradigm, the CL preceded a dorsal column axotomy (DCA) within the spinal cord. The lacerated CNS fibers, which fail to grow rostrally through and beyond the lesion site, can grow into the lesion when a CL occurs simultaneously as a DCA. When the CL takes place one week before the DCA, the injured axons can grow through and beyond the lesion site. Surprisingly, this effect is visible even if the CL and DCA are kept two weeks apart[70]. This suggests that over time the peripheral injury-initiated signal builds up a retrograde regenerative program supporting the outgrowth of CNS axons, thereby overcoming the hostile milieu of the CNS following injury.

The investigation of pathways related to a regeneration-permissive peripheral injury provides further insight into potential targets to be manipulated to achieve regeneration in the CNS. Protein kinase A (PKA) is an important regulator of the CL effect working through cyclic adenosine monophosphate (cAMP)[71]. Treatment with cAMP and neurotrophin 3 (NT-3), another neuroregenerative factor[72], following an injury to the spinal cord, allowed for growth through and beyond the injury site[73]. Another example is the phosphoinositide 3-kinase/protein kinase B (PI3K/Akt) signaling pathway. A peripheral neuronal injury subsequently activating the transcription factor SMAD family member 1 (Smad1) is indispensable for the regenerative effect of the CL[74]. Targeting this pathway showed that, when PTEN, a negative regulator of the PI3K-Akt pathway, is silenced, lesioned neurons in the optic nerve[37] can regenerate their axons. Similarly, when silenced in injured neurons in the spinal cord[75], they have enhanced supraspinal sprouting that promotes modest locomotion and motor coordination recovery[38,76].

Clearly, the aforementioned mechanisms show that the regenerative capacity of the PNS is not only based upon a permissive environment but also on intrinsic changes. It is evident that a successful regenerative strategy is complicated, and it might involve many different routes and approaches. Understanding the cytoplasmic and nuclear events associated with a

regenerative program is crucial. Recruitment of regenerative transcriptional complexes is a key component in the expression of genes that promote regeneration[60,77] and may override inhibitory transcriptional complexes. Epigenetics can orchestrate the regenerative response upon an injury, but it can also dampen a response to it. The dynamics between the epigenetic code and its outcome on gene expression is a hub of information deciding if a neuron will be repaired. Regulation of these dynamics could provide new avenues for the treatment of neuronal injuries.

## 1.1.4. The role of epigenetics in axonal regeneration

The genetic information within each cell is organized in highly dense structures in the nucleus. The expression of each gene is a combination of chromatin accessibility and recruitment of the correct repertoire of factors to initiate and execute gene transcription. Post-translational modifications of histones as well as direct changes at the DNA level control the timing of gene expression and regulate the regenerative response of the PNS or CNS. More research has recently been dedicated to the investigation of these mechanisms and their clinical translatability in cases of neuronal damage.

DNA methylation, mediated by DNA-methyltransferases (DNMTs), has been associated with dense and inaccessible chromatin, called heterochromatin. It has been shown that these modifications can regulate axonal outgrowth. For example, treatment with folic acid enhances the expression of DNMTs and the methylation status of the CNS enabling axonal regeneration[78]. These results, although promising, contradict other findings which have shown that 5-hydroxymethlylation of cytosine (5hmC), which is required for the demethylation of the DNA, is increased upon a peripheral injury. However, it remains unclear which genes are involved[79] and if 5hmC is important for axonal regeneration of the CNS[80]. Further experiments are required to elucidate the importance of the DNA methylation state and classify the underlying genes and their expression levels involved in axonal outgrowth.

Epigenetic changes are not restricted to the DNA level but also include post-translational modifications (PTMs) of histones. Histone PTMs include acetylation, methylation, glycosylation, phosphorylation, ubiquitination, proline isomerization, citrullination, SUMOylation, carbonylation and biotinylation[81,82]. Although not all of these modifications have been associated with regenerative responses upon a peripheral injury, some findings have shown that the epigenome responds to a regenerative lesion. Notably, these

modifications precede changes in the expression levels of RAGs and transcription factors associated with regeneration. In 2015, interesting work by Li and colleagues looked further into the immediate intrinsic changes upon a peripheral injury and identified three phases regarding the changes of the DRG transcriptome. Within the first 6 hours, they observed an upregulation of genes related to cellular stress. RAG expression was observed 9 hours post-injury up to 14 days, showing that the cells enter from a stress phase into a regenerative phase[83]. Earlier findings had shown that within the first 6 hours post-peripheral injury, there is a significant increase in the acetylation levels of histone 4, which is associated with active gene expression, found at the promoter loci of known RAGs[84], suggesting that these changes could set up the correct chromatin state for expression of these RAGs later on.

In addition, it has been shown that the retrograde regenerative signal initiating from peripherally injured axons exports the histone deacetylase 5 (HDAC5) from the nuclei of injured DRG. HDAC5 is responsible for histone 3 (H3) deacetylation, with its export resulting in elevated levels of histone 3 acetylation (H3ac)[85], associated with active gene expression[86,87]. Pharmaceutical inhibition of HDAC5 has been proven to facilitate axonal outgrowth of cultured sensory neurons and injured sensory neurons *in vivo*[84]. Also, peripheral injury-driven deactivation of HDAC3 is crucial for axonal regeneration *in vitro* and *in vivo* although it is not exported from the nuclei of uninjured neurons[88]. These findings support the notion that some histone modifications presage the expression of RAGs by making the chromatin more accessible (euchromatin) to transcription factors required for the establishment of a successful regenerative program.

As suggested from the aforementioned studies, histone acetylation is an epigenetic marker in general correlated to active gene expression of RAGs and enhanced axonal regeneration. Histone acetyltransferases (HATs) are enzymes that can add acetyl-groups in the tails of histones, and very often, their targets expand further than histones, thus called lysine (K) acetyltransferases (KATs). P300/CREB binding protein (CBP)-associated factor (PCAF), also known as lysine acetyltransferase 2b (Kat2b), was discovered in 1996 as an inhibitor of the adenoviral oncoprotein E1a blocking cell cycle progression and mitosis[89]. PCAF is an ortholog of another acetyltransferase called general control of amino acid synthesis protein 5 (GCN5) and belongs to the Gcn5-related-N-acetyltransferase (GNAT) family of histone acetyltransferases. It harbors a bromodomain, which recognizes acetylated lysine residues, it can interact with other KATs, such as p300 and CBP, but it cannot bind directly to the DNA as it lacks DNA binding site domains[90]. Research on the transcription factor p53 and its contribution to axonal regeneration led to discovering the importance of PCAF to the p53-

regulated regenerative signal. p53, which is a crucial tumor suppressor[91], traditionally associated with DNA damage repair and apoptosis[92], was shown to enhance axonal outgrowth of cultured neurons and its silencing interfered with the regeneration of lesioned peripheral nerves[93]. Although known that p300 and PCAF[94] acetylate p53, it was shown for the first time that PCAF overexpression *in vitro* was enough to increase p53 acetylation levels at lysine K320 and augmented its recruitment on the promoters of RAGs, enhancing the neurite outgrowth of cultured neurons[93].

The epigenome of regenerative neurons, specifically the contribution of PCAF, was further studied by Puttagunta and colleagues. They showed that epigenetic markers associated with active gene expression, such as histone 3 lysine 9 acetylation (H3K9ac)[95], were enriched on the promoters of select RAGs, such as GAP-43, Galanin and BDNF, upon a peripheral injury of adult DRG[96]. On the contrary, it was shown that an injury in the CNS failed to induce the same epigenetic changes but instead increased the occupancy of RAG promoters by epigenetic markers associated with heterochromatin[96]. PCAF, which mediates the acetylation of H3K9, also had an increased occupancy on RAG promoters upon a regenerative injury. Its inhibition interfered with the peripheral injury-induced epigenetic changes and impeded axonal outgrowth *in vitro* and *in vivo*. On the other hand, viral overexpression of PCAF enhanced axonal outgrowth *in vitro* and allowed for axonal regeneration of lacerated sensory fibers in the injured spinal cord through and beyond the lesion site[96]. These results shed further light on the contribution of epigenetics in the regenerative processes following a peripheral injury. The exact mechanisms through which PCAF functions to enhance regeneration and which other players are involved in this signaling pathway remain unknown. Therefore, the transcriptional changes associated with PCAF peripheral injury-driven activation, which transcriptional factors are involved in this process and whether pharmaceutical activation of PCAF is possible to enhance regeneration *in vitro* and *in vivo* are part of the scope of this thesis.

## 1.1.5. The role of Sp1 and MAZ in transcriptional regulation and neuronal injury

Gene expression requires the complex coordinated recruitment of factors interacting with gene promoters to form transcriptional machinery. Although PCAF acetylates cytoplasmic and nuclear proteins, it lacks a DNA binding domain, thus it recruits other factors to interact with to form a transcriptional complex. PCAF has been found as a member of

complexes along with 20 other associated proteins, most of them crucial for transcriptional initiation, such as the TAB-associated factors (TAFs)[97]. Although the contribution of PCAF in the PNS regenerative signal has been demonstrated, the transcriptional complex that is recruited due to a PCAF-dependent regenerative signal remains unknown. For this, we investigated the transcriptome (RNA-seq) of peripherally injured CD1 wild type (WT) or PCAF knockout (PCAF KO) adult mouse DRG compared to sham-injured controls. From this analysis, potential candidate RAGs were found. Transcription factor binding site (TFBS) analysis showed two transcription factors potentially regulating the expression of PCAF-dependent RAGs (PCAF-RAGs), Specificity protein 1 (Sp1) and myc-associated zinc finger protein (MAZ).

Sp1 was first isolated from mammalian cells and described by Dynan and colleagues as a TF that can bind to the Simian Virus 40 (SV40) genome and initiate the transcription of its early and late transcripts driven by RNA polymerase II[98,99]. Sp1 belongs to the Sp1-like/KLF family bearing three Cys2His2 zinc finger motifs[100]. It has four domains A, B, C and D, with domains A, B and D being essential for protein-protein interactions[101], and it recognizes GC-rich sequences present at proximal promoter sites of its target genes, which lack TATA-elements[102]. Sp1 can bind to promoters, whose CpG islands have been methylated, suggesting that the active transcription of its targets may be independent of the methylation status of the promoter[103]. Initially, Sp1 was considered mainly a regulator of housekeeping genes, but now this ubiquitously expressed TF is known to be involved in regulating a plethora of genes during development[104], tumorigenesis[105] and metabolism in response to hormones[106].

Sp1 is extensively modified post-translationally via phosphorylation, methylation, SUMOylation, ubiquitination, glycosylation and acetylation regulating its stability and trans-activation activity. Sp1 can also interact and recruit HDACs to the promoter of genes leading to their deacetylation and inhibition of their expression. On the other hand, Sp1 can recruit HATs, such as p300 and PCAF, to the promoters of target genes, mediating the acetylation of histones and allowing gene transcription[107–109]. It can bind to promoters of injury-inducible genes such as ATF3, c-Jun and STAT3, and other known RAGs suggesting a connection of this TF to neuronal injury-mediated responses[110,111]. Sp1 may have a similar role in astrocytes. Upon its activation by injury-mediated extrinsic signaling, it can interact with the Smad TFs, upregulating genes important for neuroprotection following neuronal damage[112,113]. It can act synergistically with the estrogen receptor 1 (ESR1), responding to 17beta-estradiol levels promoting the expression of their target genes bearing GC-rich domains in their promoters[114,115]. Although 17beta-estradiol has a protective function after spinal cord injury

(SCI)[116,117], it remains unclear whether Sp1 is involved in this pathway. Sp1 seems to have a range of functions depending on the environmental cues and its partners, thus we wanted to elucidate its contribution to the outgrowth of cultured neurons and whether it works in concert with PCAF in driving RAG expression.

In 1992, Bossone and colleagues isolated and characterized the protein MAZ from HeLa cells, with a molecular weight of approximately 58.5 kDa that could bind to a specific sequence present on the c-myc protooncogene promoter and the C2 gene terminator, regulating their expression levels[118]. MAZ bears six Cys2-His2 zinc finger motifs and can bind to a GA box[118]. Apart from c-myc, it can regulate other genes as well, playing an important role in cancer[119–121], immune cell development and inflammatory responses[122,123], as well as regulation of muscle-specific genes[124]. MAZ has been associated with angiogenesis in response to the vascular endothelial growth factor (VEGF)[121]. Similar to Sp1, MAZ is associated with transcriptional activation as well as mediating mechanisms of transcriptional suppression. MAZ can suppress gene expression by recruiting HDACs to its promoter binding sites[125]. Its role in neuronal regeneration and its relationship to PCAF has not been examined.

Many studies have indicated the interaction between Sp1 and MAZ as they both recognize GC-rich DNA sequences (GGGCGG for Sp1[126] and GGGAGGG for MAZ[118]) present on the same cis-elements[127]. The interaction between these two TFs is involved in different cellular processes, such as metabolism[128], neurotransmitter-mediated signaling[129], nitric oxide synthesis[130], electrolyte homeostasis[131] or expression of N-methyl-D-aspartate (NMDA) receptors, important for synaptic transmission in the CNS[132]. Similar to Sp1, its role in neuronal regeneration is unclear and we wanted to investigate its contribution to the outgrowth of cultured neurons and whether it works in concert with PCAF in driving RAG expression.

The regenerative adeptness of the PNS is usually considered as the result of the cell-autonomous intrinsic properties of its neurons. Although transcriptional and epigenetic changes are crucial, they are not necessarily the only factors in this process and there may be extrinsic factors that can contribute to PNS response to injury.

## 1.1.6. Tensile forces in axonal growth

During the development of multicellular organisms, tissues form and grow under the presence of mechanical forces[133]. The cytoskeleton receives and responds to mechanical cues

of neighboring cells, the extracellular matrix or exogenous factors[134]. The nervous system is subjected to mechanical forces that guide its development, form its shape and act as cues for perception of the internal physiology of the body (proprioception) or the outside world (mechano- and thermo-sensation)[133,135,136]. During development, growing axons of nascent neurons reach their targets prior to the completion of the overall growth of the body[137], however their neurites continue elongating during this growth period through the application of tensile strain[138]. The adult PNS is constantly subjected to mechanical forces acting either as cues to elicit a behavioral response or leading to damage. Interestingly, it has been shown that limb movement due to voluntary exercise can prime dissected cultured DRG to enhanced levels of outgrowth[139]. Hutson and colleagues have shown that wheel running exercise can prime cultured DRG outgrowth[140]. Limb movement during exercise subjects nerves to mechanical tension, thus we can infer that one factor contributing to the observed priming might be mechanical forces developed during training and applied to peripheral nerves. Although these setups involve exercise without any prior injury, tension-induced outgrowth mechanisms could shed light on new avenues of regeneration that could be applied to adult non-regenerating neurons to enhance their regenerative capacity and ability to form functional connections.

Interestingly, *in vitro* studies have shown that cultured neurons achieve long-distance elongation when subjected to tensile forces[141–143]. Pfister and his colleagues have shown that embryonic DRG neurons in culture can reach extreme levels of elongation, up to 5 cm when their axons are progressively and repetitively stretched for several days (1 mm the first day was the net result of 2 μm displacements every 172 sec, which was altered each successive day up until 14 days), similar to towing forces observed during development[144]. Likewise, adult DRG axons can reach profound levels of elongation when stretched *in vitro*[143]. This validates that adult neurons retain the capacity to respond to tensile forces even after maturity.

The movement of limbs in adult individuals subjects respective nerves to cyclic mechanical stretch of a limited amplitude[145], although the precise nerve lengthening *in vivo* by limb movement is poorly reviewed. Post-mortem studies on cadavers have shown that different nerves are stretched by the movement of the limbs they are innervating, with stretching ranging from 0 to 15%[146–155]. Therefore, given the initial responsiveness of growing neurons to mechanical stretch and the absence of the regenerative capacity of adult CNS, it remains to be addressed whether the lack of mechanical cues plays a role in the failure of the CNS to regenerate upon injury.

In the aforementioned *in vitro* studies, neurons were stretched by towing of growth cones and elongation of neurites as the extension distance grew, similar to that seen during

development. However, this does not recapitulate the physiological conditions of normal limb movement, where the nerves are stretched cyclically by the extension and contraction of the respective muscles, without towing extended distances. With SH-SY5Y human neuroblastoma cells, Higgins and his colleagues showed that 10% cyclic mechanical stretch was enough to produce statistically significant longer neurites than neurons that were not stretched[156]. Although closer to normal stretch conditions indicated *in vivo,* their approach is far from similar to the conditions *in vivo* as the cultures consist of dissociated cells. Nevertheless, they showed that when cells are let to grow for two days on a collagen-coated membrane before 10% equiaxial stretching at 0.25 Hz for 120 min/d for seven days, it led to increased neurite outgrowth similar to the level induced by the neurogenic factor, retinoic acid (10 µM). This suggests that neuronal cells can respond to mechanical forces observed during development and movement during exercise.

*In vivo* studies have also shown that exercise can enhance the regenerative capacity of peripheral[157] and central nerves[158], but how exactly mechanical forces developed in the periphery could contribute to the regeneration of the PNS and/or the CNS and if these mechanisms act in a cell-autonomous manner remains unclear.

## 1.2. Hypothesis and Aims

### 1.2.1. Hypothesis

Regeneration of injured neurons has been extensively studied in order to achieve functional regeneration of non-regenerating neuronal populations following their injury. Further understanding of mechanisms that regulate the response of regenerative peripheral nerves to trauma would allow for the recapitulation of such mechanisms in the non-regenerative neuronal populations of the CNS. Here, we hypothesize that a better understanding of PCAF-associated complexes would provide further insight into the co-regulators of the peripheral PCAF-driven regenerative signal. Additionally, the pharmaceutical activation of PCAF would be sufficient to recapitulate cell-autonomous events occurring during a regenerative peripheral lesion, promoting outgrowth *in vitro* and *in vivo*. Further, we hypothesize that mechanical stimulation of adult peripherally and centrally located nerves, simulating physiological stretch conditions during limb movement, would induce intrinsic changes in the subjected neurons and enhance their regenerative capacity.

### 1.2.2. Aims

The scope of this thesis was to investigate potential intrinsic avenues of regeneration in adult sensory neurons in response to extrinsic events. I explored PCAF-driven regenerative mechanisms and their implications *in vitro* and *in vivo* using the DRG model. Additionally, I investigated the contribution of mechanical stimulation of nerve tracts in the outgrowth of cultured DRG and its mechanisms. Collectively, the aims of my work are listed below:

#1    Identification of PCAF-RAGs and characterization of TFs important to axonal outgrowth regulating PCAF-RAGs and their synergy to PCAF.

#2    The investigation of the PCAF-driven regenerative signal following a peripheral and a central lesion and the regulation of PCAF-RAGs.

#3    Pharmaceutical activation of the PCAF-driven regenerative signal and the regulation of PCAF-RAGs *in vitro* and *in vivo* and the investigation of the regeneration of peripheral nerves upon a sciatic nerve crush coupled to pharmaceutical activation of PCAF.

#4      The investigation of the outgrowth potential of cultured DRG following mechanical stretch of different amplitudes and frequencies and the characterization of specific DRG subpopulations responding to regeneration-inducing mechanical stimulation.

#5      The exploration of potential intrinsic pathways regulated by regenerative mechanical loading.

# Materials and Methods

# 2. Materials and Methods

## 2.1. Materials

### 2.1.1. Animals

**Table 2.1.** List of animals

| Short name | Full name | Type | Description | Provider |
|---|---|---|---|---|
| **CD1** | Crl:CD1(ICR) | Outbred | Wildtype (WT) mice | Charles River |
| **CD1 PCAF$^{-/-}$** | CD1.129-Kat2b$^{tm1Nkt}$/Orl | Outbred | The exon encoding the N terminus of PCAF (Kat2b) was replaced by a neomycin resistance gene cassette in the targeting vector. | Institut de Recherche en Cancerologie de Montpellier (IRCM) INSERM U896 |

### 2.1.2. Equipment and instruments

**Table 2.2.** Equipment for DNA preparation and genotyping

| Equipment/Instrument | Usage | Manufacturer |
|---|---|---|
| NanoDrop™2000 Spectraphotometer | DNA concentration measurement | ThermoFischer Scientific, Waltham, MA, USA |
| ThermoMixer C | Digestion of biopsies for DNA isolation | Eppendorf AG, Hamburg, Germany |

| | | |
|---|---|---|
| T100™ Thermal Cycler | PCR | Bio-Rad Laboratories Inc., Hercules, CA, USA |
| UV Detector | Agarose gel image acquisition | PeqLab, VWR, Leuven, Belgium |

**Table 2.3.** Equipment and instruments for surgical procedures

| Equipment/Instrument | Usage | Manufacturer |
|---|---|---|
| BRAND® disposable micro-pipettes, intraMark | AAV5 injections | Merck, Darmstadt, Germany |
| Braunol® | Disinfection | Braun Meslungen AG, Meslungen, Germany |
| Disposable scalpel (No. 12) | DRG/Sciatic nerve dissection | FEATHER Safety Razor Co. Ltd, Osaka, Japan |
| Dumont #5 forceps | Sciatic nerve axotomy/ T9 dorsal hemisection | Fine Science Tools, Foster City, CA, USA |
| Extra Fine Micro Dissecting Scissors | DRG/Sciatic nerve dissection | Roboz surgical instrument Co., Inc., Maryland, USA |
| Inject needles 30G | T9 dorsal hemisection | Henry Schein Inc., NY, USA |
| McPherson-Westcott conjunctival scissors, | Laminectomy | World precision instruments, Friedberg, Germany |
| Michel suture clips | Surgeries | Fine Science Tools, Foster City, CA, USA |
| Micro knife – 22.5º cutting angle | T9 dorsal hemisection | Fine Science Tools, Foster City, CA, USA |

| | | |
|---|---|---|
| Picospritzer II Intracellular microinjection system | Sciatic nerve AAV5 injection | Parker Hannifin, New Hampshire, USA |
| Pipette puller Narishige Pp-830 | Pipettes preparation for AAV injections | Biosurplus Inc., SD, USA |
| Remington Razor | Surgery preparation | Remington, Wisconsin, USA |
| Rongeurs forceps | Nerve explant dissection | Fine Science Tools, Foster City, CA, USA |
| Steri250 surgical tool sterilizer | Tools sterilization | Simon Keller AG, Switzerland |
| Stryker Gaymar TP700 TPump | Temperature regulation | VWR, Leuven, Belgium |
| Surgical Microscope | Sciatic nerve axotomy/ T9 dorsal hemi-section | Olympus Deutschland GmbH, Hamburg, Germany |
| Vannas Spring Scissors – 3mm Cutting Edge | Sciatic nerve axotomy | Fine Science Tools, Foster City, CA, USA |
| Octagon Forceps | Sciatic nerve axotomy/ T9 dorsal hemi-section | Fine Science Tools, Foster City, CA, USA |

**Table 2.4.** Equipment and instruments for tissue processing

| Equipment/Instrument | Usage | Manufacturer |
|---|---|---|
| Bonn Micro Forceps | Tissue dissection | Fine Science Tools, Foster City, CA, USA |
| Cryostat Blades | Cryo-sectioning | Fine Science Tools, Foster City, CA, USA |

| | | |
|---|---|---|
| Cryostat Hyrax C60 | Cryo-sectioning | Microm GmbH, Walldorf, Germany |
| Dumont #5 forceps | Tissue dissection | Fine Science Tools, Foster City, CA, USA |
| Friedman-Pearson Rongeurs | Tissue dissection | Fine Science Tools, Foster City, CA, USA |
| ISMATEC® REGLO Digital MS-4/8 | Transcardial perfusion | IDEX Health & Science Oak Harbor, WA, USA |

**Table 2.5.** Equipment and instruments for microscopic imaging

| Equipment/Instrument | Usage | Manufacturer |
|---|---|---|
| CCD digital colour camera XC30 | Image Acquisition | Olympus Deutschland GmbH, Hamburg, Germany |
| Fluoview FV1000 confocal laser scanning microscope | Image Acquisition | Olympus Deutschland GmbH, Hamburg, Germany |
| System Microscope BX53 | Image Acquisition | Olympus Deutschland GmbH, Hamburg, Germany |

**Table 2.6.** Equipment for cell electroporation

| Equipment/Instrument | Usage | Manufacturer |
|---|---|---|
| AMAXA™ 4D-nucleofector system, X unit | DRG electroporation | LONZA Ltd., Basel, Switzerland |

**Table 2.7.** Equipment for protein quantification

| Equipment/Instrument | Usage | Manufacturer |
| --- | --- | --- |
| PHOmo microplate reader | Protein quantification | Autobio Diagnostics Co., Ltd , Zhengzhou, China |

**Table 2.8.** Equipment for nerve explant mechanical loading

| Equipment/Instrument | Usage | Manufacturer |
| --- | --- | --- |
| InVivoO$_2$ 400 Hypoxia incubator | Nerve explant incubator | I&L Biosystems GmbH, Königswinter, Germany |

**Table 2.9.** Software used

| Software | Usage | Company |
| --- | --- | --- |
| Adobe Illustrator CS6 | Image processing | Adobe Systems Inc., San Jose, CA, USA |
| Adobe Photoshop CS6 | Image processing | Adobe Systems Inc., San Jose, CA, USA |
| cell^F Imaging Software for Life Science Microscopy | Imaging software for Bright-field microscope | Olympus Deutschland GmbH, Hamburg, Germany |
| GalilTools | Nerve explant mechanical loading | Galil Motion Control, CA, USA |
| HCA-vision V2.2.0 | High throughput analysis of neurite length | CSIRO, Marsfield, Australia |

| | | |
|---|---|---|
| ImageJ | Image processing | NIH |
| nSolver™ Analysis Software | Nanostring analysis | NanoString Technologies, Inc., Seattle, USA |
| Prism 6 | Graphing and Statistical analysis | GraphPad Software Inc., La Jolla, CA, USA |

## 2.1.3. Chemicals/Kits

**Table 2.10.** List of chemicals and kits used

| Chemicals/solutions/kits | Usage | Company |
|---|---|---|
| 4',6-diamidino-2- phenylindole (DAPI) | Immunostaining | Sigma Aldrich Co., St. Louis, MO, USA |
| 5 Prime Master Mix | Genotyping/PCR | 5 PRIME GmbH, Hamburg, Germany |
| Acrylamide/Bis solution (30%, 19:1) | Protein electrophoresis | Biorad, Hercule, CA, USA |
| Agar-Agar, danish | Bacterial culture plate preparation | Carl Roth GmbH, Karlsruhe, Germany |
| Agarose Ultrapure | Gel preparation | Thermo Fisher Scientific, Invitrogen, Waltham, MA, USA |
| Ampicillin (Ampicillin-ratiopharm® 5.0 g) | Post-surgery treatment | Ratiopharm GmbH, Ulm, Germany |
| Ammonium persulfate solution (APS) | Protein electrophoresis | Biorad, Hercule, CA, USA |

| B27™ supplement, serum-free, 50x | DRG culture medium preparation | ThermoFisher Scientific, Waltham, MA, USA |
|---|---|---|
| Bovine Serum Albumin (BSA) | Immunoprecipitation | SERVA Electrophoresis GmbH, HD, Germany |
| Buprenorphine HCl (Temgesic®) | Analgesics | Reckitt Benckiser, Slough, UK |
| Chloroform | RNA preparation | neoLab Migge GmbH, Berlin, Germany |
| Citric acid (anhydrous) | Antigen retrieval | Carl Roth GmbH, Karlsruhe, Germany |
| Collagenase from *Clostridium histolyticum* | DRG digestion | Merck, Darmstadt, Germany |
| cOmplete™ protease inhibitor cocktail | Protein extraction | Roche Holding AG, Basel, Switzerland |
| Cottonseed Oil | EML76 dilution/vehicle | Merck, Darmstadt, Germany |
| Cyano Fast | Explant fixation on PEEK scaffolds | Hager & Werken GmbH & Co., Duisburg, Germany |
| D(+)-Saccharose (sucrose) | Tissue cryoprotection | Carl Roth GmbH & Co. KG, Karlsruhe, Germany |
| Distilled water (ultra-pure type 1 water) | Solutions preparation | ELGA LabWater, UK |
| Dispase (neutral protease) | DRG digestion | Worthington Biochemical Corp., NJ, USA |
| DMEM/F12 (with HEPES, L-Glutamine, phenol red) | DRG culture medium preparation | ThermoFisher Scientific, Waltham, MA, USA |

| | | |
|---|---|---|
| DNA Ladder (100 bp) | DNA electrophoresis | New England Biolabs Inc., Ipswich, MA, USA |
| DNeasy Blood & Tissue Kit | DNA preparation | Qiagen GmbH, Hilden, Germany |
| Dulbecco's phosphate buffered saline (DPBS, 1X) | Coverslips coating | ThermoFisher Scientific, Waltham, MA, USA |
| EndoFree Plasmid Mega Kit | Bacterial plasmid preparation | Qiagen, Hilden, Germany |
| Ethylenediaminetetraacetic acid (EDTA) | Whole cell lysis buffer preparation | Carl Roth GmbH & Co. KG, Karlsruhe, Germany |
| Foetal bovine serum (FBS), heat inactivated, sterile filtered | DRG culture medium preparation | Merck, Darmstadt, Germany |
| Fluoromount-G® | Imaging | Southern Biotechnology Associates, Birmingham, AL, USA |
| Gel Loading Dye, Blue (6x) | DNA electrophoresis | New England Biolabs Inc., Ipswich, MA, USA |
| Glacial acetic acid ($CH_3COOH$) | TAE buffer | neoLab Migge GmbH, Berlin, Germany |
| Hanks' balanced salt solution (HBSS), without $Ca^{2+}$ and $Mg^{2+}$ | DRG dissection | Merck, Darmstadt, Germany |
| Immunoprecipitation Dynabeads | Immunoprecipitation | Invitrogen, Carlsbad, CA, USA |
| Isoflurane | Surgeries | Baxter International Inc., Deerfield, Illinois, USA |
| Laminin from Engelbreth-Holm-Swarm murine sarcoma basement membrane | Coverslip coating | Merck, Darmstadt, Germany |

| | | |
|---|---|---|
| LB broth (Luria/Miller) | Bacterial cultures | Carl Roth GmbH, Karlsruhe, Germany |
| Liquid blocker – PAP PEN Immunostaining pen – 5mm | IHC | Kisker Biotech GmbH & Co., Steinfurt, Germany |
| Neo-Mount® | Tissue staining preservation | Merck KGaA, Darmstadt, Germany |
| Novex™ NuPAGE™ LDS-sample buffer (4X) | SDS-PAGE samples loading | ThermoFisher Scientific, Waltham, MA, USA |
| Novex™ NuPAGE™ reducing agent (10X) | SDS-PAGE samples loading | ThermoFisher Scientific, Waltham, MA, USA |
| One Shot™ TOP10 chemical competent E. coli | Bacterial transformation | Invitrogen Corp., CA, USA |
| P3 Primary Cell 4D-Nucleofector™ X Kit S | DRG electroporation | LONZA Ltd., Basel, Switzerland |
| Paraformaldehyde (PFA) | Tissue fixation | Carl Roth GmbH & Co. KG, Karlsruhe, Germany |
| Pasteur pipettes, 230mm long | DRG dissociation | neoLab Migge GmbH, Heidelberg, Germany |
| Penicillin-streptomycin (Pen/Strep) (10,000U/ml) | DRG culture medium preparation | ThermoFisher Scientific, Waltham, MA, USA |
| QIAprep Spin Miniprep kit | Bacterial DNA preparation | Qiagen, Hilden, Germany |
| Polymerase Chain Reaction (PCR) $H_2O$ | PCR | ThermoFisher Scientific, Waltham, MA, USA |

| | | |
|---|---|---|
| PeqGreen DNA/RNA dye | DNA electrophoresis | VWR, Leuven, Belgium |
| Pierce™ BCA™ protein-assay | Protein quantification | ThermoFisher Scientific, Waltham, MA, USA |
| Poly-L-ornithine hydrobromide (PLO) | Coverslips coating | Merck KGaA, Darmstadt, Germany |
| Protease inhibitors | Protein extraction | Roche, Basel, Switzerland |
| Ringer's solution | Surgeries | Braun Melsungen AG, Melsungen, Germany |
| Sodium Dodecyl Sulfate (SDS) (20%) | Protein electrophoresis | Biorad, Hercule, CA, USA |
| Sodium chloride (NaCl) | Solution preparation | VWR, Leuven, Belgium |
| Sodium dihydrogen phosphate ($NaH_2PO_4$) | Solution preparation | Carl Roth GmbH & Co. KG, Karlsruhe, Germany |
| Sodium hydroxide solution 40 % (10M, NaOH) | Solution preparation | Carl Roth GmbH & Co. KG, Karlsruhe, Germany |
| Sterile filtered donkey serum | Immunostaining | Equitech-Bio Inc., Kerrville, TX, USA |
| Sterile Saline Solution (0.9%) | Surgeries | Braun Melsungen AG, Melsungen, Germany |
| SuperScript™ III Reverse Transcriptase kit | cDNA synthesis | ThermoFisher Scientific, Waltham, MA, USA |
| N, N, N', N'-Tetramethylethylenediamine (TEMED) | Protein electrophoresis | Biorad, Hercule, CA, USA |

| | | |
|---|---|---|
| Tissue Tek® O.C.T™ compound | Cryo-sectioning | Sakura Finetek Germany GmbH, Staufen, Germany |
| TriFast (Phenol solution) | RNA preparation | VWR, Leuven, Belgium |
| Tris(hydroxymethyl)aminomethane, $(C_4H_{11}NO_3)$ - Tris | Solution preparation | neoLab Migge GmbH, HD, Germany |
| Tris-Hydrochloride (Tris-HCl) | Solution preparation | neoLab Migge GmbH, HD, Germany |
| Triton X-100 | Immunostaining | neoLab Migge GmbH, Heidelberg, Germany |
| Trypsin - EDTA solution (10X) | Cell replating | Merck KGaA, Darmstadt, Germany |
| TURBO DNA-free kit | DNA digestion | ThermoFisher Scientific, Waltham, MA, USA |
| Tween-20 | Antigen retrieval | neoLab Migge GmbH, HD, Germany |
| Xylocaine 2% | Dorsal hemisection | AstraZeneca, Cambridge, UK |

## 2.1.4. Antibodies

**Table 2.11.** List of primary antibodies

| Antibody | Host | Clonality | Dilution | Company | Cat. No. |
|---|---|---|---|---|---|
| ATF3 | rabbit | polyclonal | 1:200 | Bio-Techne GmbH, Wiesbaden, Germany | NBP1-85816 |

| | | | | | |
|---|---|---|---|---|---|
| β-III tubulin | mouse | polyclonal | 1:2,000 | Promega, Walldorf, Germany | G7121 |
| GCN5 | mouse | monoclonal | | Santa Cruz Biotechnology (SCB), TX, USA | sc-365321 |
| H3K9ac | rabbit | monoclonal | 1:1,000 | CST, MA, USA | 9649S |
| H3K9K14ac | rabbit | monoclonal | 1:1,000 | Sigma Aldrich Co., St. Louis, MO, USA | ZRB06599 |
| MAZ | mouse | monoclonal | 1:250 | SCB, TX, USA | sc-130915 |
| Normal IgG | rabbit | polyclonal | application specific | CST, MA, USA | 2729 |
| PCAF | rabbit | monoclonal | 1:500 | CST, MA, USA | 3378S |
| SCG10 | rabbit | polyclonal | 1:1,000 | Novus Biologicals | NBP1-49461 |
| Sp1 | rabbit | polyclonal | 1:300 | Merck, Darmstadt, Germany | 07-645 |

**Table 2.12.** List of secondary antibodies

| Antibody | Host | Type | Dilution | Company | Cat. No. |
|---|---|---|---|---|---|
| AlexaFluor 594, anti-mouse | donkey | IgG (H+L) | 1:1,000 | ThermoFischer, MA, USA | A21203 |

| AlexaFluor 488, anti-mouse | donkey | IgG (H+L) | 1:1,000 | ThermoFischer, MA, USA | A21202 |
|---|---|---|---|---|---|
| AlexaFluor 594, anti-rabbit | donkey | IgG (H+L) | 1:1,000 | ThermoFischer, MA, USA | A21207 |
| AlexaFluor 488, anti-rabbit | donkey | IgG (H+L) | 1:1,000 | ThermoFischer, MA, USA | A21206 |
| Cy5-AffiniPure | donkey | IgG (H+L) | 1:500 | Jackson Immuno-Research Laboratories, PA, USA | 715175151 |

## 2.1.5. DNA vectors

**Table 2.13.** Bacterial constructs

| Name | Gene of interest | Promoter | Species | Marker | Size (bp) | Provider |
|---|---|---|---|---|---|---|
| pEGFP-Sp1 | Sp1 | CMV | Human | eGFP | 6,925 | Lab of Simone Di Giovanni (ICL) |
| pcDNA3.1+ MAZ+P2A-eGFP | MAZ | CMV | Mouse | eGFP | 6,209 | GenScript, NJ, USA |
| pmaxGFP | eGFP | CMV | Renilla reniformis | - | 3,486 | LONZA, Basel, Switzerland |

**Table 2.14.** Adeno-associated viral (AAV) vectors

| Name | Serotype | Gene | Refseq | Marker | Promoter | Conc. | Provider |
|---|---|---|---|---|---|---|---|
| AAV5-hSYN1-eGFP-WPRE | AAV5 | - | - | eGFP | hSyn1 (human synapsin 1) | $8.5 \times 10^{12}$ GC/ml | Vector Biolabs, PA, USA |
| AAV5-hSYN1-eGFP-P2A-mSp1-WPRE3 | AAV5 | mSp1 | NM_013672 | eGFP | hSyn1 | $1.4 \times 10^{12}$ GC/mL | Vector Biolabs, PA, USA |

## 2.1.6. siRNAs

**Table 2.15.** Silencing RNA (siRNA) used for gene knockdown

| Name | Targeted gene | RefSeq | Species | Provider |
|---|---|---|---|---|
| Sp1 siRNA | Sp1 | NM_013672 | mouse | Santa Cruz Biotechnology, Inc., TX, USA |
| MAZ siRNA | MAZ | NM_010772 | mouse | Santa Cruz Biotechnology, Inc., TX, USA |
| Control siRNA - A | Scrabbled sequences | - | - | Santa Cruz Biotechnology, Inc., TX, USA |

## 2.1.7. Buffers and Solutions

**Table 2.16.** Animal perfusion buffers

**0.2 M sodium phosphate monobasic solution**

| Reagent | Final concentration | Volume/mass added |
|---------|--------------------|--------------------|
| $NaH_2PO_4$ | 2.76 w/v | 27.6 g |
| $ddH_2O$ | - | 1 L |
| | | **Total volume** |
| | | 1 L |

## 0.2 M sodium phosphate dibasic solution

| Reagent | Final concentration | Volume/mass added |
|---------|--------------------|--------------------|
| $NaH_2PO_4$ | 2.86 w/v | 28.6 g |
| $ddH_2O$ | - | 1 L |
| | | **Total volume** |
| | | 1 L |

## 0.2 M phosphate buffer

| Reagent | Final concentration | Volume/mass added |
|---------|--------------------|--------------------|
| Sodium phosphate monobasic solution (0.2 M) | 46 mM | 230 ml |
| Sodium phosphate dibasic solution (0.2 M) | 154 mM | 770 ml |
| | | **Total volume** |
| | | 1 L |

## Perfusion saline (0.9%)

| Reagent | Final concentration | Volume/mass added |
|---------|--------------------|--------------------|
| Sodium phosphate monobasic solution (0.2 M) | 46 mM | 230 ml |

| | | |
|---|---|---|
| Sodium phosphate dibasic solution (0.2 M) | 154 mM | 770 ml |
| | | **Total volume** |
| | | 1 L |

**Paraformaldehyde (PFA) solution (4% w/v)**

| Reagent | Final concentration | Volume/mass added |
|---|---|---|
| paraformaldehyde | 4% w/v | 40 g |
| phosphate buffer (0.2 M) | 0.1 M | 500 ml |
| ddH$_2$O | - | 500 ml |
| | | **Total volume** |
| | | 1 L |

**Sucrose solution (30% w/v)**

| Reagent | Final concentration | Volume/mass added |
|---|---|---|
| D (+)-sucrose | 30% w/v | 150 g |
| Phosphate buffer (0.2 M) | 0.1 M | 250 ml |
| ddH$_2$O | - | 250 ml |
| | | **Total volume** |
| | | 500 ml |

**Table 2.17.** DNA electrophoresis

2% Agarose solution

| Reagent | Final concentration | Volume/mass added |
|---|---|---|

| Reagent | Final concentration | Volume/mass added |
|---|---|---|
| Agarose | 2% w/v | 2 g |
| ddH$_2$O | - | 150 ml |
| | | **Total volume** |
| | | 150 ml |

**TAE buffer (50X)**

| Reagent | Final concentration | Volume/mass added |
|---|---|---|
| Tris base | 24.2 w/v | 242 g |
| Glacial acetic acid | 5.71% v/v | 57.1 ml |
| EDTA 0.5M pH 8.0 | 50 mM | 100 ml |
| ddH$_2$O | - | Up to 1 L |
| | | **Total volume** |
| | | 1 L |

**Table 2.18.** Bacterial cultures solutions

**Luria-Bertani (LB) broth**

| Reagent | Final concentration | Volume/mass added |
|---|---|---|
| LB broth | 2.5% w/v | 25 g |
| dH$_2$O | - | 1 L |
| | | **Total volume** |
| | | 1 L |

**LB-agar**

| Reagent | Final concentration | Volume/mass added |
|---|---|---|

| | | |
|---|---|---|
| LB broth | 2.5% w/v | 25 g |
| Agar | 1.5% w/v | 15 g |
| dH$_2$O | - | 1 L |
| | | **Total volume** |
| | | 1 L |

**Table 2.19.** DRG cultures solutions

**DRG culture medium**

| Reagent | Final concentration | Volume/mass added |
|---|---|---|
| DMEM/F12 | - | 14,550 μl |
| B27 (50x) | 1x | 300 μl |
| Pen/Strep | 100 U/ml | 150 μl |
| | | **Total volume** |
| | | 15 ml |

**DRG medium**

| Reagent | Final concentration | Volume/mass added |
|---|---|---|
| DMEM/F12 | - | 8,800 μl |
| B27 (50x) | 1x | 200 μl |
| FBS (100%) | 10% | 1,000 μl |
| | | **Total volume** |
| | | 10 ml |

**Replating medium**

| Reagent | Final concentration | Volume/mass added |
|---|---|---|
| DMEM/F12 | - | 8,900 µl |
| FBS (100%) | 10% | 1,000 µl |
| Pen/Strep (10000 U/ml) | 100 U/ml | 100 µl |
| | | **Total volume** |
| | | 10 ml |

**Table 2.20.** Immunofluorescence buffers/solutions

**Antigen retrieval citrate buffer (10 mM)**

| Reagent | Final concentration | Volume/mass added |
|---|---|---|
| Citric acid (anhydrous) | 10 mM | 1.92 g |
| Tween-20 | 0.05% | 500 µl |
| dH2O | - | 1,000 ml |
| | | **Total** |
| | | 1,000 ml |

**Blocking/permeabilization buffer for immunocytochemistry (ICC)**

| Reagent | Final concentration | Volume/mass added |
|---|---|---|
| TBS | 1x | 9.8 ml |
| Triton X-100 (10% v/v) | 0.1% v/v | 100 µl |
| Donkey serum (100% v/v) | 1% v/v | 100 µl |
| | | **Total volume** |
| | | 10 ml |

**Blocking/permeabilization buffer for immunohistochemistry (IHC)**

| Reagent | Final concentration | Volume/mass added |
| --- | --- | --- |
| TBS | 1x | 9,250 μl |
| Triton X-100 (10% v/v) | 0.25% v/v | 250 μl |
| Donkey serum (100% v/v) | 5% v/v | 500 μl |
| | | **Total volume** |
| | | 10 ml |

**Staining buffer for ICC (primary/secondary antibody)**

| Reagent | Final concentration | Volume/mass added |
| --- | --- | --- |
| TBS | 1x | 9,250 μl |
| Triton X-100 (10% v/v) | 0.1% v/v | 250 μl |
| Donkey serum (100% v/v) | 1% v/v | 500 μl |
| | | **Total volume** |
| | | 10 ml |

**Staining buffer for IHC (primary/secondary antibody)**

| Reagent | Final concentration | Volume/mass added |
| --- | --- | --- |
| TBS | 1x | 9,650 μl |
| Triton X-100 (10% v/v) | 0.25% v/v | 250 μl |
| Donkey serum (100% v/v) | 1% v/v | 100 μl |
| | | **Total volume** |
| | | 10 ml |

**Tris buffered saline (10X)**

| Reagent | Final concentration | Volume/mass added |
|---------|--------------------|--------------------|
| Tris-HCL | 1.32% w/v | 13.22 g |
| Tris | 0.19% w/v | 1.94 g |
| NaCl | 0.9% w/v | 9.0 g |
| dH2O | - | 1 L; adjust pH 7.4 |
| | | **Total volume** |
| | | 1 L |

**Table 2.21.** Whole cell protein extraction lysis buffer

| Reagent | Final concentration | Volume/mass added |
|---------|--------------------|--------------------|
| Tris buffer, pH 8.0 (1 M) | 20 mM | 1.0 ml |
| NaCl (5 M) | 137 mM | 1.37 ml |
| Np40 (10% v/v) | 1% v/v | 5.0 ml |
| EDTA (0.5 M) | 2 mM | 200 µl |
| | | **Total volume** |
| | | 50 ml |

## 2.1.8. Primers

**Table 2.22.** Primers used for PCAF KO genotyping

| Primer name | Size (bp) | Nucleotide sequence |
|-------------|-----------|---------------------|
| PCAF WT1 | 20 | TTCTAGATCTGCCGGTGTCC |
| PCAF WT2 | 20 | CTGCCAGACCCTGTTTACAC |

| | | |
|---|---|---|
| PCAF KO1 | 20 | TCGCCTTCTTGACGAGTTCT |

**Table 2.23.** Primers used for Sp1 and MAZ knock down and overexpression confirmation

| Primer name | Size (bp) | Nucleotide sequence |
|---|---|---|
| MAZ FW | 20 | TGAGGCAGCTTTTGCTACGA |
| MAZ RV | 21 | CCTCACCAGTACCTTTGTTGC |
| Sp1 FW | 20 | TGAGACAGCAGGTGGAGAAG |
| Sp1 RV | 20 | GGCTCTTCCCTCACTGTCTT |

**Table 2.24.** Probes used for Nanostring gene expression analysis

| Gene targeted | Accession number | Targeted gene area |
|---|---|---|
| G protein subunit gamma 4 (Gng4) | NM_010317.3 | 399-498 |
| Glutamate Ionotropic Receptor Delta Type Subunit 2 (Grid2) | NM_008167.2 | 661-760 |
| Lemur Tyrosine Kinase 3 (Lmtk3) | NM_001005511.2 | 1075-1174 |
| Nitric Oxide Synthase 1 (Nos1) | NM_008712.3 | 381-480 |
| Protocadherin Gamma Subfamily A, 8 (Pcdhga8) | NM_033591.3 | 2388-2487 |
| SH3 And Multiple Ankyrin Repeat Domains 2 (Shank2) | NM_001113373.2 | 1220-1319 |
| Tachykinin Receptor 1 (Tacr1) | NM_009313.5 | 1006-1105 |
| Xylosyltransferase 1 (Xylt1) | NM_175645.3 | 2507-2606 |
| Stum, Mechanosensory Transduction Mediator Homolog (6330403A02Rik) | NM_001081227.2 | 437-536 |
| B-Cell CLL/Lymphoma 9 Protein-like (Bcl9l) | NM_030256.2 | 2007-2106 |
| | NM_001083628.1 | 1351-1450 |

| Gene | Accession | Position |
|---|---|---|
| Growth Regulating Estrogen Receptor Binding 1- like (Greb1l) | NM_001002927.3 | 507-606 |
| Proenkephalin (Penk) | NM_021530.2 | 2891-2990 |
| Solute Carrier Family 4 Member 8 (Slc4a8) | NM_198109.4 | 885-984 |
| Slingshot Protein Phosphatase 1 (Ssh1) | XM_003085156.1 | 1445-1544 |
| Synaptic Ras GTPase Activating Protein 1 (Syngap1) | NM_008306.5 | 967-1066 |
| N-Deacetylase And N-Sulfotransferase 1 (Ndst1) | | |
| Phosphatidylinositol-4,5-Bisphosphate 3-Kinase Catalytic Subunit Delta (Pik3cd) | NM_008840.3 | 786-885 |
| Calcium Voltage-Gated Channel Subunit Alpha1 (Cacna1b) | NM_007579.3 | 4927-5026 |
| ADAM Metallopeptidase Domain 19 (Adam19) | NM_009616.4 | 1869-1968 |
| Antizyme Inhibitor 2 (Adc) | | |
| Laminin Subunit Alpha 1 (Lama1) | NM_172875.2 | 1065-1164 |
| Cartilage Acidic Protein 1 (Crtac1) | NM_008480.2 | 6878-6977 |
| Cytoplasmic FMR1 Interacting Protein 2 (Cyfip2) | NM_145123.5 | 1000-1099 |
| | NM_133769.3 | 2196-2295 |
| Pleckstrin Homology, MyTH4 And FERM Domain Containing H1 (Plekhh1) | NM_181073.3 | 4171-4270 |
| Mediator Complex Subunit 25 (Med25) | NM_029365.3 | 1315-1414 |
| Diacylglycerol Kinase Theta (Dgkq) | NM_199011.1 | 621-720 |
| | NM_001035241.2 | 295-394 |

| | | |
|---|---|---|
| Transient Receptor Potential Cation Channel Subfamily M Member 3 (Trpm3) | NM_024414.2 | 571-670 |
| Syntaxin 1B (Stx1b) | NM_001177758.1 | 467-566 |
| 6-Phosphofructo-2 Kinase/Fructose-2,6-Biphosphatase 3 (Pfkfb3) | NM_172257.3 | 705-804 |
| SID1 Transmembrane Family Member 2 (Sidt2) | NM_175514.2 | 1686-1785 |
| Family With Sequence Similarity 171 Member B (Fam171b) | NM_027882.3 | 5681-5780 |
| Capicua Transcriptional Repressor (Cic) | | |
| Myelin Transcription Factor 1 Like (Myt1l) | NM_001093775.1 | 1747-1846 |
| Ecotropic Viral Integration Site 5 Like (Evi5l) | NM_001039578.3 | 1286-1385 |
| Arrestin Beta 1 (Arrb1) | NM_177231.2 | 965-1064 |
| Collapsin Response Mediator Protein 1 (Crmp1) | NM_007765.4 | 2085-2184 |
| Protein Tyrosine Phosphatase Non-Receptor Type 1 (Ptpn1) | NM_011201.3 | 276-375 |
| Serpin Family A Member 3 (Serpina3m) | NM_009253.2 | 201-300 |
| Pleckstrin And Sec7 Domain Containing 2 (Psd2) | NM_028707.3 | 1545-1644 |
| DOT1 Like Histone Lysine Methyltransferase (Dot1l) | NM_199322.2 | 1162-1261 |
| Growth Associated Protein 43 (Gap43) | NM_008083.2 | 1123-1222 |
| Galanin | NM_010253.4 | 349-448 |
| Brain Derived Neurotrophic Factor (Bdnf) | NM_007540.4 | 948-1047 |

| | | |
|---|---|---|
| Activating Transcription Factor 3 (ATF3) | NM_007498.3 | 261-360 |
| H1 histone (h1f0) | NM_008197.3 | 699-798 |
| b actin (Actb) | NM_007393.4 | 909-1008 |
| exocyst 3 (Exoc3) | NM_177333.3 | 721-820 |
| Ribosomal Protein L13a (RPL13a) | NM_009438.5 | 348-447 |

## 2.2. Methods

### 2.2.1.  Animal subjects and experimental groups

All experiments were conducted in accordance with the European Communities Council Directive (EU and institutional guidelines) and approved by the local governing body (Regierungspräsidium Karlsruhe). Adult female and male CD1 mice (8-12 weeks old; wildtype JANVIER LABS) or PCAF knockout (PCAF KO) weighing between 25-35 g were used in the investigation of the epigenetics and transcriptomics of axonal regeneration. Also, adult female or male Fischer-344 rats (8-12 weeks old; wildtype JANVIER LABS) were used for the investigation of the contribution of mechanical stimulation in axonal regeneration. Animals were housed in groups of 4-5 mice and 5-6 rats per cage on a 12/12-hour light/dark cycle with access to water and food ad libitum. To ensure optimal conditions for housing and behavioural testing, the facility was controlled for temperature ($22°C \pm 1°C$) and humidity (45-65%) on a daily basis.

### 2.2.2. Surgical procedures

#### 2.2.2.1. Sciatic nerve axotomy (SNA)

Mice were anesthetized by delivery of nitrogen/oxygen (70%/30%) mixed with 3.5% isoflurane in a sealed box for the initial sedation. The sedated animals were fixed to a nose cone to keep a constant supply of 2.0% isoflurane. Eye lubricant was applied, and the fur of both hind limbs was shaved dorsally right next to the tail until the knee using a razor. Using blunt scissors, a 2 mm-long cut below and parallel to the femur at a mid-thigh level was made. Using blunt scissors, the biceps femoris was dissected until exposure of the sciatic nerve. The sciatic nerve was carefully separated from the connective tissue and was cut using sharp spring scissors by gently holding the distal part with #5 forceps. The muscle was put together above the sciatic nerve and the skin was clipped together. The incision was sterilized by applying iodine solution (Braunol). The animals were injected with buprenorphine (analgesics) and antibiotics (ampicillin) for two days post-injury. The animals were euthanized either by transcardial perfusion or by an overdose of anesthetics (ketamine [31.25 mg/kg], xylazine [1.58 mg/kg]).

## 2.2.2.2. Dorsal hemisection (DH) of T9 vertebral level

Animals were anesthetized as described before (Methods, 2.2.2.1 section) and were fixed in a prone position to a nose cone. Paws were fixed with tape on the surgical board, lubricant was applied on both eyes and the fur at the thoracic area was shaved. Using a scalpel No. 15, the skin from below the neck until the end of the thorax was cut, the connective tissue was slowly separated from the muscles and the skin was kept open using metal clips. The brown adipose tissue was carefully cut laterally and the T9 vertebral segment was detected using anatomical landmarks. The muscles above the vertebrae T8-T10 were dissected leaving exposed the spinal column. Carefully, the T9 vertebra was cut with spring scissors and removed exposing the spinal cord. Using a needle, a small incision of the dura was made without damaging the spinal cord. A droplet of 2% xylocaine was applied onto the spinal cord for 1 minute to numb the area before the hemisection. Then, the excess of xylocaine was removed and a 0.7 mm-deep dorsal hemisection was performed using a micro-knife. The micro-knife was passed two times through the cord to make sure that the tissue was cut thoroughly. The muscles above the cut spinal cord were sutured and the skin was clipped together. Pain killers and antibiotics were applied directly after the end of the surgery. For the control group (laminectomy), following the removal of the vertebra and the application of xylocaine without cutting the cord, the muscles were sutured, and the skin was clipped together. The recovered animals were returned to their cages and kept on a heating pad overnight.

## 2.2.2.3. AAV5 sciatic nerve injections

AAV5 virus stock solutions stored at -80°C were thawed and 2 μl of the undiluted solution was loaded into pulled micropipettes and stored at +4°C until injection. The animals were prepared for the injections as described in Methods section 2.2.2.1. The exposed sciatic nerve was placed on an 18G needle to keep it lifted. The micropipette was adjusted to the Picospritzer apparatus and it was confirmed that the viral solution was able to exit the micropipette using the stereoscope. Alternatively, the tip of the micropipette was cut until a droplet was formed after applying pressure. The micropipette was placed parallel to the longitudinal axis of the nerve and inserted 2 mm into the sciatic nerve. The micropipette was left in place for 1 minute and then 2 μl of virus solution was loaded slowly into the nerve, with a pace of 1 μl/5 minutes. The micropipette was kept in place for 2 minutes after the injection was completed and then gradually withdrawn to prevent any backflow from the pipette tip

insertion track. The control groups were injected with AAV5-hSYN1-eGFP-WPRE and the groups overexpressing Sp1 were injected with AAV5-hSYN1-eGFP-P2A-mSp1-WPRE3. The nerve was covered by the muscles and the incision was clipped together. The recovered animals were injected with analgesics and antibiotics and kept on a heating pad overnight after they were returned to their cages. The animals received a sciatic nerve crush (see following section) 3 weeks after the injections with the AAV5 viruses.

### 2.2.2.4. Sciatic nerve crush (SNC)

Similar to sciatic nerve axotomy (see 2.2.2.1. section) the animals were anesthetized with isoflurane and their sciatic nerves were exposed at a mid-thigh level. Using a No. 5 forceps, the sciatic nerve was crushed by holding the forceps tightly together for 20 seconds. The nerve tracts were severed leaving a transparent area at the crush site, but the sciatic nerve remained intact. The tip of the forceps was stained with black marker ink which also stained the crush site. This allowed for easy tracing of the crush site post-fixation. The nerve was placed back and covered by the muscles and the incision was clipped together. Immediately, the animals received an intraperitoneal (i.p.) injection of 200 μl cottonseed oil (vehicle) or 20 mg/Kg EML76. The recovered animals were injected with analgesics and antibiotics and kept on a heating pad overnight after they were returned to their cages. The animals were sacrificed and perfused transcardially (see following section) 48 hours after SNC.

### 2.2.2.5. Transcardial perfusion

Animals were transcardially perfused and fixed using 4% PFA solution. For the perfusion, the animals were anesthetized first with a mixture of ketamine/ xylazine until they lost their spinal reflexes, assessed by interdigital web pinching. The animals were placed on a perfusion board under the fume hood and secured in the supine position. Then, an incision was made with surgical scissors along the thoracic midline from just beneath the xiphoid process of the sternum to the clavicle. The sternum was lifted, and the diaphragm was cut, confirming that the liver was not injured. The thoracic musculature and the ribcage were cut on both sides up until the clavicles. The pericardial sac was grasped gently and was teared carefully. A 21G butterfly needle was inserted into the left ventricle. Immediately, the right atrium was cut and ice-cold 1X PBS was pumped into the left ventricle. 5 minutes after clearing the body's blood

with saline solution, the perfusion solution was switched to ice-cold 4% PFA solution. The animal was perfused for 5 additional minutes (~40ml fixative). Once perfused, the fur and the organs were removed, and the rest of the body was post-fixed in 4% PFA for 1 hour at RT. The post-fixed animals were either stored in 1X PBS until further use or the tissue of interest was immediately dissected.

## 2.2.3. Genotyping of CD1 PCAF knockout (PCAF KO) animals

### 2.2.3.1.  Embryo transfer of PCAF KO animals

CD1 PCAF$^{-/-}$ embryos were purchased from the ICRM INSERUM U896 (Provider: Céline Gongora, Archiving center: Institut de Transgenose, INTRAGENE, Orléans, France). Frozen embryos were transferred in a special straw in liquid nitrogen to the Interfacultary Biomedical Faculty (IBF), Heidelberg, Germany. Briefly, for the embryo thawing, the straws were removed from the liquid nitrogen and held horizontally in RT until the ice disappeared. The straw was dried out and cut open and the content was expelled into a petri dish. Under the microscope, the embryos were recovered in minimal volume of media and transferred into a drop of 40 µl of 1 M sucrose. For each straw to be thawed, 50 µl drops of M16 culture medium (Sigma, #M7292) in 4-well plates and let to equilibrate in a cell culture incubator for at least 15 minutes prior to use. 10 µl of M2 medium (Merck, M7167) were added on top of every embryo and then washed with 40 µl of M2 medium and then 40 µl of M16 medium. The embryos with normal appearance were selected and transferred into an equilibrated drop of M16 medium and mineral oil (Merck, M8410) was added to the wells to covers the drop of M16 medium. The embryos were returned to the cell culture incubator for 2 hours. Finally, embryos at 4-8-cells stage were transferred into the oviducts of 0.5-day pseudo-pregnant recipients.

Ear biopsies of pups were taken 4 weeks after birth. DNA was extracted and was used for genotyping as described below.

### 2.2.3.2.  DNA isolation

Ear biopsies were taken from 4-weeks old PCAF KO CD1 animals. DNA was processed using the DNAeasy Blood & Tissue kit (Qiagen). The tissue was digested overnight at 56ºC

by adding 20μl proteinase K (600 mAU/ml). Then, the DNA was precipitated following the manufacturer's instructions. Briefly, the lysate was mixed with 200 μl buffer AL, and vortexed thoroughly. 200μl 100% ethanol was added and the samples were vortexed. The mixture was pipetted into a DNeasy Mini Spin column placed in a 2 ml collection tube and centrifuged at 6,000 x g for 1 minute. The flowthrough and the collation tube were discarded, and the column was placed in a new collection tube. The column was filled with 500 μl buffer AW1 and centrifuged at 6,000 x g for 1 minute. The flowthrough and the collection tube were discarded. Then, the column was placed in a new collection tube, filled with 500 μl AW2 buffer and centrifuged at 20,000 x g for 3 minutes. The flowthrough and the collection tube were discarded. The DNeasy Mini spin column was placed in a 1.5 ml microcentrifuge tube and 200 μl AE buffer were added onto the DNeasy membrane and was incubated for 1 minute at RT. The column was centrifuged at 6,000 x g for 1 minute. The eluted DNA was collected, the concentration was measured by NanoDrop spectrometer and samples were stored at and stored at +4°C until further use.

### 2.2.3.3. PCR for CD1 PCAF KO genotyping

2 μl DNA (~20-100 ng) extracted from ear biopsies was used for PCR using the 5 Prime Master Mix (5 Prime GmbH). All primers were synthesized by Eurofins Genomics (Louisville, KY, USA). Lyophilized primers were reconstituted in DNase/RNase-free ddH$_2$O to a stock concentration of 100 μM and stored at -20°C. For PCR, all three primers (see Table 2.22) were used in one reaction. Table 2.25 shows the PCR reaction and Table 2.26 shows the PCR program used. PCR products were analysed using agarose gel electrophoresis. A 2.0% w/v agarose gel was prepared by dissolving 3.0 g agarose powder in 150 mL 1X TAE buffer and was boiled in a microwave. Agarose was cooled down, 4.5 μl PeqGreen was added and the agarose was poured into a gel chamber using the appropriate combs. After the gel was solidified each sample was mixed with the appropriate amount of 6X loading dye and loaded into the gel well (total of 20 μL per well). For size determination a 100 bp DNA ladder was used and loaded into the first well (3 μl). PCR products were separated by running the gel for 60 min at 110 V. Images of the gels were taken using a PeqLab UV detector (VWR).

The PCAF knockout animals were developed for the first time by the Y. Nakatani laboratory [159]. The exon coding the amino acids 1 to 88 was replaced by with a neomycin selection cassette. The knock-in of the neomycin is detected by the PCAF KO1 primer yielding

a PCR product of 600 bp. Therefore, the above PCR for a WT animal which does not harbour any neomycin, would yield a PCR product of 500 bp size, a heterozygous animal the PCR would yield two products of 500 and 600 bp and the for the knockout animals the PCR would yield a product of 600bp only, as depicted in Figure 2.1.

**Table 2.25.** Genotyping PCR reaction

| Reagent | Final concentration | Volume (1 reaction) |
| --- | --- | --- |
| DNA | ~20-100 ng | 2 μl |
| 5 Prime Master Mix (5X) | 1x | 4 μl |
| Primer WT1 (10 μM) | 0.25 μM | 0.5 μl |
| Primer WT2 | 0.40 μM | 0.8 μl |
| Primer KO1 | 0.15 μM | 0.3 μl |
| DNase/RNase-free ddH$_2$O | - | 12.4 μl |
| | | **Total** |
| | | 20 μl |

**Table 2.26.** Genotyping PCR program

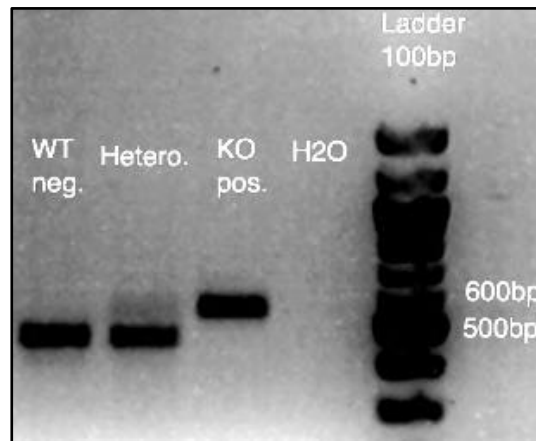| Step | Time | Temperature | |
| --- | --- | --- | --- |
| 1.  Initial denaturation | 2 minutes | 95°C | |
| 2.  Denaturation | 15 seconds | 95°C | |
| 3.  Annealing | 15 seconds | 60°C | 35 cycles |
| 4.  Extension | 30 seconds | 72°C | |
| 5.  Final extension | 5 minutes | 72°C | |

**Figure 2.1. Representative gel image of PCAF KO genotyping.** DNA sample form WT, Heterozygous (Hetero.) and PCAF KO animals was used for the PCAF KO PCR reaction. According to the 100 bp DNA ladder the reactions yields one 500 bp for the WT animals, two bands of 500 bp and 600 bp for the Heterozygous animals and a single 600 bp-band for the PCAF KO animals.

## 2.2.4. RNA-sequencing and Transcription Factor Binding Site (TFBS) analysis of PCAF-dependent genes of DRG

L4-L6 DRG from two adult CD1 animals were dissected and pooled for 3 biological replicates in ice-cold 1X PBS solution 24 hours after sciatic nerve axotomy or sham. RNA was extracted using the RNeasy Mini QIAcube Kit. RNA extraction was done by colleagues in the laboratory of Dr. Simone di Giovanni.

The RNA-sequencing was performed by the Quantitative Biology Center (QBiC) in the University of Tübingen, Tübingen, Germany. Bioinformatic analysis was performed on RNAseq data using Fastqc for quality control followed by Tophat2 for mapping and HTSeq for read counting. Differential expression analysis was performed using a linear model in DESeq2. Webgestalt, Genomatix and TRANSFAC were used for transcription factor binding site analysis of 1,237 PCAF differentially expressed RAGs and they revealed putative transcription factors binding sites that were enriched on the promoters of these genes.

## 2.2.5. DRG cell cultures

Adult CD1 mice were sacrificed by cervical dislocation. Skin and organs were discarded keeping the spinal column and limbs. DRG were dissected ventrally under a stereoscope. The

spinal cord was exposed by cutting the spinal vertebrae parallel to the spinal column axis on both sides. Peripheral and central nerves were cut as close to the DRG as possible and the DRG were kept in 1.5ml EP tubes with ice-cold HBSS.

DRG were centrifuged at 500 x g for 2 minutes and HBSS was replaced by dispase (5 mg/ml in HBSS) and collagenase (2.5 mg/ml in HBSS) solution. DRG were digested for 30 minutes at 37°C by gently shaking every 10 minutes. DRG were centrifuged at 500 x g for 2 minutes and the digestion solution was replaced by 1 ml pre-warmed DRG solution. DRG were centrifuged at 500 x g for 2 minutes. Supernatant was discarded and DRG were resuspended in 1 ml DRG solution. Using a fire-polished glass pipette, DRG were triturated to a single-cell solution. Singe-cell DRG were counted with a Neubauer hemocytometry chamber and plated on poly-L-ornithin (PLO) (100 μg/ml)- and laminin (2 μg/ml)-coated coverslips (15 mm) in DRG culture solution in a density of 3,500-4,000 cells/ coverslip. DRG were incubated for 18 hours at 37°C/ 5% $CO_2$ and then fixed with ice-cold 4% PFA for 20 minutes, rinsed once with 1X TBS and kept in 1X TBS at +4°C.

For replating, 3 days post-electroporation the growth medium was discarded the DRG were washed once with pre-warmed 1X HBSS and incubated with 1X Trypsin-EDTA solution at 37°C for 2 minutes. The digestion was stopped by adding pre-warmed 1 ml replating medium (see Materials, Table 2.19) on each coverslip and by pipetting up and down cells were detached from the coverslips. DRGs were centrifuged at 800 rpm for 5 minutes and plated on (PLO) (100 μg/ml)- and laminin (2 μg/ml)-coated coverslips.

For the treatment with SPV106, the compound was diluted in 100% DMSO. One-hour post-plating, DRG were treated with 5, 10, 25 μM SPV106 or DMSO diluted in the DRG culture medium. DMSO never exceeded 1% v/v final concentration in medium. For the treatment with EML76, the crystals were reconstituted in 100% DMSO. One hour post-plating, DRG were treated with 30, 50, 70 μM EML76 or DMSO. DMSO never exceeded 1% v/v final concentration in the medium.

## 2.2.6. DRG electroporation

Single-cell suspended DRG solution was centrifuged at 800 rpm for 5 minutes. The pellet was rinsed with 1ml pre-warmed 1X HBSS and centrifuged at 800 rpm for 5 minutes. Supernatant was discarded and the DRG pellet was mixed with the electroporation solution containing either the siRNAs or the overexpression vectors.

## 2.2.6.1. siRNA electroporation

The P3 Primary Cell 4D-Nucleofector™ X Kit S (LONZA) protocol was used for the electroporation using the Nucleocuvette™ Strip. Each siRNA (see Materials, section 2.1.6) was received lyophilized and reconstituted into 330 μl RNAse-free water and stored in -20ºC. Each siRNA's concentration was 10 μM. For the electroporation, 0.8 μg of pmaxGFP™ vector and 1 μl of 10 μM siRNA were mixed with 16.4 μl P3 Primary Cell Nucleofector™ Solution and 3.6 μl Supplement 1. Using the 4D-Nucleofector™ X Unit cells were electroporated with the program No. DR114. After electroporation, the cells were recovered for 10 minutes under the hood, then mixed with prewarmed DRG medium and plated on PLO- and laminin-coated coverslips.

## 2.2.6.2. Overexpression vectors electroporation

Similarly to the siRNA electroporation, the DRGs were electroporated with the overexpressing vectors using the P3 Primary Cell 4D-Nucleofector™ X Kit S (LONZA) protocol and the Nucleocuvette™ Strip. Each construct (see Materials, section 2.1.5, table 2.13) was received lyophilized and was prepared as described below. For the electroporation, 0.8 μg of pmaxGFP™ vector (control group), 1.6 μg pEGFP-Sp1 vector or 1.75 μg pcDNA3.1+MAZ+P2A-eGFP (Figure 2.2) were mixed with 16.4 μl P3 Primary Cell Nucleofector™ Solution and 3.6 μl Supplement 1. The molecular ratio was kept the same for each electroporation: pEGFP-Sp1 was 1.98 times bigger than pmaxGFP and pcCDNA3.1+MAZ+P2A-eGFP was 2.19 times bigger than pmaxGFP, thus 1.6 μg (1.98 x 0.8 μg) of pEGFP-Sp1 and 1.76 μg (2.19 x 0.8 μg) of pcCDNA3.1+MAZ+P2A-eGFP were used. The electroporation of DRG was performed with the 4D-Nucleofector™ X Unit with the program No. DR114. After electroporation, the cells were recovered for 10 minutes under the hood, then mixed with prewarmed DRG medium and plated on PLO- and laminin-coated coverslips.
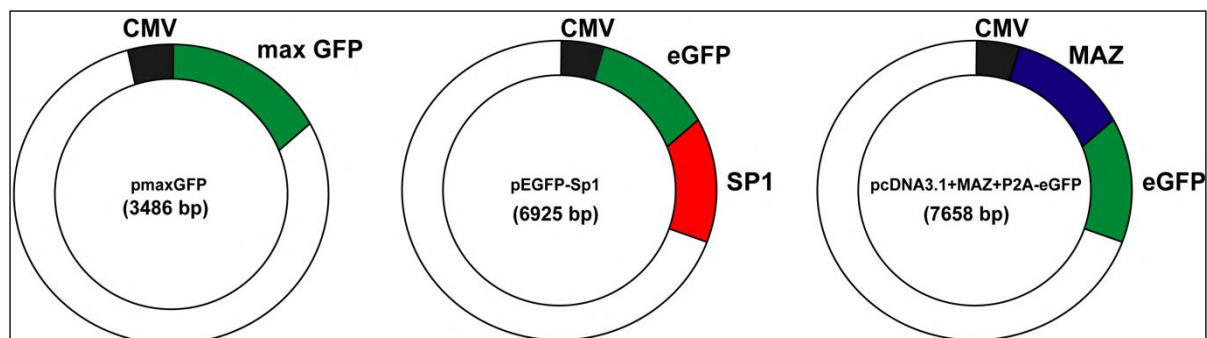
**Figure 2.2. Overexpression vectors used for DRG electroporation.** DRG were electroporated either with pmaxGFP (3,486 bp), pEGFP-Sp1(6925 bp) or pcDNA3.1+MAZ+P2A-eGFP (7,658 bp).

## 2.2.7.   Bacterial constructs

pEGFP-Sp1 was kindly provided by the laboratory of Prof. Simone Di Giovanni, ICL, London, UK and the pcDNA3.1+MAZ+P2A-eGFP was purchased by GenScript, NJ, USA. pEGFP-Sp1 vector's backbone is pEGFP-C (Takara Bio Inc., Shiga, Japan [former Clontech]) with insert gene *Sp1* by H. sapiens (human) fused at its N-terminal with eGFP cloned between XhoI (5' cloning site) and KpnI (3' cloning site) and has a kanamycin resistance gene. pcDNA3.1+MAZ+P2A-eGFP vector's backbone is pcDNA3.1+P2A-eGFP and mouse *MAZ* gene was cloned between HindIII (5' cloning site) and XbaI (3' cloning site) and has an ampicillin resistance gene.

### 2.2.7.1. Bacterial transformation and minipreps

10 μg of pEGFP-Sp1 or pcDNA3.1+MAZ+P2A-eGFP were received lyophilized. After overnight incubation in DNAse/RNAse-free water at 37°C, 2 μl of each vector was added to 50 μl OneShot® E. coli cells. Cells were incubated for 30 minutes on ice and then for exactly 30 seconds at 42°C. Then, the cells were placed on ice and 250 μl of pre-warmed S.O.C. medium was added. The cells were shaken at 37°C for 1 hour at 225 rpm in a shaking thermo-mixer. 100 μl of each reaction was spread on LB agar. Cells transformed with pEGFP-Sp1 were plated on kanamycin-containing LB-agar plates, while cells transformed with pcDNA3.1+MAZ+ P2A-eGFP were plated on ampicillin-containing LB-agar plates and incubated at 37°C overnight. The following day, random colonies were picked and cultured in 5 ml LB medium containing the respective antibiotic at 37°C in a shaking bacterial incubator overnight. DNA from each culture was extracted using the QIAprep Spin Miniprep kit using

the manufacturer's instructions. Successfully transformed colonies were tested by restriction enzyme digestion as shown in Figure 2.3. pEGFP-Sp1 was digested with XhoI and KpnI yielding two bands 4,733 bp and 2,200 bp and pcDNA3.1+MAZ+P2A-eGFP was digested with HindIII and XbaI yielding two bands 6,000 bp and 1,500 bp. The digestion products were run in an 1.5% agarose gel for 1 hour at 100 V. A 1-Kb DNA ladder was used.
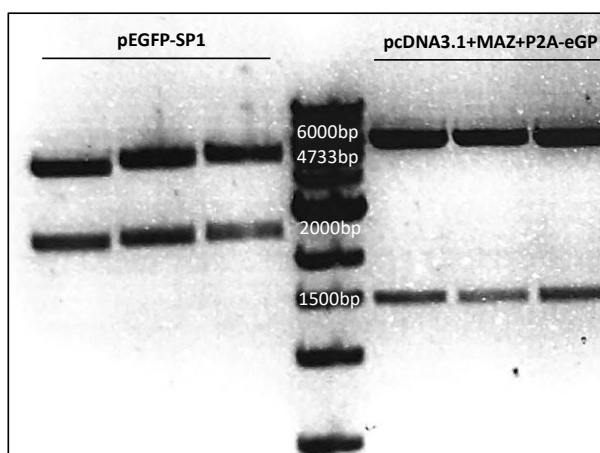


**Figure 2.3. Restriction enzyme digestion of Sp1 and MAZ overexpressing vectors.** pEGFP-Sp1 was digested with XhoI and KpnI yielding two bands 4,733 bp and 2,200 bp and pcDNA3.1+MAZ+P2A-eGFP was digested with HindIII and XbaI yielding two bands 6,000bp and 1,500bp

## 2.2.7.2. Constructs preparation (Maxi-prep)

One positive colony was selected from the mini-prep for a maxi-prep culture. For this, the EndoFree plasmid maxi kit (Qiagen) was used. 1 ml from the mini-prep culture was used to inoculate 250 ml of LB medium containing the respective antibiotic for each plasmid. The DNA extraction was performed according to the manufacturer's instructions. After overnight incubation, the cultures were centrifuged in 50 ml falcon tubes at 6,000 x g for 15 minutes at +4°C. The pellets were resuspended in 10 ml P2 buffer and incubated at RT for 5 minutes. 10 ml of P3 buffer was added and the samples were mixed. The lysate was added to the QIAfilter Cartridge and incubated for 10 minutes until the lysate exited the column, removing the cell debris. 2.5 ml ER buffer was added to the lysate and incubated for 30 minutes on ice. The lysate was poured into an equilibrated Qiagen-tip, with 10 ml QBT buffer, and the lysate exited by gravity. The tip was washed 2 times with 30 ml QC buffer and the DNA was eluted 15 ml QN buffer into a 50 ml endotoxin-free tube. The DNA was precipitated by adding 10.5 ml

isopropanol and centrifuging at 15,000 x g for 30 minutes at +4°C. The supernatant was discarded, and the DNA pellet was washed with 5 ml of endotoxin-free 70% ethanol and centrifuged at 15,000 x g for 10 minutes. The supernatant was discarded and then pellet was air-dried or 10 minutes. The DNA pellet was resuspended with 2 ml endotoxin-free ddH$_2$O. The DNA was stored at -20°C.

## 2.2.8. PCR to confirm TF knock-down or overexpression in DRG

In order to confirm that Sp1 and MAZ were either knocked down 72 hours post-electroporation with the respective siRNAs or overexpressed 72 hours post-electroporation with the respective bacterial vector, RNA was extracted with phenol-chloroform (see Methods, section 2.2.9) and cDNA was prepared using the SuperScript™ III reverse transcriptase kit and following the manufacturer's instructions. Briefly for each reaction, 9 µl of 500 ng or 1 µg RNA was mixed with 1 µl random primers (50 ng/µl), 1 µl oligo(dT)$_{20}$ (50 µM) and 1 µl dNTP mix (10 mM each) in a 1.5 ml tube and heated at 65°C for 5 minutes. Then, 4 µl 5X 1$^{st}$ strand buffer, 2 µl 0.1M DTT and 1 µl RNAseOUT™ (40 units/ µl) were added to the mix and heated to +25°C for 2 minutes, then to 42°C for 2 minutes and finally 1 µl SuperScript reverse transcriptase II was added. The reaction was incubated at +25°C for 10 minutes followed by incubation at +42°C for 50 minutes. Reverse transcriptase was inactivated by incubation at +70°C for 15 minutes. cDNA samples were stored diluted five times and stored at -20°C. 2 µl cDNA (10 ng – 20 ng) were used for end-point PCR to determine whether the TFs were knocked-down or overexpressed. Table 2.23 shows the primers used. Table 2.27 shows the reactions prepared for the PCRs and Table 2.28 shows the PCR program used.

**Table 2.27.** PCR reaction for confirmation of TF knockdown or overexpression

| Reagent | Final concentration | Volume (1 reaction) |
| --- | --- | --- |
| DNA | ~10-20 ng | 2 µl |
| 5 Prime Master Mix (5x) | 1x | 4 µl |
| Primer FW (10 µM) | 0.25 µM | 0.5 µl |
| Primer RV (10 µM) | 0.25 µM | 0.5 µl |

| DNase/RNase-free ddH$_2$O | - | 12.4 µl |
|---|---|---|
| | | **Total** |
| | | 20 µl |

**Table 2.28.** PCR program for confirmation of TF knockdown or overexpression

| Step | Time | Temperature | |
|---|---|---|---|
| 1. Initial denaturation | 2 minutes | 95$^o$C | |
| 2. Denaturation | 30 seconds | 95$^o$C | |
| 3. Annealing | 30 seconds | 60$^o$C | 35 cycles |
| 4. Extension | 30 seconds | 72$^o$C | |
| 5. Final extension | 1 minute | 72$^o$C | |

## 2.2.9. RNA extraction and gene expression analysis by the Nanostring Technology

For RNA extraction from DRG tissue, DRG were dissected and kept in ice-cold 1X PBS. DRG were centrifuged at 500 x g for 2 minutes and the supernatant was replaced by 1ml of phenol (TriFast, VWR) and homogenized with a homogenization pestle. Lysate was incubated for 5 minutes at RT and then 200 µl chloroform was added and samples were vortexed vigorously for 15 seconds. Samples were incubated at RT for 3 minutes and centrifuged at 12,000 x g, +4$^o$C for 15 minutes. After centrifugation, three phases were formed, a lower phenol/ chloroform phase which contains the DNA, an upper aqueous phase which contains the RNA and a middle phase containing the proteins. Carefully, the upper aqueous phase was transferred to a clean pre-chilled 1.5 ml tube. 10 µg glycogen was added to each sample together with 500 µl of isopropanol, samples were vortexed and incubated for 10 minutes at RT. Then, they were centrifuged at 12,000 x g, +4$^o$C for 10 minutes. The supernatant was discarded, and the pellet was resuspended in 1ml ice-cold 75% ethanol by vortexing and then

centrifuged at 7,500 x g, +4°C for 5 minutes. Supernatant was discarded and the last step was repeated. The pellet was air-dried for 10 minutes and resuspended in 18 μl RNase-free water.

To rule out any contamination of the RNA samples by genomic DNA, samples were treated with DNase (DNA-free™ kit) using the manufacturer's instructions. Briefly, 2 μl 10X DNAse I buffer and 1 μl rDNase I (2 Units) were added to the RNA samples and mixed gently. Samples were incubated at +37°C for 25 minutes. To block the DNAse I enzymatic activity, 2 μl DNase Inactivation Reagent was added and incubated for 2 minutes by mixing occasionally. Samples were centrifuged at 10,000 x g, +4°C for 1.5 minutes and supernatant was transferred to a clean pre-chilled RNase-free 1.5 ml tube. RNA concentration was measured by spectrophotometry by NanoDrop. Samples were stored at -80°C until use. For RNA extraction from DRG cultures 1 ml phenol was used per group to harvest cells from glass coverslips and then the same protocol was followed.

RNA samples were transferred to the Nanostring Ncounter facility of the University of Heidelberg, Heidelberg, Germany for further analysis of the gene expression levels of the different samples. RNA concentration was confirmed using fluorescence (Quibit Fluorometer) and RNA integrity was evaluated by calculating the RNA Integration Number (RIN) using an Agilent Bioanalyzer. Electropherograms were created based on the 18S and 28S rRNA quality. RIN values range from 1-10, with 1 representing totally degraded RNA and 10 being the highest quality of RNA. For downstream analysis of RNA, a cut-off of RIN=7.0 was set. Nanostring nCounter Technology does not require the production of cDNA or any enzymatic amplification step. Briefly, the RNA is hybridized with a color-coded reporter probe specific for the gene of interest and with another probe called the capture probe. The reporter probe-RNA-capture probe complex is immobilized on an imaging surface and then scanned by a fluorescence microscope. The labelled bar-codes for each gene are automatically counted and raw counts for each gene of interest are created. A list of all the targeted genes is shown in Table 2.24. The raw data from the nCounter facility was analyzed by the nSolver software in order to normalize the raw counts and to create the ratios and the heatmaps between the control groups and the groups of interest. For each analysis, .RCC files were loaded into nSolver and the samples of interest were selected and added to a New Study → New Experiment. Annotations were given to the different groups. Using the geometric mean of the negative controls the background was subtracted from each sample. Each group was normalized to the positive control's geometric mean and a normalization factor was calculated by the geometric mean of reference genes (beta-actin, exocyst 3, H1 histone and RPL13a). The ratios were built comparing each group to each respective control group. For the heatmaps, the fold changes

were calculated by the Euclidean distance which calculates the distance between two samples as the square root of the sum of squared differences in their log count values.

### 2.2.10.       Immunocytochemistry

Coverslips from DRG cultures were transferred to a 24-well plate and washed once with 0.1 M Tris-buffered saline. DRG were permeabilized and blocked with 1X TBS/ 0.1% TritonX-100/ 1% donkey serum for 30 minutes at RT. Then, DRG were incubated with primary antibodies diluted in the same permeabilization/ blocking solution overnight at +4°C. After primary antibody incubation, DRG were rinsed 3 times with 1X TBS for 5 minutes and then incubated with secondary antibodies for 1 hour at RT in the dark. After secondary antibody incubation, DRG were rinsed 3 times with 1X TBS for 5 minutes and then incubated for 10 minutes at RT with DAPI (1:2,000) diluted in 1X TBS. DRG were rinsed 3 times in 1X TBS for 5 minutes and then mounted on glass slides with Fluoromount-G.

Microphotographs of the stained DRG were taken by a confocal microscope using the Olympus FluoView software and analysed by ImageJ or HCAvision.

### 2.2.11.       Cryo-sectioning

Dissected tissue after fixation was kept in 30% sucrose solution for at least 24 hours until saturated. The tissue was dried out and embedded in Tissue Tek® O.C.T™ compound and frozen at -50°C. Samples were cut with thickness an angle of 10° with object temperature -21°C and knife temperature -18°C. The thickness of the slices of each tissue was as follows: DRG slices 18 μm thick and longitudinal sciatic nerve slices 14 μm thick.

### 2.2.12.       Immunohistochemistry

Immunohistochemical labelling was performed on positively charged glass slides with serial sections of the lumbar (L4-L6) DRG and sagittal sections of thoracic spinal cord around the T9 hemisection. When antigen retrieval was needed, slides were submerged in citrate buffer at 96-100°C for 20 minutes. After incubation, slides were cooled down at RT for 30 minutes. Slides were rinsed once with 1X TBS, slightly dried and then encircled with a liquid blocker. Sections were blocked and permeabilized by incubating in 1X TBS/ 0.25 % TritonX-100/ 5 %

donkey serum for 1 hour at RT. All primary antibodies were diluted in 1X TBS/ 0.25% TritonX-100/ 1% donkey serum and the samples were incubated overnight in a humid box at +4°C.

After primary antibody incubation, sections were washed 3 times in 1X TBS at RT shaking for 10 minutes each. Secondary antibodies and DAPI were diluted in 1X TBS/ 1% donkey serum and the sections were incubated for 2.5 hours at RT in the dark. Then, sections were washed 3 times in 1X TBS for 10 minutes, briefly dried and coverslipped with Fluoromount-G.

## 2.2.13.    Neurite length analysis of DRG cultures

Cultured DRG photomicrographs were taken in 10x magnification. Neurites were traced by βIII-tubulin staining. Raw images were saved as .tiff files and neurite length analysis was performed manually by the NeuronJ plugin of Fiji (ImageJ). The average neurite length was calculated by dividing the total length of neurites calculated by all cells counted for each group. For the compound screening using the neurite length in vitro assay, the HCAvision software was used according to the manufacturer's instructions.

## 2.2.14.    Whole cell protein extraction and quantification

L4-L6 DRG were collected in ice-cold 1X PBS + 1X protease inhibitors. DRG were centrifuged at 500 x g for 2 minutes and supernatant was replaced by 100 μl whole cell extraction lysis buffer (Table 2.21). Using a mini-homogenization pestle, DRG were homogenized manually and kept on ice for 30 minutes, while shaking gently every 10 minutes. Lysate was centrifuged at 16,000 x g for 10 minutes at +4°C. The supernatant containing the proteome was collected in a clean pre-chilled 1.5ml tube and kept on ice until protein quantification or stored at -80°C.

For protein quantification, the Pierce™ BCA Protein Assay Kit was used according to the manufacturer's protocol using known concentrations of BSA for the standard curve. Briefly, for the creation of the standard curve 2,000 μg/ml, 1,000 μg/ml, 500 μg/ml, 250 μg/ml, 125 μg/ml, 62.5 μg/ml of BSA and blank were used. Each sample was diluted 10 times in final volume of 20 μl distilled $H_2O$ and then mixed with 200 μl of BCA Reagent A: BCA Reagent B mix (50:1) in clear flat round-bottom 96-well plates. BSA and unknown samples were

incubated for 30 minutes at +37°C and then the absorbance at 582 nm was detected by a spectrophotometer. Standard curve was plotted in Excel as OD versus Concentration (mg/ml) using the known concentrations of BSA and the protein concentration were calculated based on the standard curve.

### 2.2.15.  Nuclear and cytoplasmic fractionation of DRG

DRG were dissected in 1X PBS + 1X protease inhibitors. For the nuclear and cytoplasmic fractionation, the NE-PER Nuclear and Cytoplasmic extraction kit (ThermoScientific) was used. DRG were spun down at 500 x g for 5 minutes. The supernatant was discarded and by using a mini homogenization pestle the tissue was homogenized by using 200 µl CERI solution + 1X protease inhibitors. Samples were vortexed vigorously for 15 seconds and incubated on ice for 10 minutes. Then, 11 µl of CERII was added and samples were vortexed for 5 seconds and incubated for 1 minute. Samples were centrifuged for 5 minutes at 16,000 x g, +4°C. The supernatant containing the cytoplasmic fraction was collected in a pre-chilled 1.5 ml tube. The pellet was resuspended into 50 µl NER + 1X protease inhibitors and vortexed for 15 seconds. The lysate was incubated for 40 minutes on ice and was vortexed for 15 seconds every 10 minutes. Samples were centrifuged at 16,000 x g for 10 minutes. The supernatant containing the nuclear fraction was transferred to a pre-chilled 1.5 ml tube. Both cytoplasmic and nuclear fractions were stored at -80°C.

### 2.2.16.  Co-Immunoprecipitation of PCAF-complexes and mass spectrometry

The proteome of L4-L6 DRG was extracted by pooling three CD1 animals per group. DRG were kept in ice-cold 1X PBS + 1X protease inhibitors. The proteome was extracted by following the whole cell protein extraction protocol (see Methods, 2.2.14 section). 10% of each sample was stored at -80°C until use as input. For the immunoprecipitation, the Dynabeads™ Protein G Immunoprecipitation Kit was used. 50 µl (1.5 mg) of magnetic bead slurry was transferred to a clean 1.5 ml tube and using a magnetic rack the supernatant was discarded and the beads were washed once with Ab Binding and Washing buffer. To avoid unspecific binding of protein on the beads surface, beads were incubated for 1 hour at RT under constant rotation with 10 % BSA in 1X TBS/ 0.1 % TritoX-100. After incubation, supernatant was discarded

using the magnetic rack and the beads were incubated for 1 hour at RT with 10 μg PCAF antibody (CST) diluted into 500 μl Ab Binding and Washing buffer under constant rotation. Using the magnetic rack, the supernatant was discarded together with the excess of antibodies that were not bound to the beads and the complex was rinsed gently three times with 500 μl Ab Binding and Washing buffer. The antibody-beads complex was added to 150 μg of the proteome in a final volume of 500 μl of 1X PBS + 1X protease inhibitors. As a negative control normal rabbit IgG was used the same way as the PCAF antibody and loaded on 150 μg of the lysate as well. Samples were incubated overnight at +4°C under constant rotation. Then, using the magnetic rack the antigen-antibody-beads complex was rinsed three times with 500 μl Washing buffer by gently pipetting up and down. To elute the adsorbed protein complex from the antibodies and the magnetic beads the antigen-antibody-bead complex was resuspended in 20 μl Elution buffer, 7 μl 4X NuPage Loading buffer and 3 μl 10X Reducing Agent and boiled for 5 minutes at +95oC and then kept at +4°C. Samples were sent on ice to the mass spectrometry facility at the Ruhr Universität Bochum (Working group of Prof. Dr. Katrin Marcus, Medical Proteome Center, Ruhr University Bochum).

## 2.2.17. Nerves mechanical loading

### 2.2.17.1. Nerve explants mechanical loading

Upon decapitation, the skin and viscera were removed sparing the spinal column and the hind limbs. The animal was fixed in the supine position and the lumbosacral plexus nerves was exposed ventrally removing the surrounding muscles and connective tissue. The sciatic nerves were identified, and the ventral half of the spinal column was removed carefully using Rongeurs forceps without damaging the spinal cord or the DRG. For the sciatic nerve bifurcating to L4-L5 DRG explant, the nerve was cut 2.5 cm distal to the DRG which were also dissected from their CNS side. For the central nerves connected to either the L4 or the L5 DRG, the nerves were cut 2.5 cm distal to their respective DRG which were also dissected from their PNS side. The explants were kept in ice-cold HBSS. Each DRG-nerve explant was mounted on two poly-ether-ether-ketone (PEEK, 11 mm x 4 mm x 4 mm) bars fixed on the bioreactor by screws. The two opposing PEEK bars were 1 cm apart and the explants were glued on each bar using acrylic adhesive (CYANO-Fast) normally used for extra-oral work. The explant was kept in a metal container (7.5 cm x 2.5 cm x 2.0 cm) filled with a solution of

1X F12/ DMEM, 10% fetal bovine serum, 1X B27 serum-free supplement, 1% Pen/ strep and was placed into the mechanical stretch incubator (Ruskinn, Invivo2 400) for 3 hours at 37ºC under 5% $CO_2$. The explants for the static control group were kept in the same solution and incubation conditions, glued on a Petri dish 60mm $\varnothing$ without any mechanical tension applied to them.

For the mechanical stretch of the nerve explants a stretch bioreactor was built in-house. One metal plate (a) (8 cm x 4 cm x 2.5 cm) was fixed on a metal rail (16 cm). Another metal plate (b), with the same dimensions to (a), was also built on the same rail, free to move back and forth in order to change the distance from plate (a) but able to be fixed on the rail by a screw to keep the distance from plate (a) constant when needed. Each plate had small square openings (4 mm x 4 mm x 1 cm) next to each other to fit the PEEK bars which could be fixed on the plates by small screws. The free part of the PEEK bars from the two metal plates were facing towards each other. The bars had a distance of 1 cm apart by adjusting plate (b). After nerve explants were glued on the fixed PEEK bars, the metal rail and Plate (b) were fixed on an oscillator able to move the plate back and forth at a specific amplitude and frequency when not fixed on the metal rail. Half of the oscillator was built inside the incubator chamber through the incubator's plexiglass door, controlling the movement of plate (b) and the other half was sitting outside connected to an electronic controller (Steimeyer, Germany). The controller was also connected to a laptop (HP, Windows 7 Pro). The GalilTools program (Galil Motion Control Inc., USA) was used to set the parameters of the cyclic movement of the oscillator/bioreactor. The nerves were stretched with either 10% or 20% mechanical stretch. The part between the two glued spots was 1 cm, thus 10% stretch was achieved with 1 mm dislocation towards the long axis of the nerve and respectively 20% stretch with 2 mm dislocation.

The program for the GalilTools used for the mechanical loading of nerve explants is shown below:

```
#OSZI01
WT2000
NO_____REFERENCE
MOVE_____
NO
SHX
```

```
DP0;NO              SET POSITION COUNTER TO ZERO
#INDEX
NO                  MOVE TO FIND HARD END
JG20000
BGX
MG"SUCHE HARDANSCHLAG"
#LOOP1;NO           CHECK BUILDUP OF POSITION ERROR
JP#LOOP1,_TEX<10000;NO    IF NO MORE MOOVEMENT EXIT LOOP1
NO
STX
AMX
NO               FIND INDEX
JG-10000
MG"STARTE INDEX SUCHLAUF"
FIX
BGX
AMX
MG"INDEX GEFUNDEN, NULLPUNKT GESETZT"
WT20000;NO          WAIT 20 SEC
NO
NO_____SINUSOIDIAL                              MOVE
PROGRAMM_____
NO
#SINUS
NO                  SETTING VECTOR MOVE PROPERTIES
VM XN;NO            N IS THE VIRTUAL AXIS
VA 68000000
VD 68000000
VS 31416;NO         VS=2*PI*RADIUS*f


NO                  DOING 10 CYCLES (3600 DEG)
#KREIS
CR 10000,90,3600;NO     RADIUS, START DEG., STOP DEG.
VE
```

BGS

AM

JP#KREIS;NO        INFINITE LOOP

EN

NO_____PROGRAMM

END_____

The program above is controlling the moment of the oscillator with an amplitude radius of 1 mm and frequency 0.5 Hz. By modifying the VS and the radius we could achieve different amplitudes and frequencies.

## 2.2.17.2. DRG cultures after mechanical loading of nerve explants

Following 3 hours of oscillatory stretch of the DRG-nerves explants, the DRG were dissected and kept in ice-cold HBSS. DRG were spun down at 300 x g for 1 minute and HBSS was replaced by 500 μl of a digestion mixture of 2.5 mg/ml collagenase and 5 mg/ml neutral protease (dispase) in HBSS and incubated at 37$^o$C for 35 minutes by gently shaking every 10 minutes. Then, the DRG were centrifuged at 300 x g for 2 minutes, the digestion solution was discarded and the DRG were washed once with prewarmed DRG medium consisting of DMEM/F12, 10% FBS and 1X B27 serum-free supplement solution. DRG were centrifuged at 300 x g for 2 minutes, the medium was discarded and fresh DRG medium was added to mechanically triturate them by a fire-polished glass pipette to a single cell solution. DRG were centrifuged at 300 x g for 5 minutes, supernatant was discarded, and they were resuspended into DRG medium. 100 μl of the single-cell resuspension was loaded onto 15 mm-diameter glass coverslips coated with 100 μg/ml PLO and 2 μg/ml laminin in a density of 4000 cells/ coverslip. DRGs were incubated at 37$^o$C 5% $CO_2$ for 1 hour and then each well was filled up with DRG culture medium consisting of DMEM/ F12, 1X B27 supplement and 1% Pen/ Strep. Cells were incubated for 17 more hours and then fixed for 20 minutes with ice-cold 4% PFA/ 0.1 M phosphate buffer. PFA solution was discarded, cells were rinsed with 1X TBS once and kept at +4$^o$C in 1X TBS.

## 2.2.17.3. Nerve and DRG cryo-sectioning and Hematoxylin-Eosin (H&E) staining

After mechanical stretch, the 1cm-long nerve part between the two glued spots was dissected and fixed into 4% PFA for two hours, washed once with 1X TBS and then immersed into 30% sucrose/ 0.1 M phosphate buffer and stored at +4°C until sectioning. Nerves were immersed into Tissue-Tek O.C.T compound and cut in 10 μm-thick slices parallel to their long axis using a cryostat (Zeiss, knife -20°C, object -18°C) and mounted on positively charged SuperFrost Plus glass slides. Nerves were subjected to H&E staining to check the quality of the tissue after stretch. Slides were immersed into 100% propanol for 5 minutes, then into 96% propanol for 5 minutes, 70% propanol for 5 minutes, 50% propanol for 5 minutes, and washed twice with distilled water for 5 minutes. Slides were immersed into Hemalum acid solution for 6 minutes and washed once with distilled water for 5 minutes. Slices were stained with 1% Eosin solution for 3 minutes and washed with distilled water until the desired contrast was achieved. Slides were immersed into 96% propanol for 1 minute, then 100% propanol twice for 1 minute and then 4 times into Roti-Histol for 5 minutes each. Finally, slices were coversliped using Neo-Mount and stored at RT until imaging.

DRG were cut as mentioned above (see section 2.2.11) and were stained using the immunofluorescence protocol described above (see section 2.2.12)

# Results – Part I

## 3.1  Results – Part I

### 3.1.1. Regeneration-associated genes regulated by PCAF

As found previously, PCAF is involved in regulating the regenerative signal in sensory neurons induced by an injury in the PNS [96]. PCAF, when virally overexpressed in DRG, is sufficient to promote axonal regeneration of ascending sensory axons via the mitogen-activated protein kinase (MAPK) signaling pathway. Based upon these results, we wanted to examine which genes associated with regeneration are controlled by PCAF, the corresponding transcriptional regulators involved, and finally, if mimicking the activation of the PCAF-regulated regenerative signal can enhance regeneration of injured neurons.

The first step to study the PCAF-dependent regenerative signal was by comparing the transcriptome of wild-type and PCAF knock-out (KO) CD1 mice. Both groups received a sciatic nerve axotomy (SNA), that induces a retrograde regenerative signal in WT animals. 24 hours post-injury, their transcriptomes were compared to the transcriptomes of WT or PCAF KO animals that had received a sham injury (**Figure 3.1A**). PCAF KO mice do not show overt differences from WT CD1 mice and can mate normally[159]. Additionally, to ensure that gene expression in the DRG is not drastically altered by the deletion of PCAF alone, the DRG transcriptomes of uninjured WT and PCAF KO animals were compared. A linear relationship between the two transcriptomes indicates that baseline expression levels of all genes between the two groups are relatively similar and not significantly affected by the inherent absence of PCAF, perhaps due to compensation by other HATs (**Figure 3.1B**).

The comparison of the transcriptome of peripherally injured and sham-injured WT and PCAF KO animals is shown in Figure 3.1C (24,062 genes included). Specific clusters of genes are upregulated after a regenerative peripheral injury (green) or downregulated (red), indicating overall gene expression differences due to injury between WT and PCAF KO mice. From our analysis, 1,237 genes were found to be differentially expressed in WT mice following injury compared to PCAF KO. From those, 647 genes were upregulated after SNA in WT but not PCAF KO mice. These genes will be termed regeneration-associated PCAF-dependent genes or PCAF-RAGs for short, given these genes are expressed by a regenerative injury and appear to be regulated by PCAF.
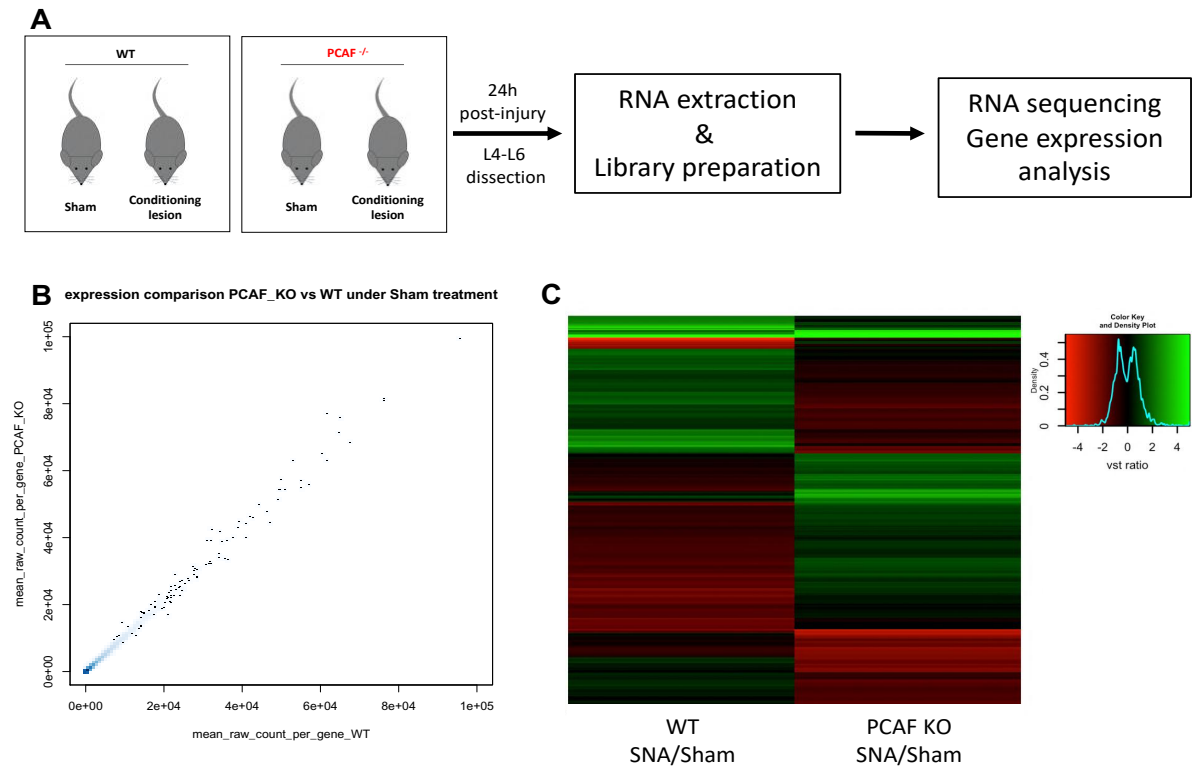
**Figure 3.1. Gene expression analysis of WT and PCAF KO CD1 mice. A)** Schematic workflow of lumbar DRG RNA-seq following a regenerative injury between WT and PCAF KO CD1 mice compared to non-injured mice. Bioinformatic analysis was performed on RNAseq data using Fastqc for quality control followed by Tophat2 for mapping and HTSeq for read counts. Differential expression analysis was performed using a linear model in DESeq2. **B)** Scatter plot of gene expression differences between WT and KO uninjured mice shows a linear relationship between the two, indicating that baseline gene expression does not change significantly in PCAF KO mice. **C)** Heatmap of gene expression differences between WT and PCAF KO animals 24h following sciatic nerve axotomy compared to sham injured animals (N=3 per group, each sample was pooled from two mice). Expression ratios range from -4 (red) to +4 (green).

## 3.1.2. PCAF regulates the increase of H3K9ac after a regenerative injury in the periphery

PCAF is a lysine acetyltransferase with various targets in the nucleus as well as the cytoplasm[160,161]. Previously, it has been shown that the acetylation of H3K9 (H3K9a), mediated by PCAF and GCN5[162], is upregulated after a peripheral injury[96]. To confirm that the observed increased levels of this epigenetic marker is linked to the activation of PCAF specifically, a peripheral injury in both WT and PCAF KO mice was used. For this, DRG were collected 24 hours post-sciatic nerve axotomy, and stained for PCAF and H3K9ac. The peripheral injury

induces nuclear translocation of PCAF, promoting its HAT activity leading to acetylation of H3K9ac (**Figure 3.2**). Importantly, the lack of PCAF does not allow this to occur, confirming that H3K9ac is PCAF-driven following SNA (**Figure 3.2**).
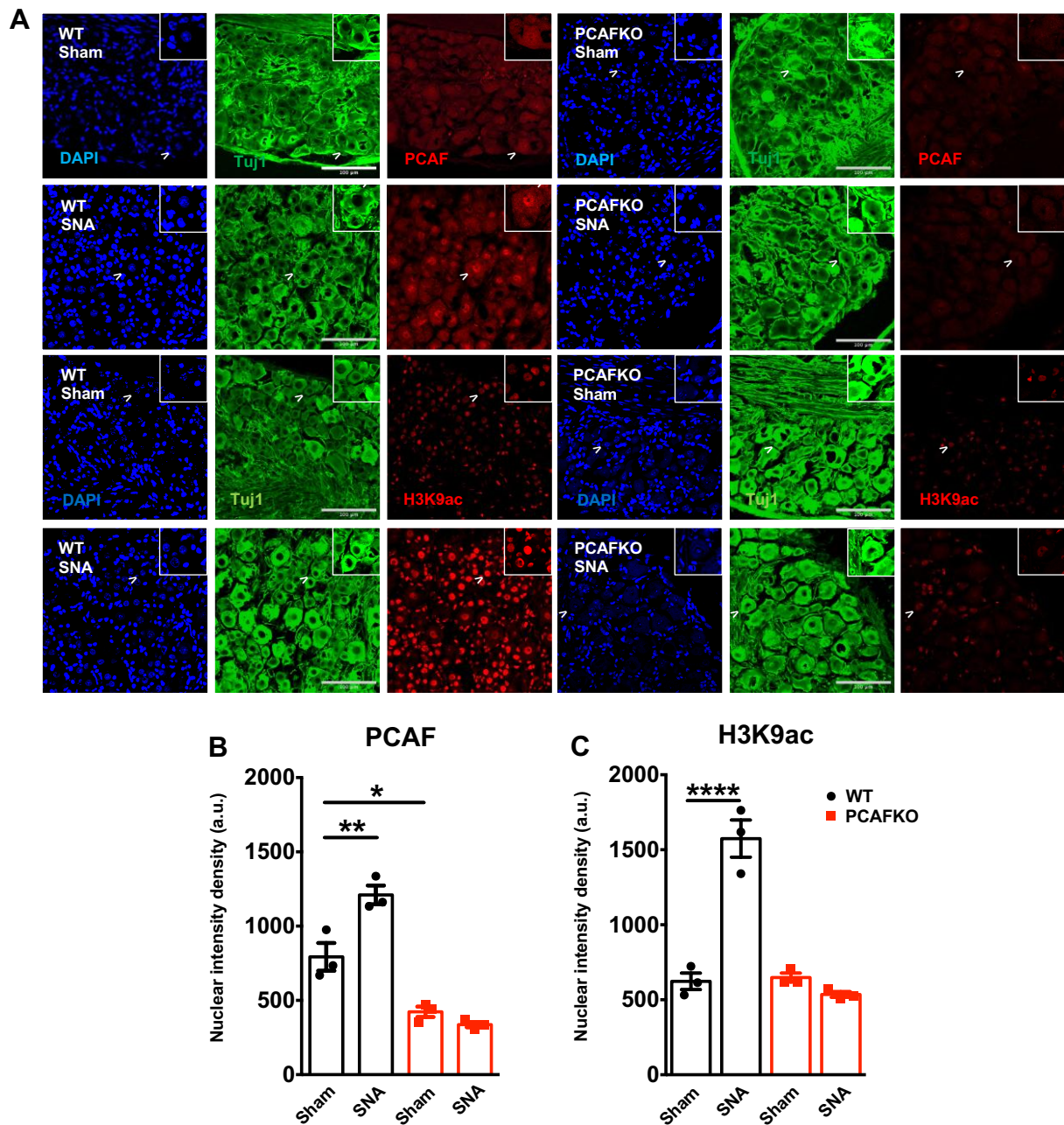


**Figure 3.2. SNA induces PCAF nuclear translocation and PCAF-dependent increased H3K9ac levels. A)** Immunohistochemistry photomicrographs (20x) of WT or KO lumbar (L4-L6) DRG after Sham or SNA stained for PCAF and H3K9ac. Arrowheads indicate magnified regions of interest (ROIs). Scale bar, 100μm. **B, C)** Quantitative analysis of PCAF (**B**) and H3K9ac (**C**) nuclear intensity density in WT or KO lumbar DRG after Sham or SNA. Two-way ANOVA, mean ± SEM, **p<0.01, ****p<0.0001, N=3.

### 3.1.3. Sp1 and MAZ can regulate PCAF-RAGs

It is known that PCAF does not bind to DNA by itself as it lacks DNA-binding domains[89]. PCAF binds to histones and recruits transcriptional complexes [163–165]; however, which transcriptional factors are involved following a regenerative injury remains unknown. For this, we analyzed the promoter sequences of all the PCAF-RAGs that were found from our RNA-seq analysis. *In silico* Transcription Factor Binding Site (TFBS) analysis was applied with Webgestalt, TRANSFAC and Genomatix. The two highest hits, Sp1 and MAZ, have binding sites in the promoters of many of the PCAF-RAGs. Their DNA binding site motifs are: 5'-GGGCGGG-3' and 5'-GGGAGGG-3' for Sp1 and MAZ, respectively. Specifically, it was predicted that 172 of the PCAF-RAGs are regulated by either Sp1 or MAZ, with Sp1 having promoter binding sites in 69 and MAZ in 71 PCAF-RAGs. 32 genes had binding sites for both TFs (**Figure 3.3**).


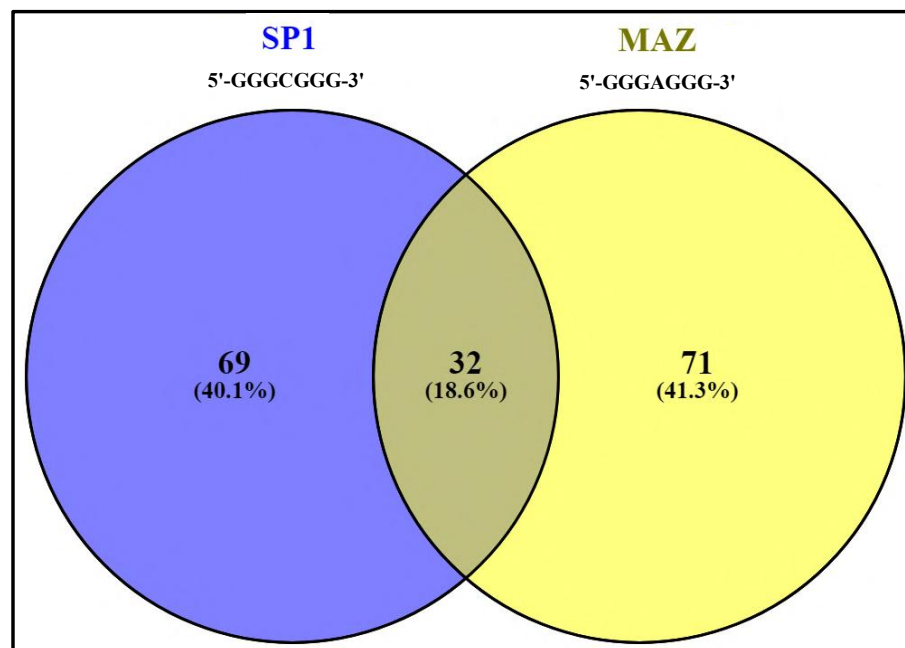
**Figure 3.3. Sp1 and MAZ are predicted to regulate PCAF-RAGs.** A Venn diagram of PCAF-RAGs whose promoters have binding sites for Sp1 (5'-GGGCGGG-3') and/or MAZ (5'-GGGAGGG-3') derived from the Transcription Factor Binding Site (TFBS) analysis.

These *in-silico* results suggest that Sp1 and MAZ may play a role in the peripheral lesion-initiated PCAF-mediated regenerative signaling. Based upon our hypothesis that, PCAF should be part of context-dependent transcriptional complexes which regulate the expression of RAGs upon injury, we examined if Sp1 and MAZ also translocated to the nuclei of DRG upon a peripheral injury as colocalization is required for the complex to be formed. Sp1 and MAZ nuclear localization is significantly increased 24 hours following SNA of adult WT DRG (**Figure 3.4**). Interestingly, the increased nuclear localization does not occur in PCAF KO DRG upon a regenerative injury, suggesting PCAF dependence.

Having found, histochemically, Sp1 and MAZ nuclear increase upon SNA in WT animals, we wanted to confirm these results biochemically. For this, cytoplasmic-nuclear fractionation of DRG lysates upon either SNA or sham injury was performed. Nuclear fractions were analyzed by western blot stained for Sp1, MAZ or histone 3 as a nuclear marker. These results did not show any significant changes (**Figure 3.5**). It should be noted that the cellular heterogeneity of the DRG with glial and satellite cells, have also been shown to express Sp1 and probably MAZ (**Figure 3.4**) and by using a bulk DRG protein fractionation approach these populations cannot be filtered out.

## 3.1.4. The PCAF-signal upon an injury to the CNS

Now that the PCAF-signal following an injury to the peripheral branch of the lumbar DRG is clear, the signal following a non-regenerative central lesion remains unknown. To examine this, I collected the lumbar DRG (L4-L6) of WT mice which had received a dorsal hemisection (DH) at thoracic vertebral level 9 (T9) and looked for the nuclear localization of PCAF, Sp1 and MAZ and acetylation levels of H3K9. Interestingly, shown here for the first time, a central lesion does not increase the nuclear levels of PCAF but reduces it (**Figure 3.6**). Similarly, H3K9ac levels do not increase after DH, confirming that PCAF is crucial for H3K9 acetylation. Although Sp1 levels increase after DH, MAZ nuclear levels remain unchanged (**Figure 3.6**).
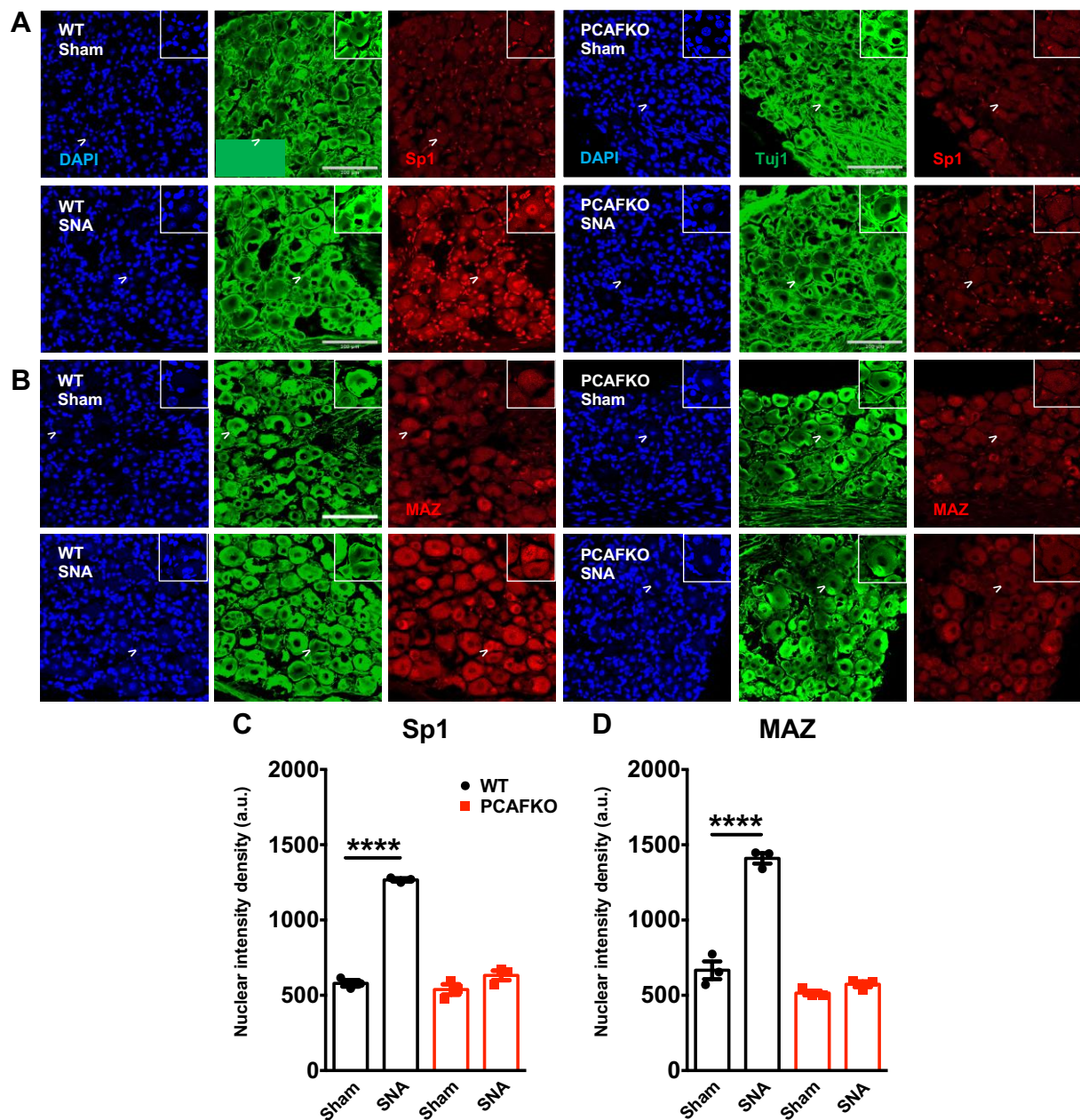
**Figure 3.4. Sp1 and MAZ show increased nuclear localization after SNA in WT but not PCAF KO mice.**
**A, B**) Immunohistochemistry photomicrographs (20x) of WT or PCAF KO lumbar DRG after Sham or SNA stained for Sp1 (**A**) or MAZ (**B**). Scale bar, 100μm. **C, D**) Nuclear intensity density analysis of the lumbar DRG showed a statistically significant increase of Sp1 (**C**) and MAZ (**D**) nuclear localization after a regenerative injury in the WT mice, while there was no increase in the KO mice after the same injury. Arrowheads indicate magnified ROIs. Two-way ANOVA, mean ± SEM, ****$p<0.0001$, N=3.

**Figure 3.5. DRG nuclear fractionation did not show an increase of Sp1 and MAZ nuclear levels upon SNA.**
**A**) Western blot of the nuclear fraction of DRG lysate after sham or SNA. **B**) Intensity density analysis of western blot showed no statistically significant differences of Sp1 and MAZ nuclear levels. Student's t-test, mean ± SEM, N=2.
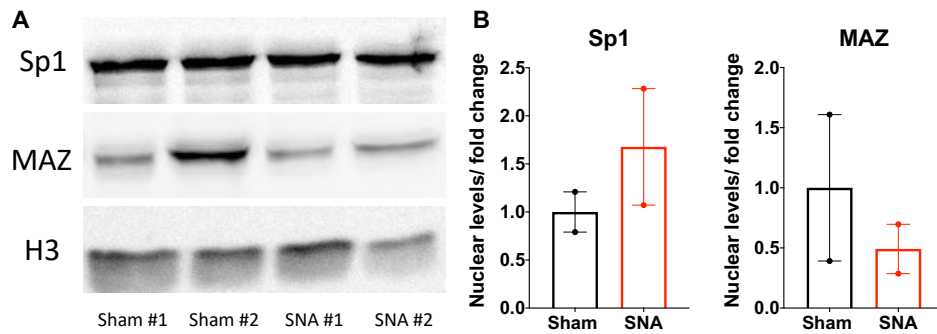
## 3.1.5. The PCAF-dependent regenerative gene panel does not respond to a CNS non-regenerative lesion

PCAF nuclear levels are reduced after a CNS lesion, but it remains unclear if the expression of PCAF-RAGs has a different pattern compared to their expression after a regenerative peripheral lesion. In place of confirming RNA-seq results with time-consuming and inefficient single primer set q-PCR, I exploited a new technology, called Nanostring, which detects differences in the mRNA levels without any prior enzymatic reaction and amplification step in a fast and cost-effective way. With this method, custom-designed color-coded probes hybridize specifically to the mRNA of genes of interest. By counting the different color codes, the raw expression levels of respective genes in the different groups can be measured. Thus, color-coded RNA probes were designed for 43 PCAF-RAGs (Materials 2.1.8 section, Table 2.24). Examples of PCAF-RAGs are shown in Figure 3.7A. Raw counts were normalized with four housekeeping genes, H1 histone (h1f0), beta-actin (Actb), exocyst 3 (Exoc3) and RPL13a. The house keeping genes were chosen as their expression levels remain stable after injury both in WT and PCAF KO animals (RNAseq data not shown). ATF3 is an indicator of a peripheral injury, as it is known that its DRG expression levels always increase after SNA. Also, classical RAGs, such as BDNF, galanin and GAP43 were included as indicators of a regenerative injury.

First, with our custom-made panel of regenerative gene probes, I confirmed the majority of our RNAseq results. As shown in the heatmap in Figure 3.7B, most of the genes are upregulated in WT SNA compared to WT sham as suggested by the RNAseq results. Further confirmation showed that PCAF-RAG upregulation is not observed in the PCAF KO mice after a peripheral injury when compared to PCAF KO sham-injured mice.
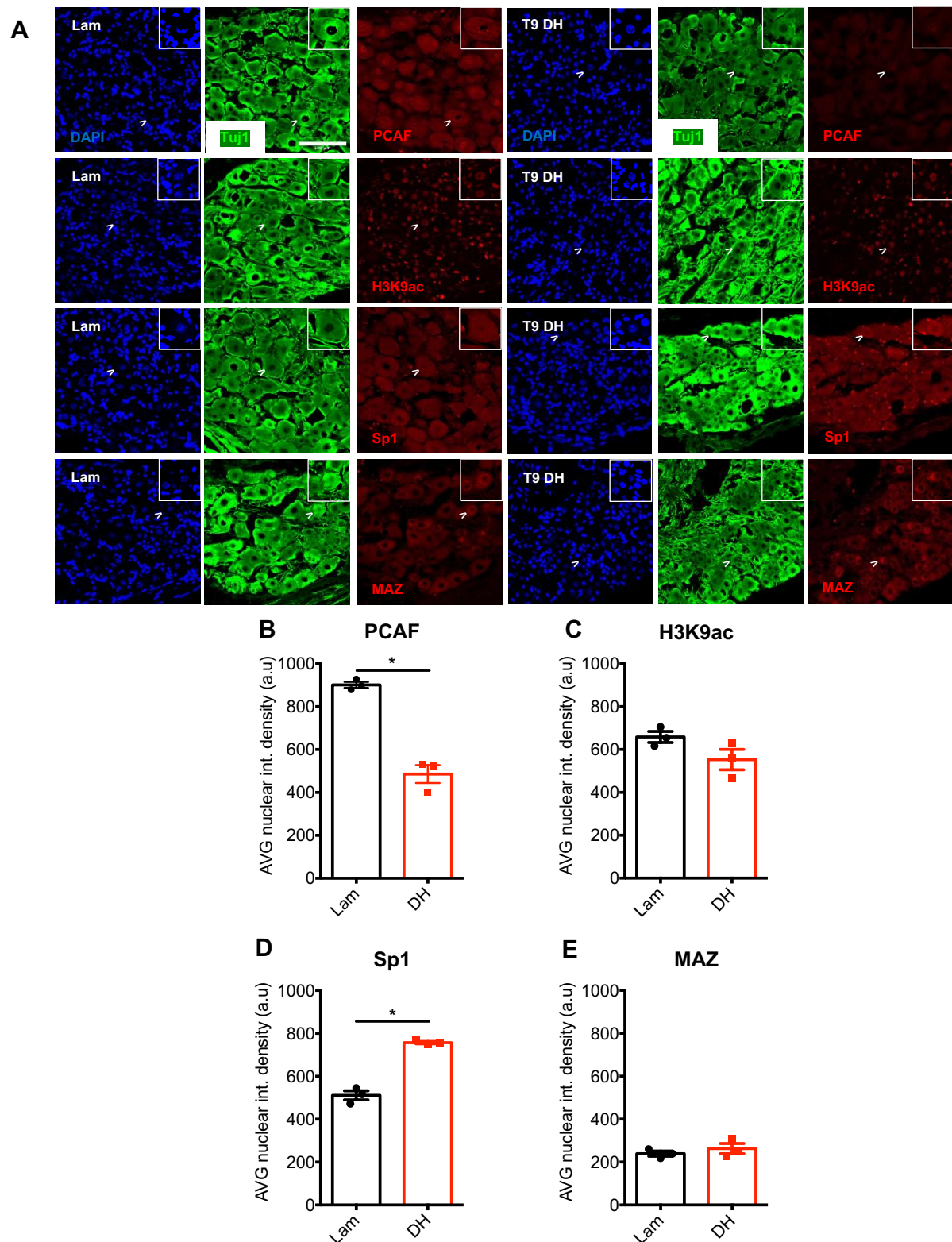
**Figure 3.6. CNS injury does not activate the entire PCAF-dependent regenerative signal. A)** Immunohistochemistry photomicrographs (20x) of WT lumbar DRG stained for PCAF, H3K9ac, Sp1 and MAZ after laminectomy or T9 DH. Arrowheads indicate magnified regions of interest (ROIs). Scale bar, 100μm. **B-E)** DRG nuclear intensity density analysis of PCAF (**B**), H3K9ac (**C**), Sp1 (**D**) and MAZ (**E**) after T9 DH compared to laminectomy. Student's t-test, mean ± SEM, ***$p<0.001$, N=3.

Second, I investigated the expression levels of the PCAF-RAGs upon a non-regenerative CNS lesion. mRNA from lumbar DRG (L4-L6) 24 hours following a dorsal T9 hemisection (T9 DH) was compared to a laminectomy (lam). Strikingly, PCAF-RAGs are confirmed to be expressed in a regenerative paradigm and not after a CNS lesion or a peripheral lesion lacking PCAF (**Figure 3.7B**).

**Figure 3.7. The PCAF-RAG regenerative panel confirms RNA-seq results and does not respond to non-regenerative lesions. A**) Some representative PCAF-RAGs from RNA-seq chosen to design probes for Nanostring technology, Two-way ANOVA, mean ± SEM, *p<0.05, **p<0.01, N=3, *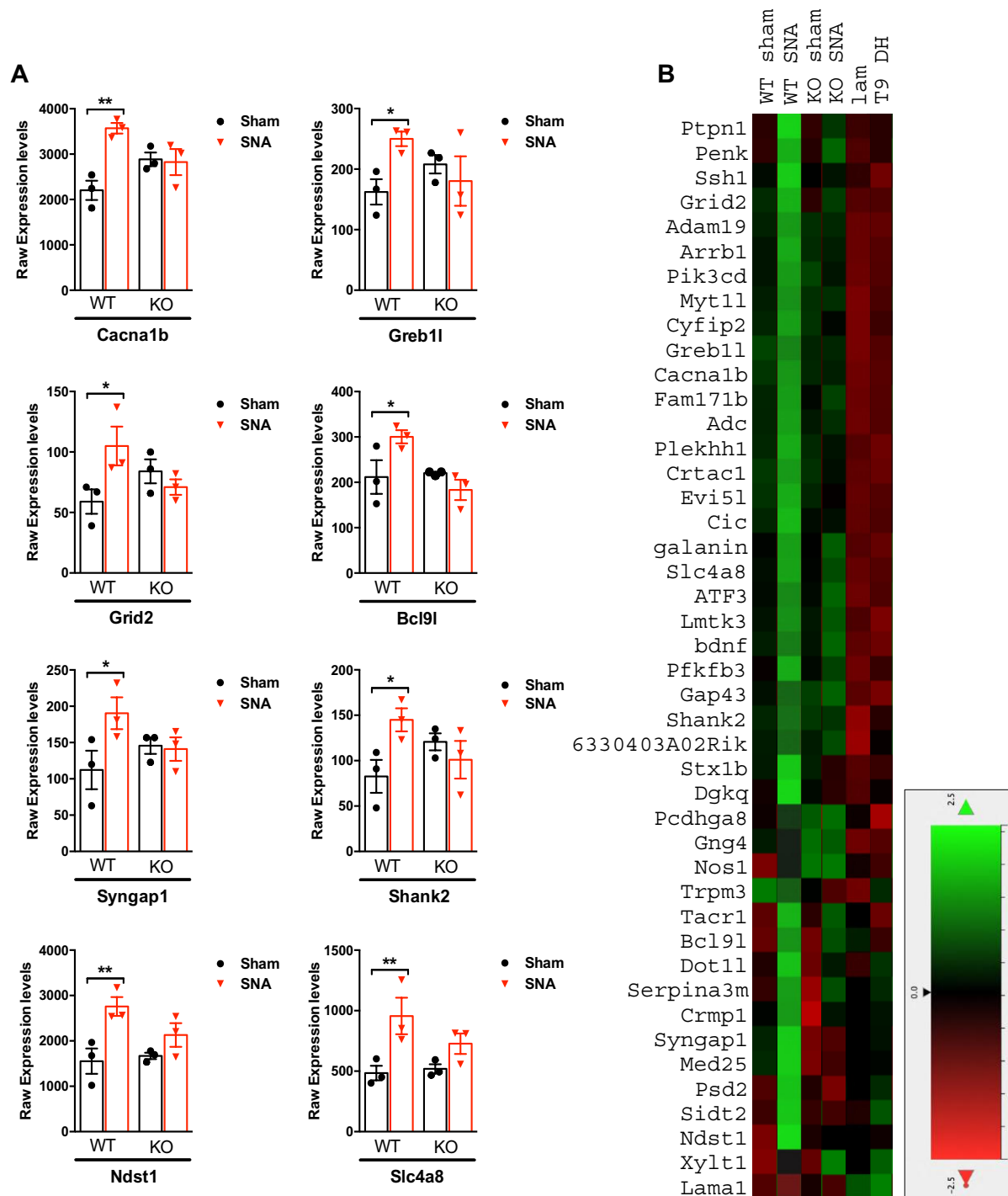*B**) Gene expression analysis of the PCAF-dependent injury-upregulated genes after either a PNS (SNA) injury in WT and PCAF KO animals or CNS (DH) injury compared to a Sham injury or laminectomy (N=3 per group). Expression fold change ranges from -2.5 (red) to +2.5 (green).

## 3.1.6. Sp1 and MAZ regulate the expression of PCAF-RAGs and are important for neurite outgrowth *in vitro*

As mentioned before, Sp1 and MAZ were found through RNA-seq and TFBS analysis to be involved in the PCAF-driven regenerative pathway. Sp1 and MAZ were shown here to be translocated to the nuclei of peripherally injured DRG together with PCAF, however it remains unclear if these two TFs are important for axonal regeneration.

To examine if Sp1 and MAZ are essential for neurite outgrowth, all DRG from adult mice were collected and co-electroporated with siRNA against either *Sp1* or *MAZ* mRNA or scrambled siRNA and a vector overexpressing eGFP (**Figure 3.8**). Cells were cultured for 3 days on a permissive substrate (laminin) to allow a sufficient reduction of the TFs mRNA and protein levels, then the DRG were replated, to sever already growing neurites. Neurite outgrowth was measured 18 hours post-replating. Pmax-GFP was used as a rudimentary co-electroporation efficiency marker and only GFP+ cells were used for the measurement of neurites.

As shown in Figure 3.9, *Sp1* and *MAZ* mRNA (**Figure 3.9.A, F**) and protein levels (**Figure 3.9. B-C, G-H**) were significantly reduced 72 hours and 90 hours post-electroporation, respectively. Although DRG were cultured on permissive laminin substrates, the knock down of either Sp1 or MAZ resulted in a significant reduction of DRG neurite outgrowth compared to DRG electroporated only with scrambled siRNA (**Figure 3.9. D-E, I-J**).

In contrast, we examined if Sp1 and MAZ could enhance neurite outgrowth on their own accord. Again, all DRG of adult WT mice were electroporated with constructs expressing either Sp1 fused with GFP or MAZ linked with eGFP through a P2A linker or the pmaxGFP vector expressing only eGFP (**Figure 3.10**). The fused Sp1-eGFP localized to the nuclei of DRG, however MAZ localized to the nucleus while the linked GFP was found both in the cytoplasm and the nucleus of cultured DRG. Only GFP+ cells were used for neurite length analysis.
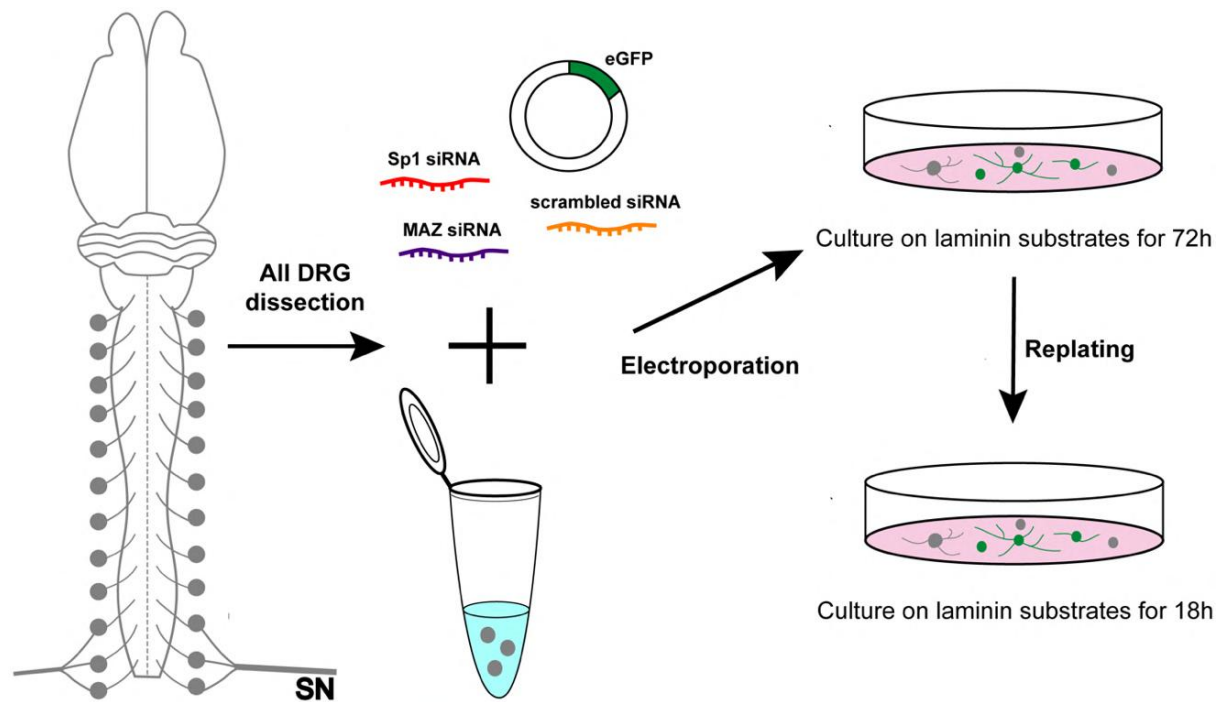
**Figure 3.8. Schematic representation of Sp1 and MAZ knockdown.** All DRG of adult WT CD1 mice were dissected and dissociated. DRG cells were mixed with *Sp1* siRNA, *MAZ* siRNA or scrambled siRNA and pmaxGFP vector and co-electroporated. Electroporated cells were cultured on laminin substrates for 72 hours for full silencing to occur and then replated and fixed 18 hours post-replating. Only GFP+ cells were used for neurite length analysis with the NeuronJ plugin of Fiji (ImageJ).

*Sp1* and *MAZ* mRNA (**Figure 3.11A**) and protein (**Figure 3.11B, C**) levels were significantly increased 72 and 90 hours post-electroporation, respectively. Neurite length analysis of cultured DRG overexpressing either Sp1 or MAZ compared to control DRG, showed enhanced neurite outgrowth *in vitro* (**Figure 3.11D**).

The knockdown and overexpression approaches shed more light on the importance of Sp1 and MAZ in the regeneration of sensory neurons *in vitro,* but it still remained unclear if they could regulate the expression levels of PCAF-RAGs. Notably, not all PCAF-RAGs that we designed Nanostring probes for have binding sites for Sp1 or MAZ (**Table 3.1**), thus it was not clear if their expression levels would respond to the overexpression of either Sp1 or MAZ. Nanostring Technology was used to analyze the expression levels of selected PCAF-RAGs of either Sp1 or MAZ compared to control eGFP-overexpressing DRG. As seen in Figure 3.11E, more than half of PCAF-RAGs were upregulated after Sp1 overexpression (Sp1OE) compared to the control. Remarkably, MAZ overexpression (MAZOE) induces the expression of almost all PCAF-RAGs when compared to the control.
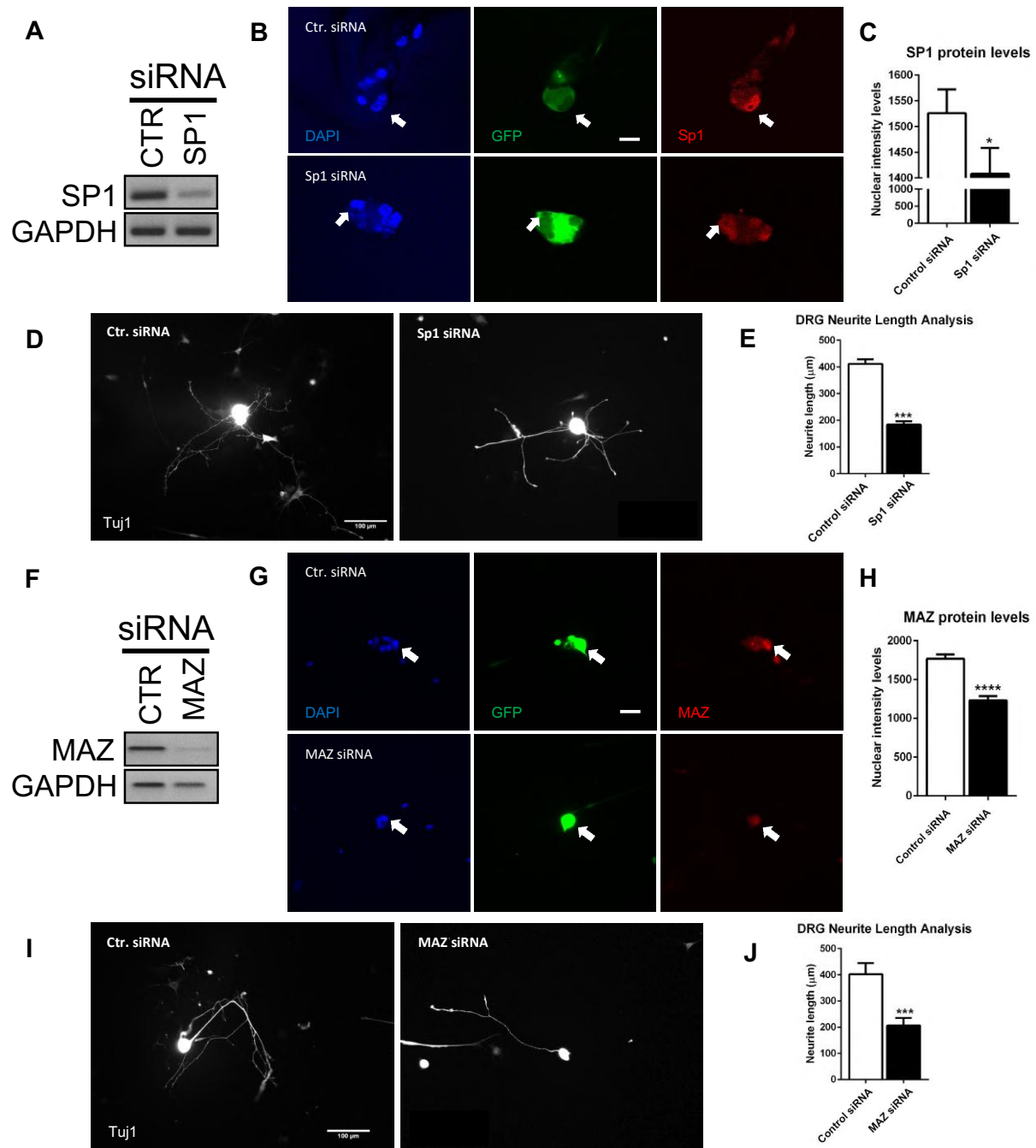
**Figure 3.9. Sp1 and MAZ knockdown results in a reduction of neurite outgrowth *in vitro*. A, F)** siRNA treatment of primary DRG against either *Sp1* (**A**) or *MAZ* (**F**) mRNA resulted in downregulation of *Sp1* or *MAZ* gene expression 72 hours post electroporation. **B, G)** Immunohistochemical analysis (40x) of DRG treated with either *Sp1* (**B**) or *MAZ* (**G**) siRNA for 90 hours. Scale bars, 50μm. Arrows indicate successfully co-electroporated cells. The treatment with the siRNA results in a significant reduction of the protein levels of either Sp1 (**C**) or MAZ (**H**). **D, I)** Neurite length analysis of DRG 18 hours post-replating and 90 hours post-electroporation with either Sp1 (**D**) or MAZ (**I**) siRNA. Sp1 or MAZ knockdown significantly reduced the neurite outgrowth of cultured DRG (**E, J**). Statistical analysis, Student t-test, mean ± SEM, *p<0.05, ***p<0.001, ****p<0.0001, N=3.
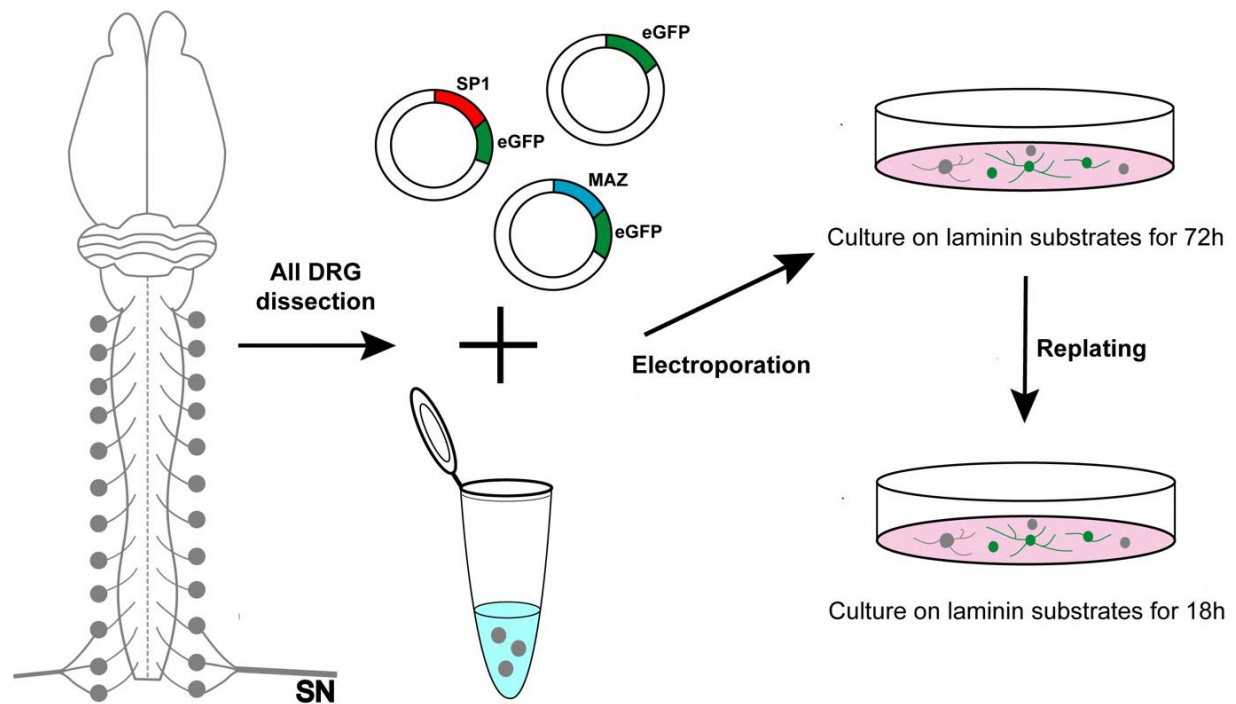
**Figure 3.10. Schematic representation of Sp1 and MAZ overexpression.** All DRG from adult WT or PCAF KO CD1 mice were dissected and dissociated. DRG cells were electroporated with either Sp1- or MAZ expressing plasmids or pmax-GFP as control and cultured on laminin substrates for 72 hours. Then, they were replated and fixed 18 post replating. Only eGFP overexpressing cells were used for neurite length analysis with the NeuronJ plugin of Fiji (ImageJ).

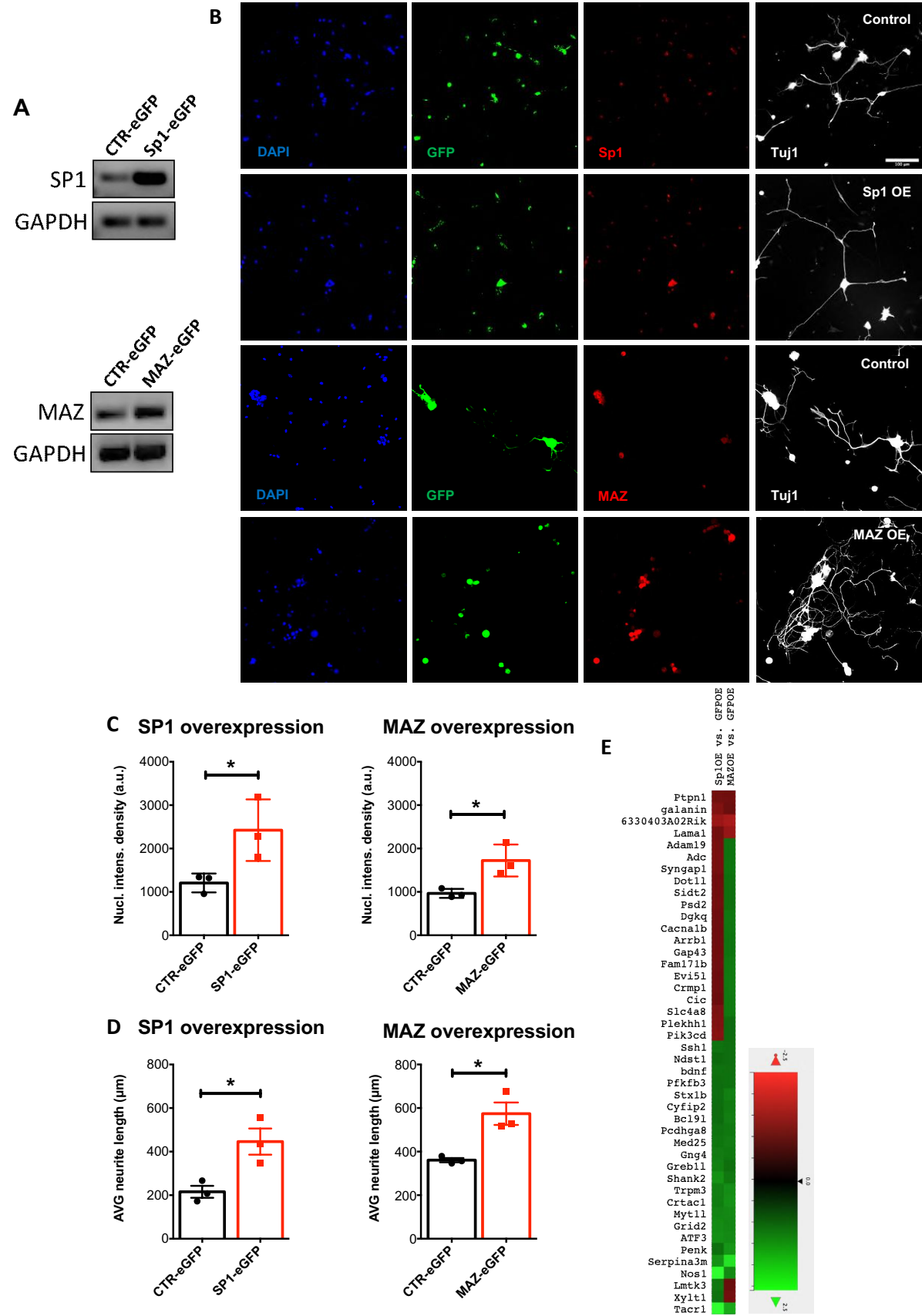**Figure 3.11. Sp1 and MAZ overexpression enhances neurite outgrowth *in vitro*. A**) DRG electroporation with Sp1 or MAZ expressing vectors results in an increase of *Sp1* or *MAZ* mRNA as shown by PCR. **B**) Immunohistochemical analysis (10x) of DRG overexpressing either Sp1 or MAZ and GFP. GFP+ cells were selected for the neurite length analysis. Scale bar, 100μm. **C**) Nuclear intensity density analysis of DRG overexpressing either Sp1 or MAZ compared to control cells showed a significant increase of Sp1 and MAZ nuclear levels 90 hours post-electroporation. Student's t-test, mean ± SEM, *p<0.05. **D**) The overexpression of the transcription factors correlated to a significant increase of average neurite length of cultured DRG, 18 hours post-replating. Student's t-test, mean ± SEM, *p<0.05. **E**) mRNA was extracted 3 days post-electroporation with either Sp1 or MAZ overexpressing constructs. Gene expression of PCAF-RAGs was analyzed by Nanostring. Samples were normalized to housekeeping genes. Expression levels ratios range from -2.5 (red) to +2.5 (green).

**Table 3.1. Sp1 or MAZ regulated PCAF-RAGs predicted to have binding sites for them**

| Target Genes | Predicted SP1 | Predicted MAZ | Nanostring SP1 | Nanostring MAZ |
|---|---|---|---|---|
| Gng4 | X | | X | X |
| Grid2 | | X | X | X |
| Lmtk3 | | | X | X |
| Nos1 | | X | X | X |
| Pcdhga8 | | | X | X |
| Shank2 | | X | X | X |
| Tacr1 | | | X | X |
| Xylt1 | | | X | |
| 6330403A02Rik | | | | |
| Bcl9l | X | X | X | X |
| Greb1l | | | X | X |
| Penk | | X | X | X |
| Slc4a8 | | | | X |
| Ssh1 | | | X | X |
| Syngap1 | X | X | | X |
| Ndst1 | X | | X | X |
| Pik3cd | | | | X |
| Cacna1b | | | | X |
| Adam19 | | X | | X |
| Adc | | | | X |
| Lama1 | | X | | |
| Crtac1 | X | | X | X |
| Cyfip2 | | | X | X |
| Plekhh1 | | | | X |
| Med25 | | | X | X |
| Dgkq | | | | X |
| Trpm3 | | | X | X |
| Stx1b | | | X | X |
| Stx1b | X | | X | X |

| | | | | |
|---|---|---|---|---|
| Sidt2 | | | | X |
| Fam171b | | | | X |
| Cic | | | X | X |
| Myt1l | | **X** | X | X |
| Evi5l | **X** | **X** | | X |
| Arrb1 | | | | X |
| Crmp1 | **X** | **X** | | X |
| Ptpn1 | **X** | | | |
| Serpina3m | | | X | X |
| Psd2 | | **X** | | X |
| Dot1l | | | | X |
| Gap43 | | | | X |
| galanin | | | | |
| bdnf | | | X | X |
| ATF3 | | | X | X |

**Table 3.1. PCAF-RAGs, some of which were predicted to have binding sites for Sp1 and MAZ, are partially regulated by the overexpression of Sp1 and MAZ *in vitro*.** X indicates the genes that were upregulated upon Sp1 or MAZ overexpression. Bold X (**X**) indicates genes that were predicted to have binding sites on their promoters or Sp1 or MAZ. Highlighted genes are these for whom the prediction for Sp1 or MAZ agreed with upregulated gene expression levels upon overexpression of Sp1 or MAZ.

## 3.1.7. Sp1 and MAZ regenerative potential *in vitro* is regulated by PCAF

Thus far, we have shown that the SNA-induced regenerative signaling recruits transcriptional complexes which induce genetic and epigenetic changes in sensory neurons. As shown above, Sp1 and MAZ's nuclear localization does not occur after SNA in DRG that lack PCAF suggesting a strong relationship between our TFs and PCAF. Also, Sp1 and MAZ can enhance axonal outgrowth of cultured sensory neurons. Nevertheless, it was not clear if PCAF is crucial for the regenerative capacity of cultured DRG when overexpressing either Sp1 or MAZ. We assumed that if PCAF works together with Sp1 and MAZ to enhance neurite outgrowth, then the Sp1 or MAZ overexpression-related regenerative effect will not occur in DRG lacking PCAF.

For this, PCAF KO DRG were electroporated with either Sp1- or MAZ-expressing vectors and neurite length was measured compared to PCAF KO DRG overexpressing only GFP. As shown in Figure 3.12, when Sp1 or MAZ are overexpressed in DRG lacking PCAF the previously observed regenerative effect is abolished as no significant differences were found between the control group, the Sp1OE or MAZOE groups' average neurite length.
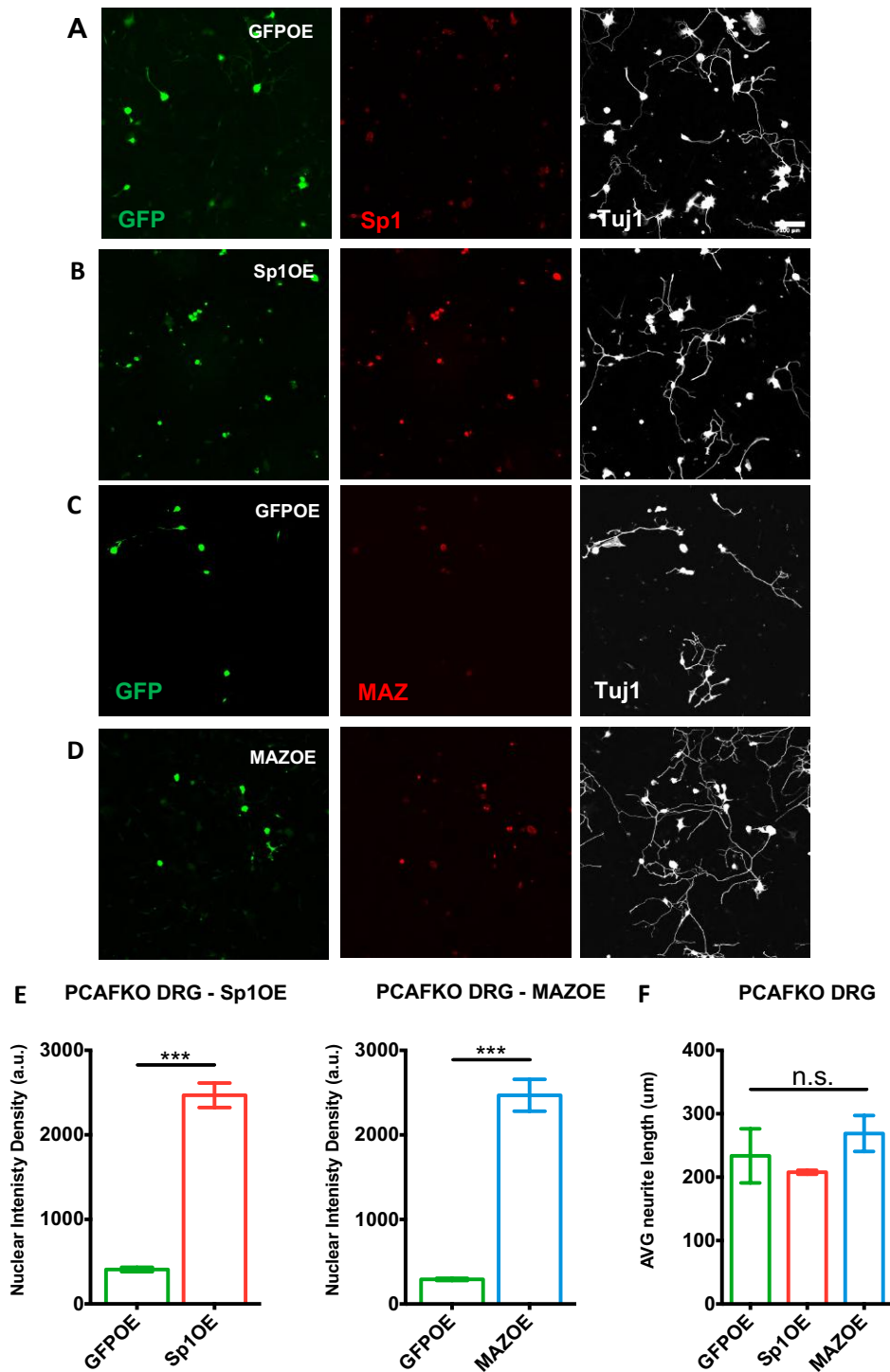
**Figure 3.12. Sp1- and MAZ-overexpression regenerative efficacy *in vitro* requires the presence of PCAF.** DRG from PCAF KO mice were dissected and electroporated with either Sp1OE, MAZOE or GFPOE vectors. Cells were cultured for 72 hours, replated and fixed 18 hours post-replating. **A-D**) Immunocytochemistry of DRG overexpressing GFP (**A, C**) SP1 (**B**) or MAZ (**D**) stained for GFP and Sp1 (**A, B**) or MAZ (**C, D**) and Tuj1. **E**) Nuclear intensity density analysis of DRG overexpressing either Sp1 or MAZ compared to their respective GFPOE control. Student's t-test, mean ± SEM, ***$p<0.0001$, N=3, **F**) Neurite length analysis of cultured DRG showed no significant differences between GFP-, SP1- or MAZ-overexpressing in PCAF KO DRG. One-way ANOVA, mean ± SEM, N=3.

### 3.1.8. Activation of PCAF by SPV106 *in vitro* can enhance neurite outgrowth of sensory neurons

PCAF has an important role in the regenerative signal allowing sensory tracts of the PNS to regrow after their damage, and the regenerative signal that primes axonal outgrowth of the injured CNS following a conditioning lesion. Nevertheless, the approaches exploited so far to investigate the regenerative potential of PCAF involved the use of adeno-associated viruses (AAV) or the use a regenerative peripheral lesion model [96]. These techniques are commonly used in basic research into mechanistic understanding of nervous systems, but they lack strong clinical translatability. Thus, we aimed to find ways to pharmaceutically activate PCAF and mimic the PCAF-driven regenerative signal. The search into the literature led us to a compound called pentadecylidenemalonate 1b, or SPV106, which is an analogue of anacardic acid[166]. SPV106 is a known activator of PCAF and has been used *in vivo* in experiments related to fear extinction[167]. Since SPV106 had not been used in the field of neuronal regeneration before, we decided to use it on DRG cultures in order to investigate its regenerative potential *in vitro* prior to use *in vivo*.

Adult mouse WT DRG cultured on permissive substrates were treated with SPV106. Given the lack of previous knowledge for use in neuronal cultures, I used a range of concentrations of SPV106, 5 µM, 10 µM, 25 µM or vehicle (DMSO) for 24 hours, to determine which concentration would be the most beneficial without detrimental effects (**Figure 3.13A**). Neurite length analysis showed that 5 µM SPV106 had the strongest effect on neurite outgrowth of cultured DRG compared to those treated with vehicle and 25 µM had the poorest effect, showing the highest levels of cell death. Interestingly, diameter analysis of the SPV106 effect (5 µM) showed that medium to large (20-40 µm) and large diameter (>40µm) DRG, which only partially represent nociceptive neurons but mostly represent mechanoreceptor and proprioceptive neuronal populations, respectively[168], had significantly longer neurites compared to the ones that were treated with the vehicle. Although DRG treated with 10 µM SPV106 did not have a significant increase in their overall neurite outgrowth compared to control, the diameter analysis did show that the medium to large diameters had a slight increase. In both cases the small diameter neurons (<20 µM), representing nociceptive neurons[169], did not show any increased axonal outgrowth compared to the control.

We tested whether the regenerative effect of SPV106 is species-specific. For this, I cultured DRG were derived from Fischer-344 rats. As shown in Figure 3.13D, E, 5 µM SPV106 had a similar effect on rat DRG as it had on mouse DRG. Additionally, diameter analysis of

the treated and untreated cultured DRG showed that medium to large-diameter DRG seem to respond to SPV106 treatment (**Figure 3.13F**).
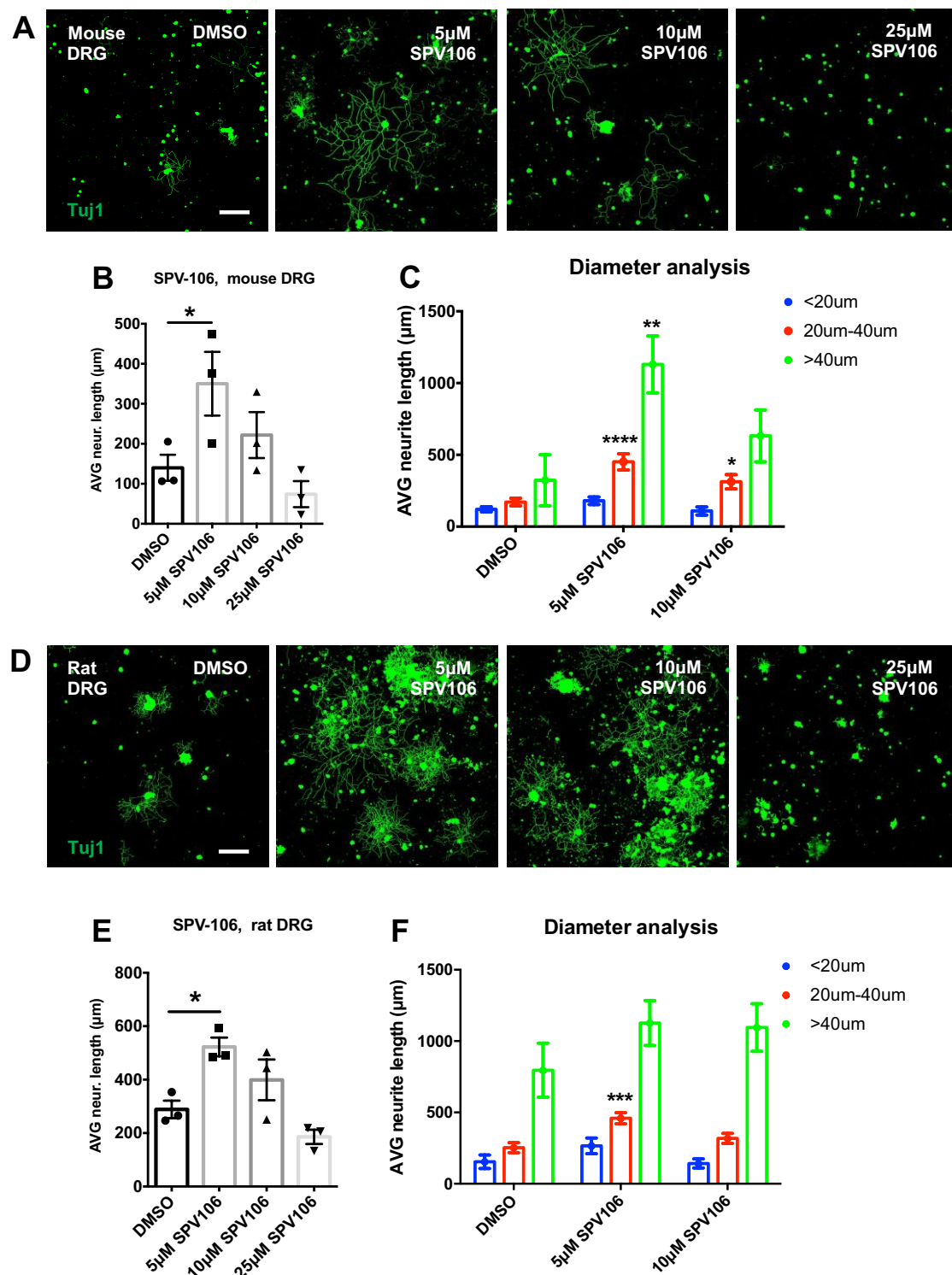


**Figure 3.13. SPV106 treatment enhances neurite outgrowth of medium to large diameter mouse and rat adult DRG. A)** Photomicrographs (10x) of cultured mouse DRG treated for 24 hours with DMSO, 5 μM, 10 μM

or 25 µM SPV106. Scale bar, 100 µm. **B)** Treatment of mouse DRG with 5 µM SPV106 significantly increased their neurite outgrowth. One-way ANOVA, mean ± SEM, *$p<0.05$, N=3. **C)** Diameter analysis of cultured DRG treated with DMSO, 5 and 10 µM SPV-106. Two-way ANOVA, mean ± SEM, **$p<0.01$, ****$p<0.0001$, N=3. **D)** Photomicrographs (10x) of cultured rat DRG treated for 24 hours with DMSO, 5 µM, 10 µM or 25 µM SPV106. Scale bar, 100 µm. **E)** Treatment of rat DRG with 5 µM SPV106 significantly increased their neurite outgrowth. One-way ANOVA, mean ± SEM, *$p<0.05$, N=3. **F)** Diameter analysis of cultured DRG treated with DMSO, 5 and 10 µM SPV106. Two-way ANOVA, mean ± SEM, **$p<0.01$, ****$p<0.0001$, N=3.

### 3.1.9. EML76 can enhance neurite outgrowth *in vitro* by activating PCAF without blocking CBP

Although SPV106 seemed like a potential candidate for the activation of PCAF *in vivo,* there are two caveats. According to the laboratory which initially produced it, SPV106 has a high apoptotic activity [166] compared to other similar compounds. This made it difficult to infer the side effects when administered systemically *in vivo*. Secondly, in 2019 T. Hutson and colleagues demonstrated the importance of another histone acetyltransferase called, CBP, in the regeneration of injured neurons. Specifically, they proved that CBP plays an important role in the enriched environment-induced regenerative potential of DRG, and specifically of the propriospinal neurons both *in vitro* and *in vivo* [140]. Milite and colleagues have demonstrated that SPV106 is able to strongly active PCAF and block CBP at the same time[166] (**Figure 3.14**).

Given these reasons we looked to collaborate with the laboratory of Prof. Gianluca Sbardella (Università di Salerno, Italy) and his colleague, Dr. Ciro Milite, who produced SPV106 to find a PCAF specific activator that did not inhibit other HATs. We were introduced to EML76. Its use was limited to *in vitro* enzymatic assays or treatment of U937 leukemia cells to measure the apoptotic efficacy of this compound. Unlike SPV106, EML76 had a low toxicity profile. We were the first to use this drug in neurons to investigate its effect on neurite outgrowth. We were able to determine the best concentration to enhance neurite outgrowth and with limited observed cellular toxicity.

As shown in Figure 3.15A, cultured DRG were treated for 24 hours with a range of EML76 concentrations (30, 50, 70 µM) or with DMSO. Notably, it was found that the treatment with 30 µM EML76 can increase the outgrowth capacity of cultured DRG almost 5 times compared to the DRG cultured with DMSO. Lower concentrations did not reach the potential of 30 µM and interestingly, higher concentrations did not have a greater effect on enhancing the neurite outgrowth of cultured DRG (**Figure 3.15B**).
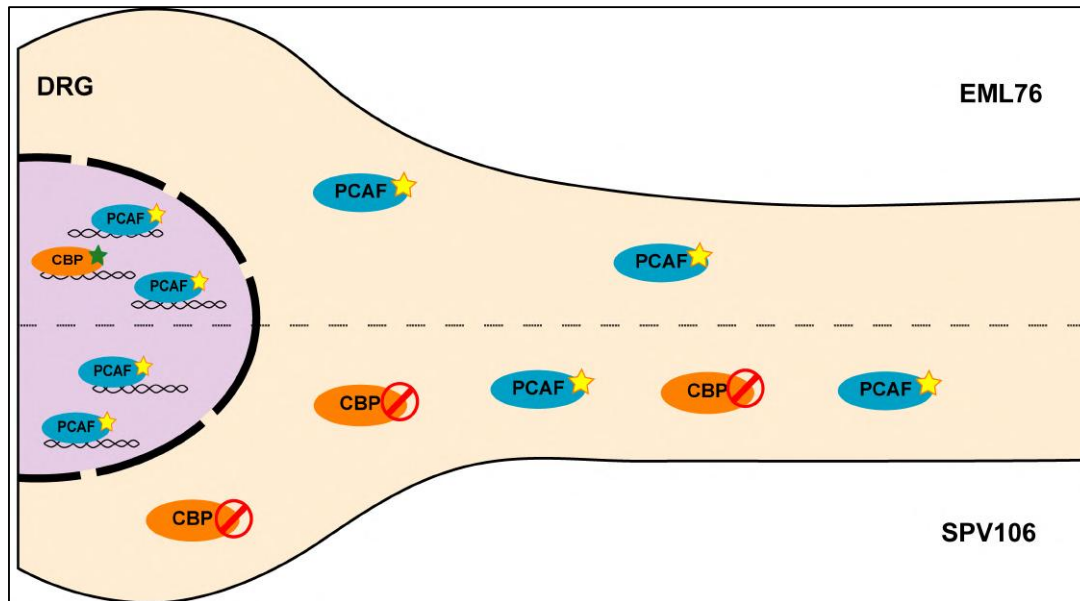
**Figure 3.14. Both SPV106 and EML76 can activate PCAF, but EML76 does not inhibit CBP.** EML76 can specifically activate the acetyl-transferase activity of PCAF without blocking the activity of CBP making it a better candidate for specific activation of PCAF in sensory neurons both *in vitro* and *in vivo*.

Next, to explore if the observed effect was indeed due to the activation of PCAF by EML76, PCAF KO DRG were treated with 30, 50 and 70 μM EML76 or DMSO for 24 hours. The neurite length analysis showed no significant differences between the different concentrations and the DMSO group, suggesting that EML76 works through PCAF for the enhancement of neurite outgrowth *in vitro.* Although not significant, 30 μM EML76 had showed great variability in the PCAF KO DRG, indicating that EML76 could have additional targets having an ancillary contribution to neuronal outgrowth unable to reach full potential without PCAF. This would require further investigation outside the scope of this thesis.

For further mechanistic focus on EML76, I measured the nuclear levels of H3K9ac, which is known to be increased after an SNA-induced activation of PCAF. It was found that H3K9ac levels significantly increase after treatment with 30 μM EML76 (**Figure 3.15**). On the other hand, when PCAF KO DRG were treated with 30 μM EML76, no significant increase of H3K9ac was observed (**Figure 3.15C**), further supporting our hypothesis that EML76 activates PCAF, inducing epigenetic changes that can enhance neurite outgrowth of sensory neurons. Furthermore, the diameter analysis of cultured WT DRG treated with either 30 μM EML76 or DMSO showed that large diameter neurons (primarily thought to be mechanoreceptors and proprioceptive neurons) are the ones responding to the regenerative effect of EML76 (**Figure 3.15D**). These results suggest EML76 to be an ideal candidate for use *in vivo.*

Lastly, given that EML76 can induce epigenetic changes through PCAF activation that can enhance neurite outgrowth *in vitro,* we wondered whether PCAF-RAGs would respond to EML76 treatment. For this, mRNA of cultured DRG 24 hours post-treatment with either 30 μM EML76 or DMSO was collected and expression levels of our top PCAF-RAGs were analyzed with Nanostring Technology. As shown in Figure 3.15E, 30 μM EML76 was sufficient to induce the upregulation of numerous PCAF-RAGs. Interestingly, several genes overlap between our *in vitro* regenerative approaches, Sp1 or MAZ OE or EML76 treatment, and would be of interest for further investigation into their possible related pathways.

### 3.1.10. EML76 can enhance neurite outgrowth *ex vivo*

EML76 successfully replaces SPV106 without blocking CBP and enhances neurite outgrowth of sensory neurons *in vitro,* thus we took the next step and administered the compound *in vivo*. Previous research with SPV106 showed that it crossed the blood brain barrier (BBB) when administered systemically[167], although EML76 is quite similar to SPV106 this has not been explored for the new compound.

For this, we collaborated with the laboratory of Prof. Sbardella, who produces EML76 for us, and conducted the *in vitro* parallel artificial membrane permeability assay (PAMPA) which measures the ability of different compounds to cross through an artificial membrane resembling the BBB. EML76 and SPV106's permeation ability was compared to other chemical compounds, furosemide, propranolol and chlorpromazine, whose ability to cross the BBB is already known (**Figure 3.16**). Furosemide permeation value was $4.62 \pm 0.21 \times 10^{-8}$ $P_a$ cm/s and does not cross the BBB. Propranolol has a permeation value of $7.37 \pm 0.04 \times 10^{-6}$ $P_a$ cm/s and the BBB is highly permeable to it. Chlorpromazine has a permeation value of $5.74 \pm 10^{-7}$ $P_a$ cm/s which indicates a medium permeability of the BBB to this compound. We found that EML76 has a permeation value of $4.98 \pm 0.18 \times 10^{-7}$ $P_a$ cm/s and SPV106 has a value of $3.56 \pm 0.11 \times 10^{-7}$ $P_a$ cm/s, similar to the permeation levels of chlorpromazine, suggesting that these two compounds have both medium permeation ability to the BBB. Chlorpromazine is an FDA-approved drug used in anti-psychotic therapy, such as of schizophrenia [170], with known targets in the CNS [171–173] indicating that compounds with similar BBB crossing abilities should reach the CNS successfully.
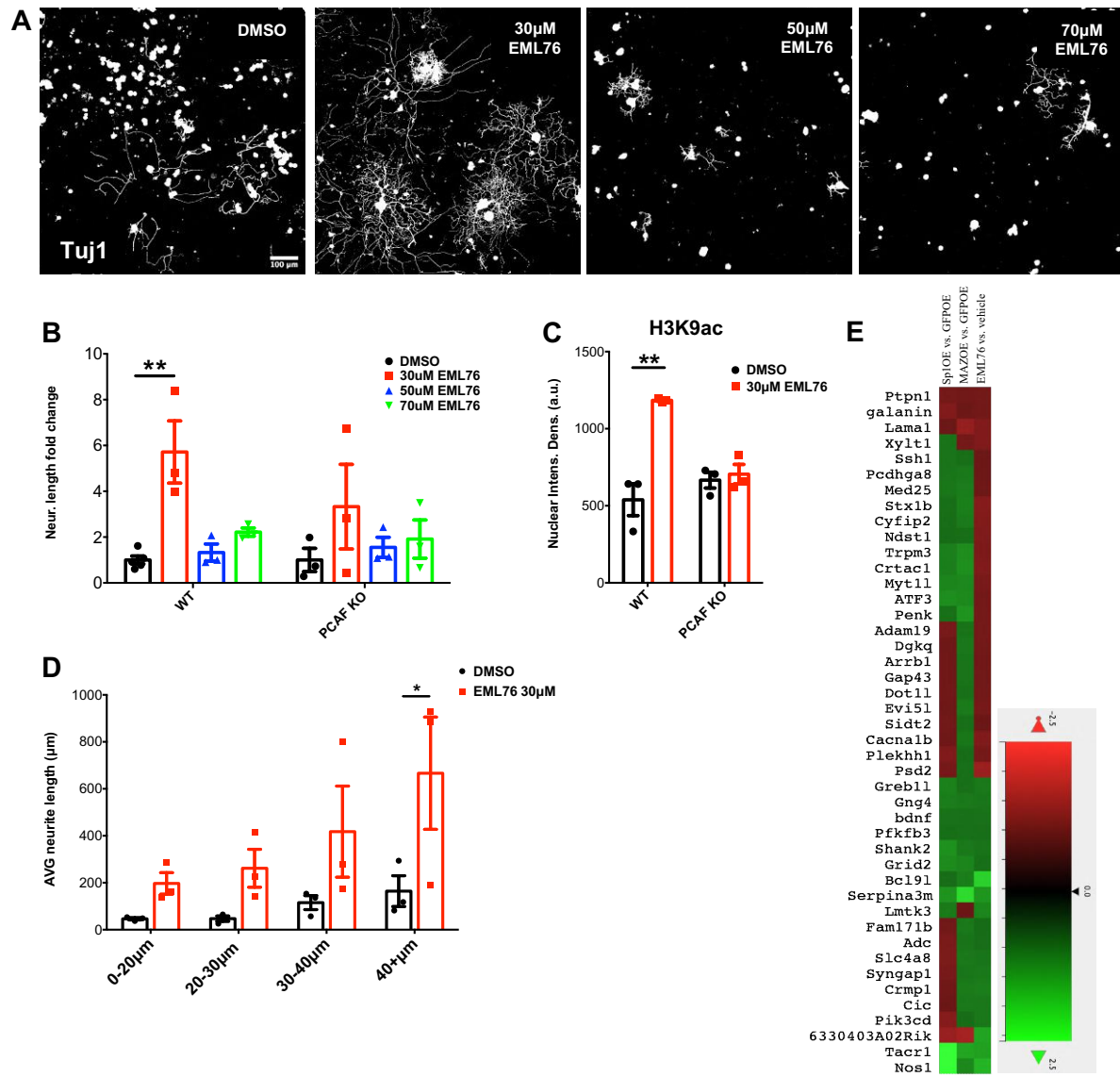
**Figure 3.15. EML76 treatment of mouse WT adult DRG enhances the outgrowth of large diameter DRG.**
**A)** Representative photomicrographs (10x) of cultured DRG treated either with EML76 or DMSO. Scale bar, 100 µm. **B)** Neurite length analysis of cultured WT and PCAF KO DRG treated with EML76 (30-70 µM) compared to DMSO treatment. Two-way ANOVA, mean ± SEM, **p<0.01, N=3. **C)** H3K9ac nuclear intensity density analysis of WT and PCAF KO DRG treated *in vitro* either with DMSO or 30 µM EML76. Two-way ANOVA, mean ± SEM, **p<0.01, N=3. **D)** Diameter analysis of WT DRG treated with 30µM EML76 or DMSO showed that large diameter neurons (40+µm) grow longer neurites when treated with EML76 when compared to the control DRG. Two-way ANOVA, mean ± SEM, **p<0.05, N=3. **E)** Gene expression analysis of the PCAF-RAGs by Nanostring technology comparing all *in vitro* regenerative approaches: Sp1OE, MAZOE (compared to GFPOE) and EML76 treatment (compared to DMSO treatment). Expression fold change ranges from -2.5 (red) to +2.5 (green).

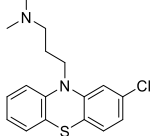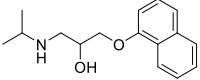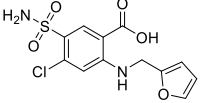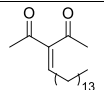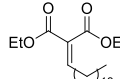| # | Structure | $P_a$ cm/s | | |
|---|---|---|---|---|
| Chlorpromazine | | $5.74 \pm 0.12 \times 10^{-7}$ | ⇨ | Medium permeability |
| Propranolol | | $7.37 \pm 0.04 \times 10^{-6}$ | ⇨ | High permeability |
| Furosemide | | $4.62 \pm 0.21 \times 10^{-8}$ | ⇨ | No permeability |
| EML76 | | $4.98 \pm 0.18 \times 10^{-7}$ | ⇨ | Medium permeability |
| SPV106 | | $3.56 \pm 0.11 \times 10^{-7}$ | ⇨ | Medium permeability |

**Figure 3.16.** *In vitro* **PAMPA BBB permeability assay.** EML76 and SPV106's ability to cross the artificial BBB was compared to chemicals for whom the BBB permeability is already known. Chlorpromazine has medium permeation ability, propanolol has a high one and furosemide does not cross the BBB. EML76 and SPV106 have medium permeation through the BBB, similar to chlorpromazine.

Given that medium permeation allows sufficient chlorpromazine to cross the BBB and previous findings showing that systemic administration of SPV106 is potent to induce changes in the cortex[167], strengthened our hypothesis that systemic use of EML76 *in vivo* could activate PCAF without any prior peripheral lesion or viral overexpression of PCAF in the DRG. First, EML76 was used in an *ex vivo* experiment where the mice were subjected to only a sham injury and then intraperitoneally (i.p.) injected with EML76. Due to the lack of previous knowledge regarding the working *in vivo* concentration of EML76, I used two different concentrations, 20 mg/kg which was similar to what has been previously used for i.p. injections of SPV106[167], and a higher concentration , 40 mg/kg, to test whether it will have a greater effect. 24 hours post-injection all DRG were dissected and cultured on a permissive substrate for 18 hours. Then, DRG were fixed and analyzed for neurite length outgrowth (**Figure 3.17A**). Due to solubility issues of EML76 in high concentrations, we used cottonseed oil (CSO) as a diluent, since EML76 could not be completely dissolved in DMSO. CSO dissolves completely high concentrations of EML76 and has not been reported to have high toxicity when used *in vivo*[174–176].

As shown in Figure 3.17B, C, a single injection of 20 mg/kg was enough to enhance neurite outgrowth of treated cells compared to vehicle-treated cells, with a higher concentration

showing no beneficial outcome. These results indicate that PCAF activation through EML76 increases H3K9ac levels (**Figure 3.17D**). Surprisingly, although 40 mg/kg EML76-treated DRG had increased levels of H3K9ac, it did not result in significantly increased neurite outgrowth.
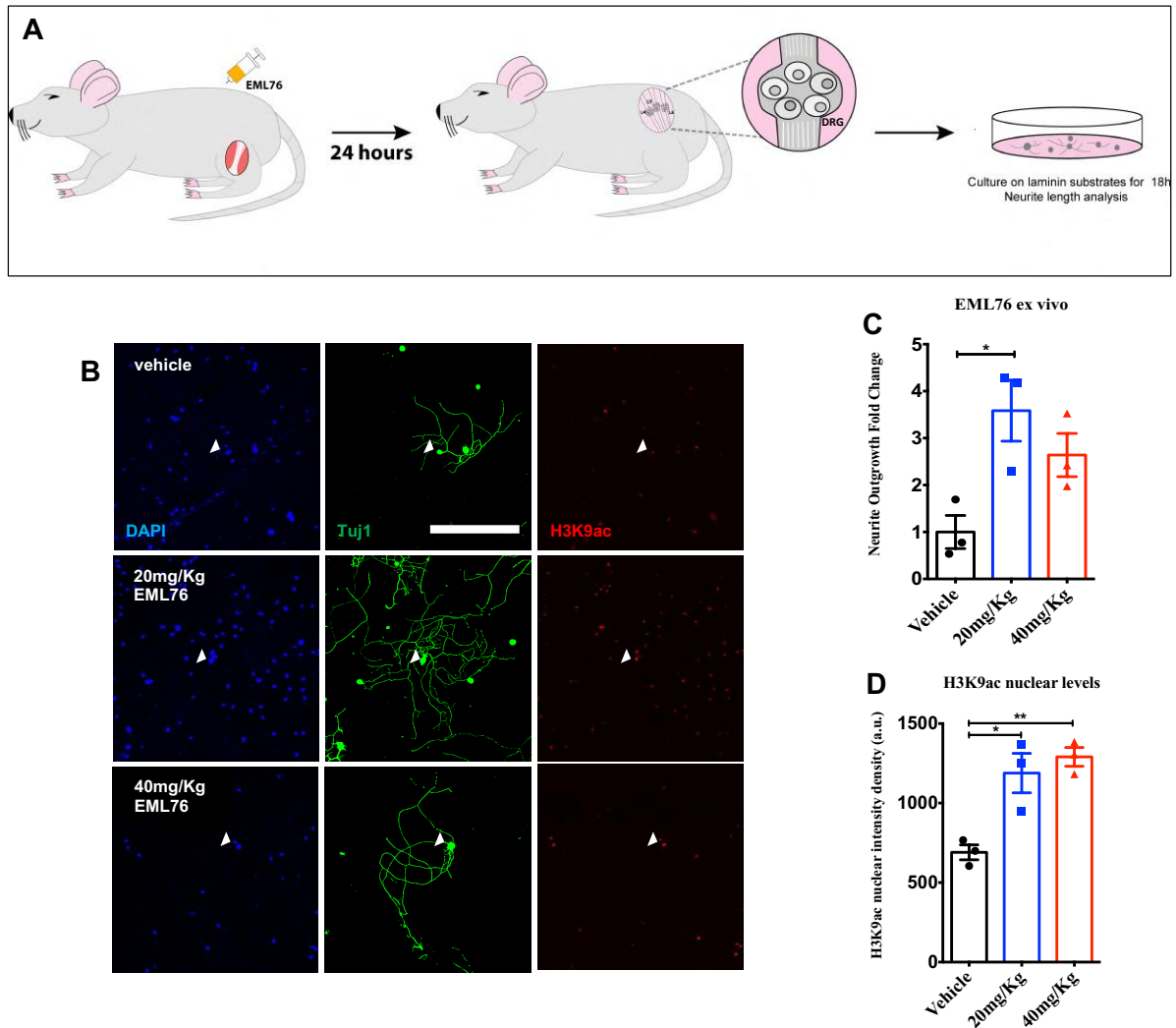


**Figure 3.17. Systemic administration of EML76 in WT CD1 mice can induce epigenetic changes and enhance the neurite outgrowth of *ex vivo* cultured DRG. A)** WT CD1 mice were treated with vehicle (CSO), 20mg/kg or 40mg/kg EML76 for 24 hours then DRG were collected and cultured for 18 hours on permissive (laminin) substrates. Fixed cells were stained for DAPI, βIII-tubulin and H3K9ac. H3K9ac intensity density was measured by Fiji (ImageJ) and the cells were subjected to neurite length analysis. **B)** Representative photomicrographs (10x) of DRG cultured for 18 hours stained for DAPI (blue), βIII-tubulin (green) and H3K9ac (red). Arrowheads indicate the nuclear area of single DRG neurons. Scale bar, 200μm. **C)** Neurite length analysis of *ex vivo* DRG cultures treated with EML76 or vehicle. One-way ANOVA, mean ± SEM, *$p<0.05$, N=3. **D)** H3K9ac nuclear intensity analysis of *ex vivo* DRG cultures treated with EML76 or vehicle. One-way ANOVA, mean ± SEM, *$p<0.05$, **, $p<0.01$, N=3.

### 3.1.11. Systemic administration of EML76 *in vivo* can regulate the PCAF-dependent regenerative signal

Next, I investigated the PCAF-associated regenerative signal after systemic administration of EML76, based upon the aforementioned *in vitro* and *ex vivo* results where EML76 increased neurite outgrowth of treated DRG. For this, sham-injured animals were injected with the effective working dose, 20 mg/kg EML76 or vehicle, after 24 hours lumbar DRG were dissected, fixed and analyzed for nuclear H3K9ac levels and nuclear localization of PCAF, Sp1 and MAZ. Figure 3.18A, B shows a significant increase of nuclear localization of PCAF which is associated with a significant increase of H3K9ac nuclear levels. Interestingly, the nuclear localization of Sp1, but not of MAZ, is also significantly increased.

Lastly, I investigated if a single i.p. injection of EML76 is sufficient to induce genetic changes that lead to the expression of the PCAF-RAGs. Nanostring Technology was used to analyze the expression levels of our top PCAF-RAGs of lumbar DRG dissected from WT animals injected i.p. with 20 mg/Kg. As shown in Figure 3.18E, almost half of the PCAF-RAGs were upregulated after EML76 treatment, suggesting that a single systemic administration of EML76 is sufficient to initiate transcriptional changes in the DRG that remain for 24 hours.

### 3.1.12. Systemic administration of EML76 can increase axonal regeneration of the sciatic nerve after crush

Thus far, we have shown the contribution of PCAF to the peripheral lesion-initiated regenerative signal together with Sp1 and MAZ. Specific RAGs are regulated by PCAF and some of them by Sp1 and MAZ as well. Importantly, it was shown that pharmaceutical activation of PCAF by EML76 *in vitro* and *ex vivo* is able to enhance neurite outgrowth of sensory neurons *in vitro*. However, although systemic administration of EML76 can activate PCAF in DRG, it remained unclear whether this activation could enhance axonal outgrowth of injured neurons *in vivo* as well.

For this, the sciatic nerve crush (SNC) injury model was used, where the sciatic nerve is crushed with forceps, leaving the nerve intact but lacerating the residing axons. WT CD1 mice were subjected to a bilateral SNC for 20 seconds and immediately received an i.p. injection of 20 mg/kg EML76 or vehicle (**Figure 3.19A**). 48 hours post-injury the mice were sacrificed and fixed, and the sciatic nerves were dissected. Sciatic nerves were cryosected longitudinally and stained for SCG10, visualizing regenerating axons exclusively[177,178].
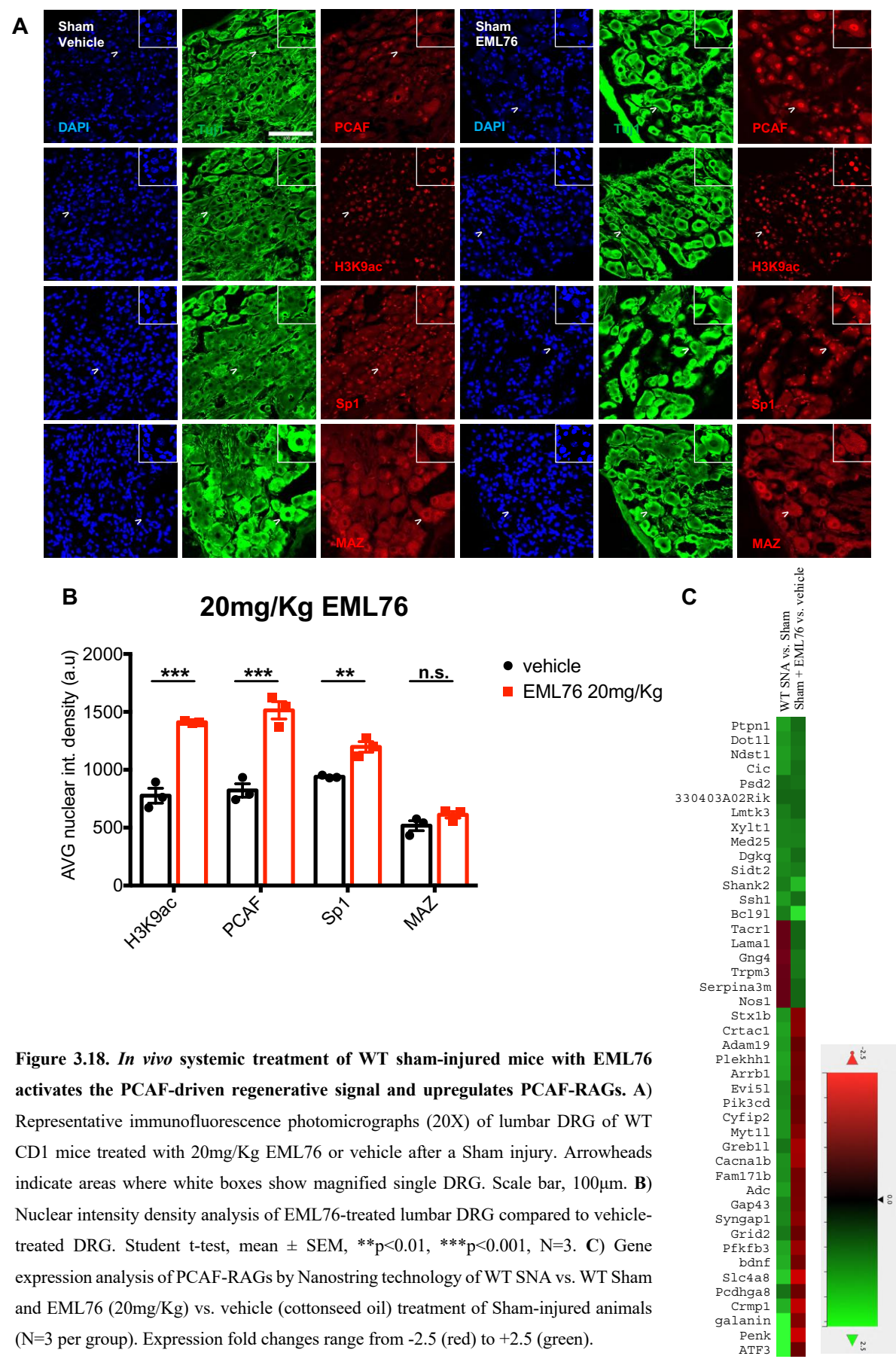
**Figure 3.18.** *In vivo* **systemic treatment of WT sham-injured mice with EML76 activates the PCAF-driven regenerative signal and upregulates PCAF-RAGs. A)** Representative immunofluorescence photomicrographs (20X) of lumbar DRG of WT CD1 mice treated with 20mg/Kg EML76 or vehicle after a Sham injury. Arrowheads indicate areas where white boxes show magnified single DRG. Scale bar, 100μm. **B)** Nuclear intensity density analysis of EML76-treated lumbar DRG compared to vehicle-treated DRG. Student t-test, mean ± SEM, **p<0.01, ***p<0.001, N=3. **C)** Gene expression analysis of PCAF-RAGs by Nanostring technology of WT SNA vs. WT Sham and EML76 (20mg/Kg) vs. vehicle (cottonseed oil) treatment of Sham-injured animals (N=3 per group). Expression fold changes range from -2.5 (red) to +2.5 (green).

Then, the intensity density of SCG10 was measured across the length of the sciatic nerve at 1 mm intervals distally to the crush site, with each point being compared to the intensity density at the crush site. Given that SCG10 is expressed only by regenerating axons[179], the percentage of regenerating axons was calculated as a ratio between the intensity density of SCG10 from 1-5 mm distally to the crush site and the intensity density of SCG10 proximal to the crush site.

As shown in Figure 3.19B, C, EML76 treatment of mice subjected to a sciatic nerve crush resulted in a significantly higher number of axons regenerating; even growing from 3 to 5 mm past the crush site. The control group which received the crush and CSO had also regenerating axons, but only a small portion of the regenerating axons reached 5mm beyond the crush site. As indicated by the regenerative index, 50% of the regenerated axons treated with EML76 reached 2.5 mm beyond the injury site, while their control counterparts only reached 1.5 mm. Apparently, a single injection of EML76 was enough to accelerate the regeneration of peripheral axons and promote outgrowth of a higher number of neurons surpassing the regenerative levels of the control.

Thus far, I have shown that Sp1 or MAZ overexpression *in vitro* enhances the axonal outgrowth of cultured DRG. Additionally, it was found that the regenerative potential of Sp1 and MAZ is dependent upon PCAF, as no enhanced outgrowth was observed after overexpression of either Sp1 or MAZ in PCAF KO DRG. Based upon these results and the fact that EML76 was able to enhance regeneration of the crushed sciatic nerve through PCAF, we wondered whether its regenerative capacity could be enhanced by the concomitant overexpression of Sp1 or MAZ in lumbar DRG. For this, I used adeno-associated viruses (AAVs) of serotype 5 expressing either GFP or Sp1 (see Materials, section 2.1.5, Table 2.14). Viruses were injected directly into the sciatic nerves 3 weeks prior to a sciatic nerve (2 μl of each virus). Unfortunately, it was found that 3 weeks were not enough for sufficient expression of the genes of interest in the respective DRGs (data not shown). To rule out that the lack of expression was not due to deficit viruses, I used the viruses on cultured DRG. They were transduced with two different titers of viruses. For GFP, I used $8.5 \times 10^9$ Genome Copies (GC) (1 μl) and $17 \times 10^9$ GC (2 μl) and for Sp1, I used $1.4 \times 10^9$ GC (1 μl) and $2.8 \times 10^9$ GC (2 μl). 7 days post-transduction, DRG were fixed and stained for GFP in order to count the transduction efficiency of the viruses *in vitro*.
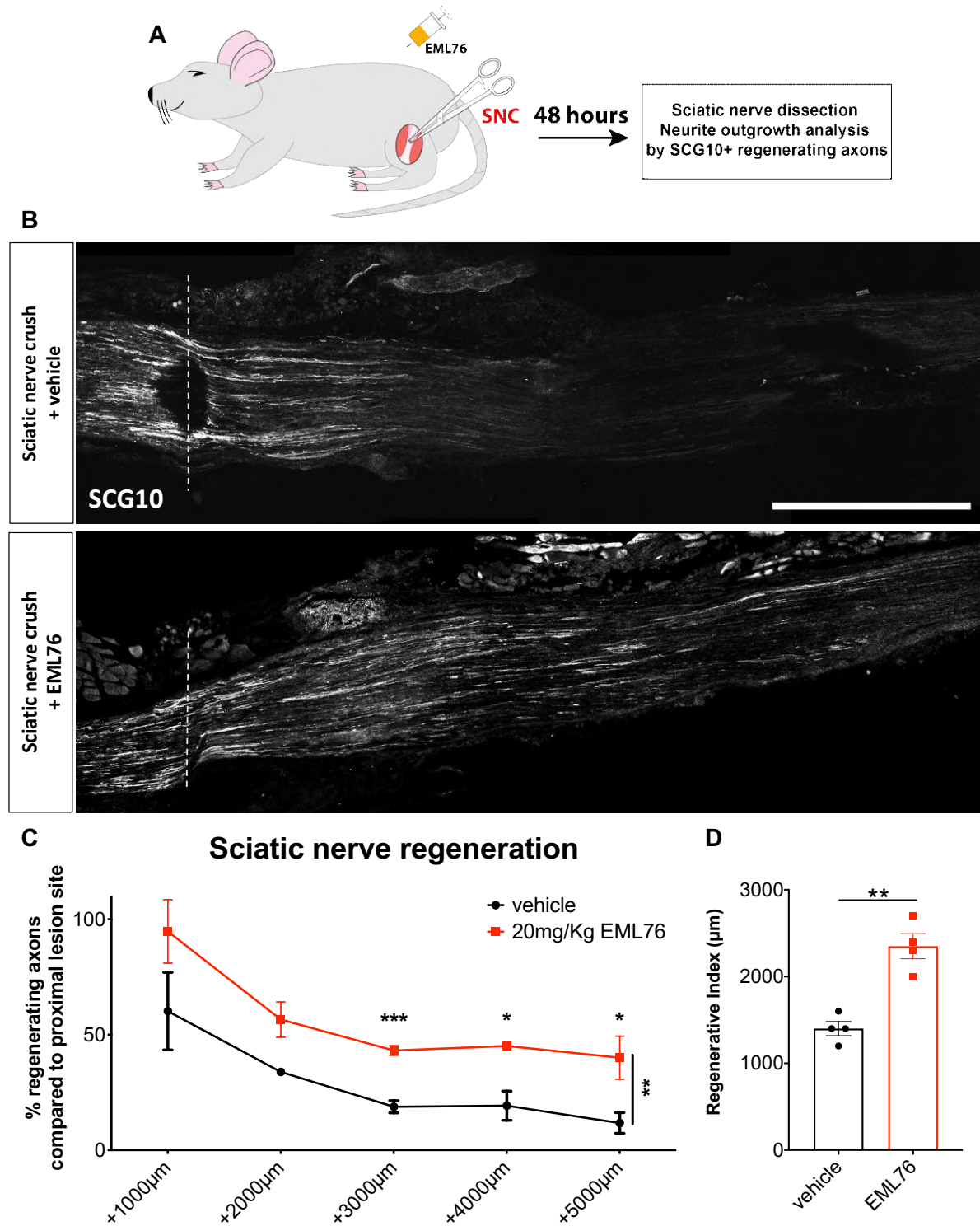
**Figure 3.19. Systemic EML76 administration can increase the axonal regeneration of the injured sciatic nerve. A)** WT mice were subjected to sciatic nerve crush and immediately received a single i.p. injection of 20 mg/kg EML76 or vehicle (cottonseed oil). 48 post-injury the animals were sacrificed, their sciatic nerves were dissected and stained for SCG10 staining regenerating axons, **B)** Representative photomicrographs (10x) of sciatic nerves stained for SCG10. Images were stitched together using the stitching plugin of Fiji (ImageJ). Dashed lines indicate the crush site. Scale bar, 1cm. **C)** Axonal regeneration percentage analysis was performed by measuring

the intensity density of SCG10 (regenerating axons) at 1mm intervals and comparing it to the intensity density proximal to the crush site. Intensity density values were corrected for background intensity. Repeated measures Two-way ANOVA, Fisher's LSD multiple comparisons test, mean ± SEM, *p<0.05, ***p<0.001. N=4, **D**) The regenerative index shows the distance from the crush site to the location where SCG10 level is 50% of the level proximal to the crush site. Student's t-test, mean ± SEM, **p<0.01, N=4.

This pilot experiment showed that 7 days post-transduction with the GFP- or Sp1-expressing AAVs, the lower titers resulted in ~60% GFP-AAV transduction of DRG and ~20% Sp1-AAV transduction of DRG. The higher concentration (more relevant to what was used *in vivo*) resulted in ~75% GFP-AAV transduction efficiency while for Sp1-AAVs the efficiency was the same (data not shown). Seemingly, there is no obvious deficit with the viruses although there is a significant difference between the two virus' transduction efficiencies. The size of the viral constructs is also different. AAV5-hSYN1-eGFP-P2A-mSp1-WPRE3 is significantly larger than the AAV5-hSYN1-eGFP-WPRE since the open reading frame of Sp1 is 7706 bp and this might also affect the transduction efficiency of AAV-Sp1. In the future, since timing seems to be important for how efficiently the viruses are expressed, it will be examined if a longer incubation time (more than 3 weeks) would allow for a sufficient expression of the GFP and Sp1 constructs.

# Results – Part II

## 3.2 Results – Part II

In conjunction with examining the underlying mechanisms of regenerative injury response of the PNS to be able to replicate with pharmaceutical interventions, I also examined the neuronal response to extrinsic stimuli. In particular, I examined if centrally located nerves have the intrinsic capacity to respond to mechanical stimulation as peripherally located nerves. Fischer-344 rats were used for dissection of lumbar DRG connected to either their peripheral (sciatic nerve) or central branches and stretched using an in-house built bioreactor. It should be noted that parts of this section have been used in a manuscript that is currently under review at *Cells* journal with Manuscript ID: cells-1040747 and Title: Cyclic stretch of either PNS or CNS located nerves can stimulate neurite outgrowth.

### 3.2.1. An in-house built bioreactor was used to apply mechanical stretch to DRG-nerve explants

In order to investigate whether mechanical loading would affect the regenerative capacity of subjected DRG, a bioreactor was built with the assistance of Mr. Wolfgang Roth (Experimental Neurorehabilitation, Universitätsklinikum Heidelberg, Heidelberg, Germany). A hypoxia incubator (Invivo2 400 hypoxia workstation, Ruskin, kindly loaned by Prof. Wiltrud Richter) was modified to achieve normal culture conditions with constant supply of 5% $CO_2$ and able to host the stretch bioreactor. The nitrogen and compressed air supply was replaced by a tank of compressed 25% $O_2$/75% N controlled by a gas exchanger (**Figure 3.20C**)

More specifically, as shown in Figure 3.20, the window of the hypoxia incubator (**Figure 3.20B**) was replaced by a new one, having a door to allow entry to the inner part of the incubator and an opening where the oscillator (**Figure 3.20D, E**) could enter from outside with its metal arm and attach to the bioreactor (**Figure 3.20F**). The bioreactor consisted of two metal plates (a and b), placed on a metal rail. Plate (a) was fixed on the rail and metal plate (b) was able to move back and forth when attached to the metal arm of the oscillator. Each plate had small square openings where the polyetheretherketone (PEEK) scaffolds could be fixed with metal screws. PEEK was chosen due to its high durability and low cytotoxicity [180,181]. PEEK scaffolds were kept 1 cm apart and nerve explants were glued onto them. Once glued, the nerves were kept in a metal boat containing the culture medium and the bioreactor was fixed to the oscillator. The nerve explants of the static control group were glued on a petri dish

instead and kept in the same incubator for as long as the stretch lasted without receiving any mechanical loading. The cyclic movement of the oscillator was driven by the controller



**Figure 3.20. In-house built bioreactor setup**. **A**) The controller connected to GalilTools software and the oscillator. **B**) The incubator chamber keeping constant temperature, humidity and $CO_2$ conditions. **C**) The gas mixer analyzing the air constitution of the incubator chamber, 5% $CO_2$. **D**) The bioreactor mounted on the oscillator. **E**) The oscillator, the mechanical part sits outside the incubator chamber connected to the controller, while the metal bar of the oscillator is connected to the mobile metal plate of the bioreactor. **F**) The two metal plates have openings into which the PEEK bars fit. The metal plate (b) can move back and forth, while the metal plate (a) is fixed to the stage and the metal rail.

(**Figure 3.20A**), which converts the digital signal from the connected computer to the cyclic movement of the oscillator. The program used to define the different parameters of the oscillatory movement of the oscillator is called GalilTools (Galil Inc.).

With the incubator and oscillator built, the next step was to establish the DRG-nerve explant isolation and culture parameters. To develop our DRG-nerve explant model, I first examined which part of the DRG, and nerve could be dissected consistently, without damage and withstand strain. I began with the central side from DRG L4 and L5 of Fischer-344 rats. I could consistently extract the dorsal roots prior to the dorsal root entry zone (~2.5cm residing within the vertebral column) without issue. An equivalent length was taken from the peripheral sciatic nerve (**Figure 3.21A**). It should be noted that the anatomy of either side is not equivalent since the sciatic nerve is bifurcating into L4 and L5 with each of these DRG projecting thinner central branches that are not fused into one common nerve, such as the sciatic nerve.

The nerves were fixed to the bioreactor without additional strain directly on the DRG itself. This was accomplished with the use of two PEEK bars and acrylic adhesive (**Figure 3.21B**). Next, I optimized the growth media that allowed for explant viability over a period of

time of mechanical strain prior to DRG culture as it was observed that mechanical stretch of explants longer than 3 hours did not allow for survival (data not shown), which limited the time for cyclic stretch and recovery time. Finally, it was important to establish the percent of stretch that would result in neurite length extension. The various parameters tested are listed in Table 3.2.
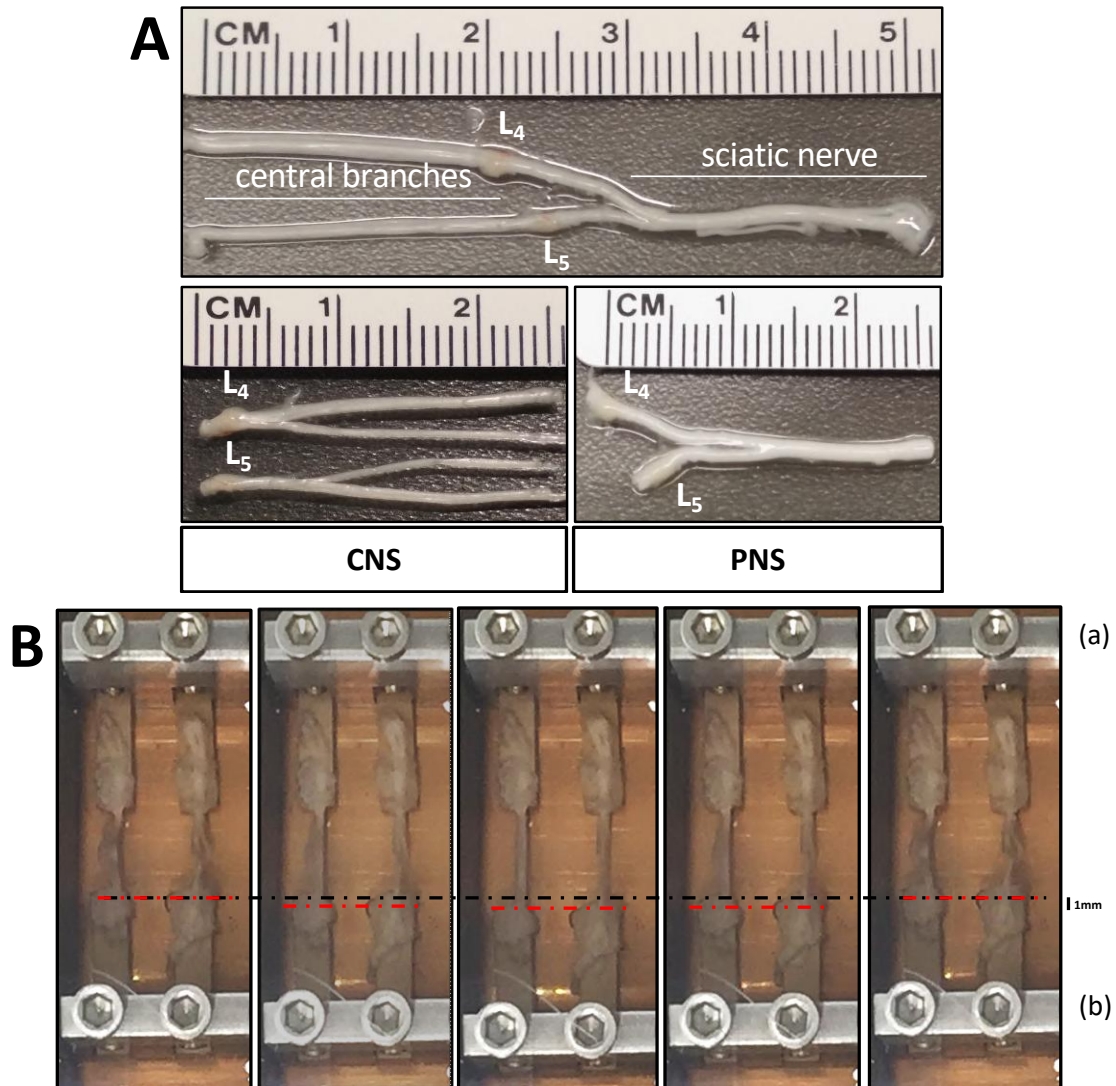


**Figure 3.21. Sciatic nerve and central DRG branches dissection and stretch**. **A**) ~2.5 cm of the sciatic nerve connected to both L4 and L5 DRG was dissected. Similarly, ~2.5 cm of the central branches of the L4 and L5 DRG were dissected and subjected to mechanical stretch. **B**) The dissected DRG-nerve explants were glued onto PEEK bars fixed on the metal plates of the bioreactor. The PEEK bars had a 1 cm distance between each other. Different stretch amplitudes and frequencies were applied as the metal (b) moved towards and away from the plate (a) while in the DRG culture medium. This figure depicts 10% stretch.

| % Stretch | Time of stretch | Recovery time |
|---|---|---|
| 2.5%, 0.5Hz | 3h | 0h |
| 5%, 0.5Hz | 6h | 0h |
| 5%, 0.5Hz | 3h | 3h |
| 5%, 0.5Hz | 3h | 0h |
| 10%, 0.25Hz | 3h | 0h |
| 10%, 0.5Hz | 3h | 0h |
| 20%, 0.25Hz | 3h | 0h |
| 20%, 0.5Hz | 3h | 0h |

**Table 3.2. Various mechanical stretch conditions tested**. Sciatic nerves or central branches connected to their respective lumbar DRG were stretched using specific amplitudes (2.5 - 20%) and two different frequencies (0.25 Hz and 0.5Hz). The optimal explant culture conditions was found to be 3 hours in the bioreactor, followed by no recovery time and direct DRG dissection and culture.

## 3.2.2. 20% stretch can cause tearing damage to the subjected nerves, while 10% stretch has no apparent morphological changes

Upon analysis of the aforementioned stretch parameters, I, firstly, examined whether the morphological physiology of the nerves is affected by the mechanical stretch. For this, the longitudinally sectioned nerves were stained with H&E and examined with a brightfield microscope. In general, nerves consists of an outer collagen layer surrounding the whole nerve, called perineurium; the epineurium, which surrounds individual fascicles; and lastly the endoneurium which is composed mostly by neuronal axons, myelin Schwann cells and vessels ensheathed by connective tissue [182]. It should be noted that the epineurium is not very visible on the central nerves. These nerves are surrounded by meninges instead, but these layers are removed when the central nerves are dissected. Figure 3.22 shows sciatic nerves (A, B, C) and central nerves (D, E, F) either after no stretch (A, D), 10% mechanical stretch (B, E) or 20% mechanical stretch (C, F) longitudinally dissected and stained with H&E.

As expected, the static controls have a very dense and thick epineurium and their overall morphology appears intact. The first to be affected by the stretch of nerves is the epineurium which detaches from the perineurium compared to the static controls. 10% mechanical stretch both of PNS and CNS explants exhibit normal morphological cytoarchitecture of the perineurium and the endoneurium. Notably, most of the damage was caused by 20% mechanical loading was both in the epineurium (sciatic nerves) and the perineurium (sciatic nerves and central nerves), while in the central branches it even caused tear damage to the endoneurium (**Figure 3.22F**).
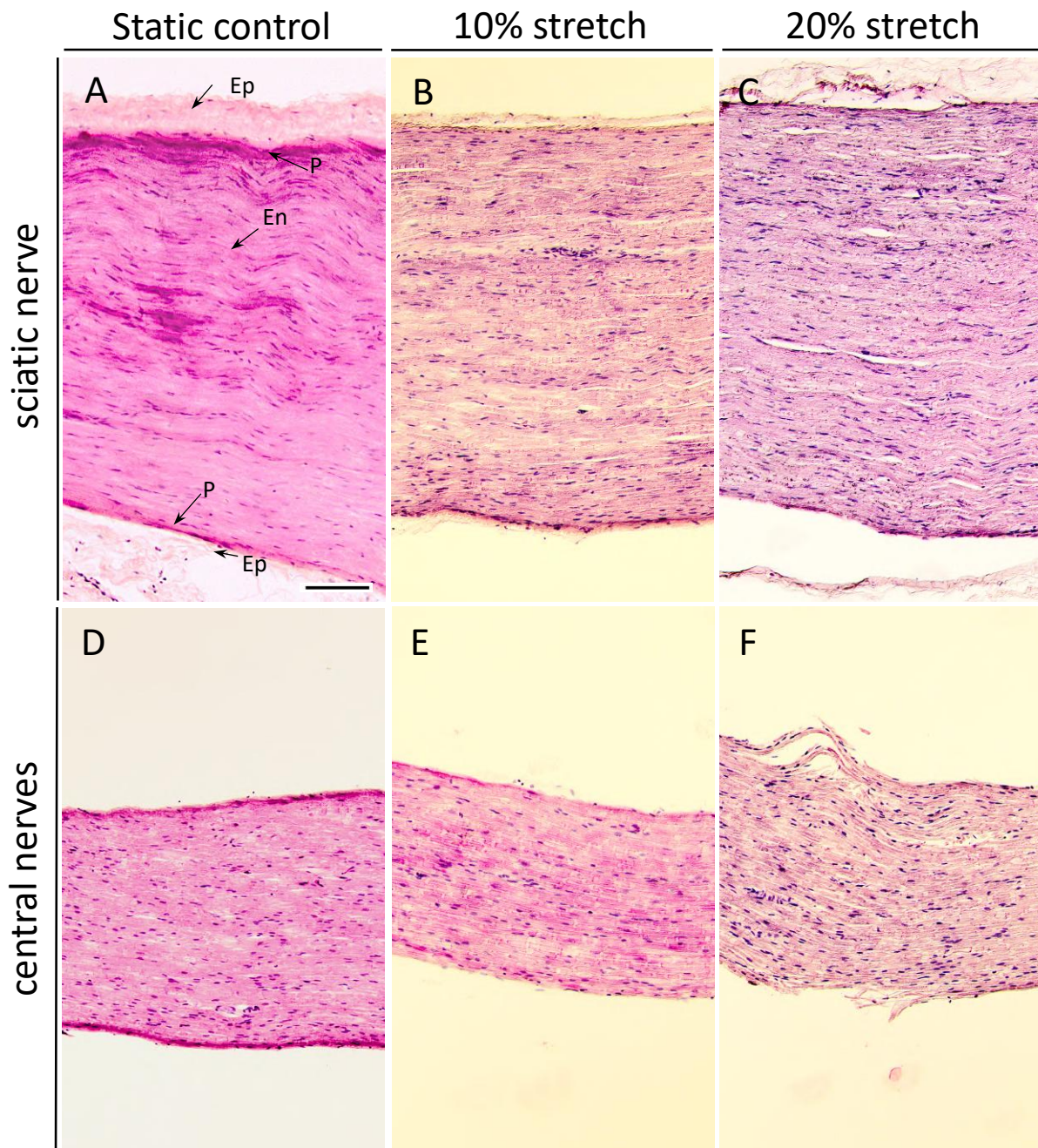
**Figure 3.22**. **3 hours of 10% stretch does not significantly alter the microarchitecture of the nerve, although 20% stretch does. A-F)** Photomicrographs (10x) of H&E staining of sciatic nerves (**A-C**) and central nerves (**D-E**). Nerves were subjected to either no stretch (**A, D**) 10% (**B, E**) or 20% (**C, F**) mechanical stretch. Arrows in (**A**) indicate the epineurium (Ep), perineurium (P) and endoneurium (En). The epineurium (sciatic nerves) is densely formed in the static controls but upon 20% stretch begins to unravel. The perineurium, a protective sheath covering nerve fascicles, was found to slowly thin with increasing amounts of stretch, with some tears in the 20% samples. Importantly, the naturally occurring nerve undulation noted in the static control is progressively lost upon mechanical stretch. Scale bar, 500μm.

### 3.2.3. 10% 0.5Hz mechanical stretch of central branches can enhance neurite outgrowth of sensory neurons *in vitro*

Given that 10% stretch does not cause any drastic damage to the subjected nerves, I investigated whether mechanical stimulation could enhance axonal outgrowth *in vitro*. Sciatic nerve-L4/L5 DRG or central nerves-L4/L5 DRG explants were subjected to 3 hours of stretch, with an amplitude of 10% (1 mm dislocation of 1 cm-long nerve) and a frequency of 0.5 Hz. Interestingly, it was found that mechanical stimulation of the central nerves connected to their respective DRG led to enhanced neurite outgrowth of DRG compared to the control (**Figure 3.23A, B**). Although the trend appeared similar, the sciatic nerve stretch did not lead to significantly enhanced neurite outgrowth (**Figure 3.23A, B**).

The DRG is a heterogeneous population of neurons (nociceptive, mechanoreceptive and proprioceptive neurons) that partially sort via diameter size. Therefore, we questioned whether all DRG neurons respond to mechanical stimulation or only a subpopulation of neurons are affected by mechanical strain. Applying diameter analysis to the cultured DRG, it was found that the large diameter neurons (40+μm), which represents mostly mechanoreceptor and proprioceptive neurons, of the mechanically loaded groups had increased outgrowth compared to the static controls (**Figure 3.23C**).

### 3.2.4. 10% 0.5Hz mechanical stretch of central branches can stimulate the initiation of outgrowth in cultured DRG

Additionally, it was observed that mechanical loading induced the switch from non-growing neurons to growing neurons in the CNS explants (**Figure 3.24A**). *In vitro,* not all of the cultured DRG start growing although it is not clear why some do, and others do not, even when they are plated on permissive substrates. Apparently, mechanical stretch of the central nerves connected to their respective DRG facilitates the initiation of their axonal growth. Moreover, those that make up the growing population of neurons represent the medium to large diameter neurons compared to the small-diameter neurons of the non-growing group (**Figure 3.24B**).
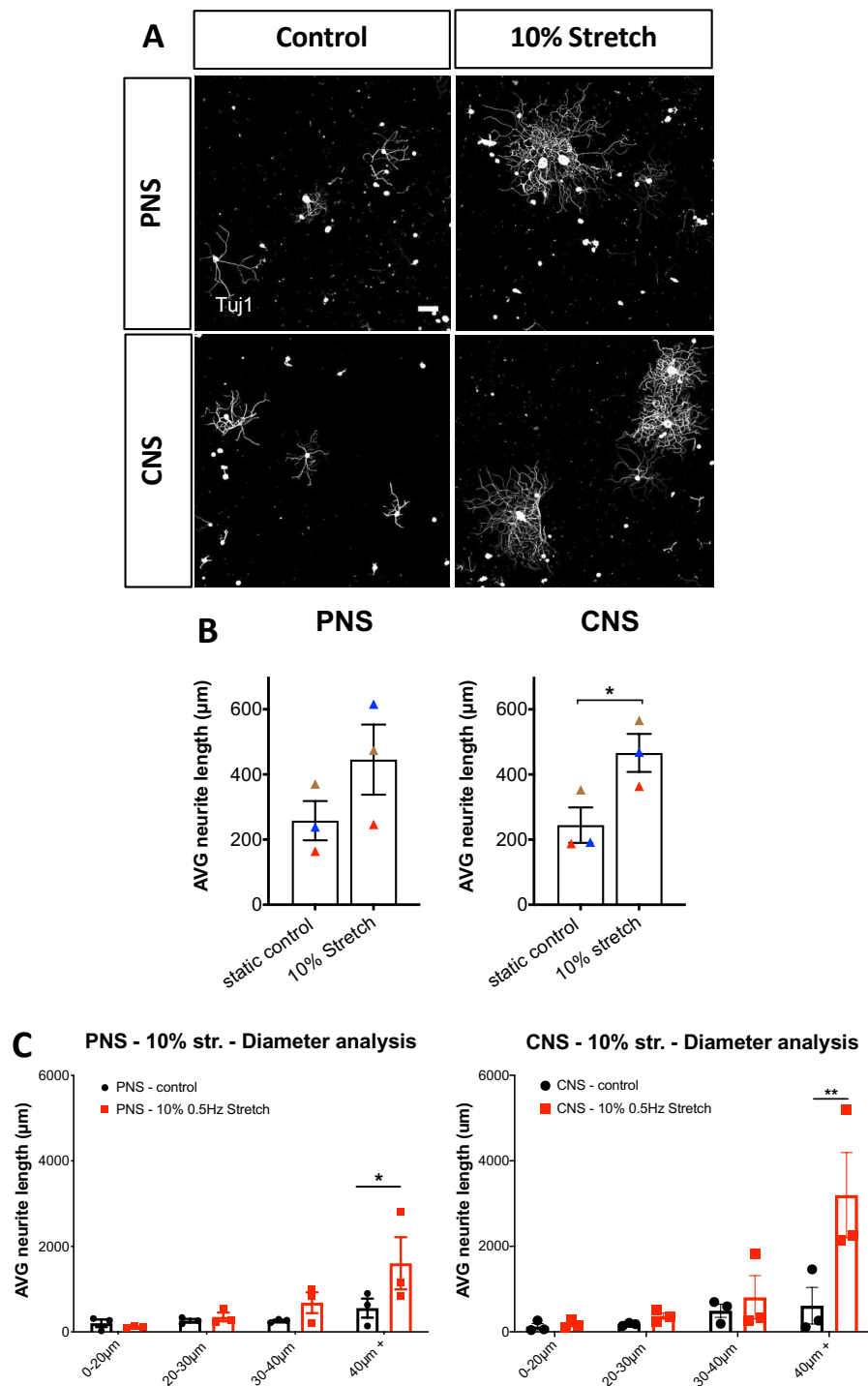
**Figure 3.23. 10% 0.5 Hz stretch of central nerves-DRG explants can enhance neurite outgrowth of respective cultured DRG neurons.** Three hours following mechanical stretch of either the sciatic nerve connected to L4-L5 DRG or connected to their respective central nerves, DRG were dissected and cultured for 18 hours on laminin substrates. **A)** Immunohistochemical staining of βIII-tubulin (Tuj1) was used to trace all neurites of the DRG. Scale bar, 100μm, **B)** 10% mechanical stretch with a frequency of 0.5Hz was able to enhance axonal outgrowth of DRG derived from the CNS explant but not from the PNS explant. Two-tail paired Student t-test, mean±SEM, *p<0.05, N=3, **C)** Diameter analysis of DRG outgrowth comparing the static controls to the stretched explants shows the largest neurons responding to stretch from both the PNS and CNS stretch samples. Two-way ANOVA, mean ± SEM, * p<0.05, ** p<0.01, N=3.

**A**



**B**
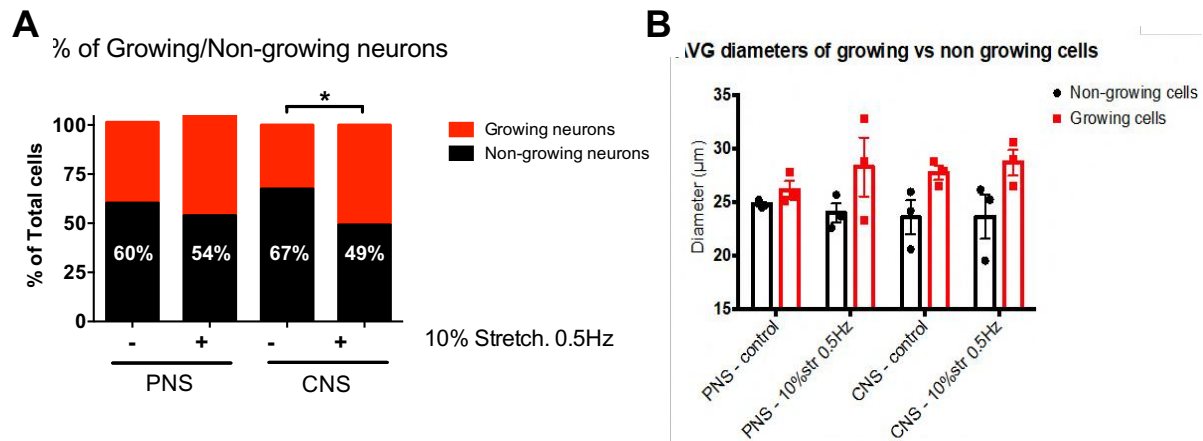


**Figure 3.24. Mechanical stretch promotes DRG neurite outgrowth initiation of CNS stretched nerves *ex vivo*. A**) Quantification of growing vs non-growing neurons in each group showed that non-growing neurons decreased in the CNS group upon stretch. Two-way ANOVA, mean ± SEM, * $p<0.05$, N=3, **B**) Examination of the average size of growing versus non-growing neurons shows non-growing neurons to be consistently of smaller diameters than growing neurons.

## 3.2.5. 20% mechanical stretch has detrimental effects on neurite outgrowth of cultured DRG

Given that high levels of mechanical stretch, over 15%, have been associated to neuropathic pain[183], we questioned whether 20% mechanical stretch would increase the outgrowth of nociceptive neurons, which in general is represented by small diameter DRG. Interestingly, it was shown that 20% stretch not only did not enhance the neurite outgrowth of DRG neurons of stretched nerves but it had the opposite effect (**Figure 3.25**). This was further supported by our previous H&E results, showing that 20% mechanical stretch leads to tearing damage of the subjected nerve which could explain the dramatic impact of high levels of mechanical stretch on DRG outgrowth.

## 3.2.6. TrkC+ neurons respond to mechanical stretch but CGRP+ neurons do not

As previously discussed, the DRG is a heterogeneous population of sensory neurons that consist of differently sized neurons, having different properties and responding to different modalities (touch, pain, itch, proprioception). One way to distinguish between these neurons
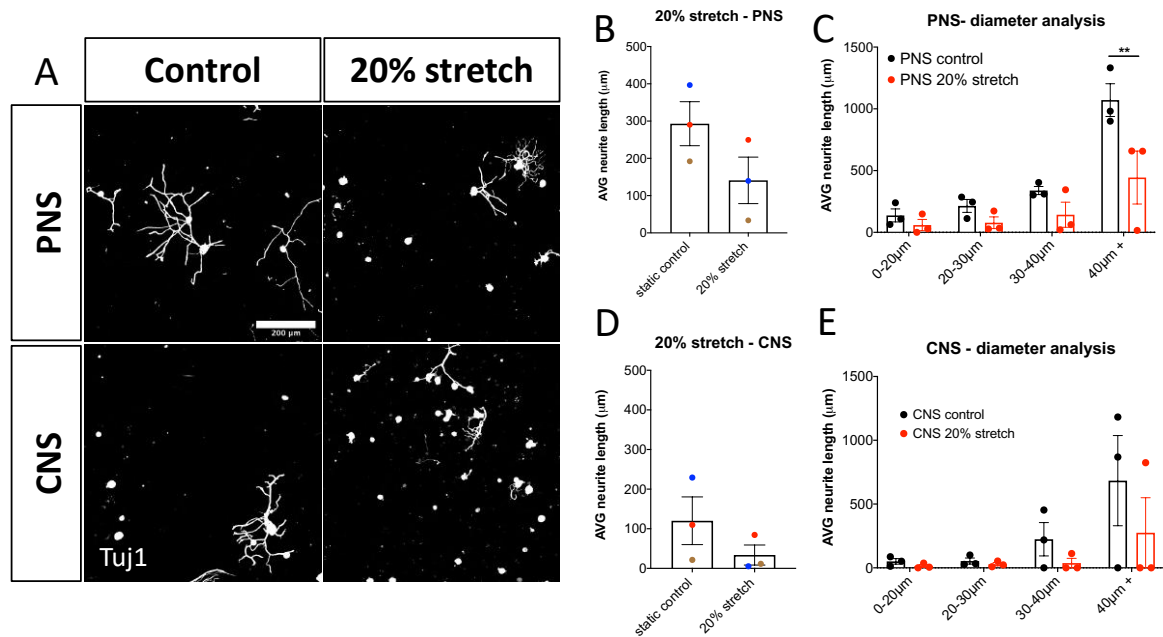
**Figure 3.25. 20% 0.5 Hz stretch has a negative impact on the neurite outgrowth of DRG neurons *in vitro* . A)** Representative photomicrographs (10x) of cultured rat DRG following 20% 0.5 Hz stretch or no stretch and stained for βIII-tubulin (Tuj1). Scale bar, 200μm. **B)** Neurite length analysis of DRG cultured after 20% 0.5Hz stretch of the PNS-nerve explant compared to static control. Stretch appeared to have a negative impact on the neurite outgrowth although not statistically significant. Student's t-test, mean ± SEM, N=3. **C)** Diameter analysis shows a significant reduction in the outgrowth of large diameter neurons after 20% stretch of the PNS-nerve explant. Two-way ANOVA, mean ± SEM, **$p<0.01$, N=3 **D)** Neurite length analysis of DRG cultured after 20% 0.5Hz stretch of the CNS-nerve explant compared to static control showed no significant difference between the stretched and the static control groups. Student's t-test, mean ± SEM, N=3. **E)** Diameter analysis shows a reduction trend in the outgrowth of all DRG populations after 20% stretch of the CNS-nerve explant, Two-way ANOVA, mean ± SEM, N=3.

is by markers expressed only by a specific sub-population of the DRG. Thus far, it has been shown that mild mechanical stretch can enhance the axonal outgrowth *in vitro* of the large diameter neurons derived from both the PNS- and the CNS-DRG nerve explants (**Figure 3.23C**). Although, it is generally accepted that the medium to large diameter neurons represent mainly the proprioceptive and mechanoreceptor sensory neurons while the small to medium diameter neurons are the nociceptive ones [184,185], it still remained unclear which specific population responded to our mechanical loading of the nerves.

Thus, upon 10% 0.5 Hz mechanical stretch, DRG cultured *in vitro* were stained for Neurotrophic Receptor Tyrosine Kinase 3 (TrkC), the receptor for neurotrophin-3 (NT-3), which is expressed by proprioceptive neurons and low-threshold mechanoreceptors [186–188]. For neurite length analysis, only double positive neurons for TrkC and βIII-tubulin were analyzed

to include only the proprioceptive neurons and the low-threshold mechanoreceptors, which mediate innocuous touch. Importantly, as shown in Figure 3.26, 10% 0.5Hz mechanical stretch of PNS-DRG explants was sufficient to increase the axonal outgrowth of cultured DRG compared to their static control. For the CNS, although there may be a trend there was no significant difference due to the high variability of the control group. Surprisingly, the difference observed here was lost, when a frequency of 0.25 Hz was used instead of 0.5 Hz, indicating the significance of the frequency apart from the amplitude of the cyclic stretch, although the mechanism behind this remains unclear.

Previously, hindlimb stretching of spinal cord injured rats led to increased sprouting of nociceptive fibers in the dorsal horn of the spinal cord[189]. Before, we investigated if small to medium diameter neurons would grow more upon 20% mechanical stretch, that is associated to neuropathic pain. To be more specific on which neurons are targeted, I stained DRG following stretch or static conditions with the antibody for calcitonin gene-related peptide (CGRP), a marker of peptidergic nociceptive neurons (**Figure 3.26A**). Under our standard amplitude (10%) conditions, axonal outgrowth of CGRP+ neurons were not altered from either PNS or CNS stretch at either frequency examined (**Figure 3.26C**). Notably, Figure 3.26C shows that no changes were observed.

### 3.2.7. Mechanical loading does not significantly increase the neurite outgrowth of neurofilament 200 (NF200) positive neurons

10% 0.5 Hz mechanical stretch affected large-diameter neurons, which does not include only proprioceptive neurons but also TrkB+ mechanosensitive neurons [190]. However, this proved difficult as the TrkB marker did not work in immunocytochemistry as it does on tissues with immunohistochemistry. Therefore, we turned to staining with neurofilament 200 (NF200), which stains all A myelinated fibers [191,192]. Although we observed an overall trend, significance was not reached, which may be due to the high variability with this staining that contains medium Aγ peptidergic nociceptors and medium to large Aβ mechanoreceptors as well as large Aα proprioceptors (**Figure 3.27**). Interestingly, when diameter analysis was performed, the 30-40 μm group of the PNS nerve-DRG explant did respond with increased neurite outgrowth. It should be noted that explant and primary culture conditions coupled with the lower cell numbers in the medium to large diameter cell populations leads to high variability between biological replicates.

**A**

**B**

PNS - TrkC+ neurons

CNS - TrkC+ neurons

- static control
- 0.25Hz
- 0.5Hz

**C**

PNS - CGRP+ neurons

CNS - CGRP+ neurons
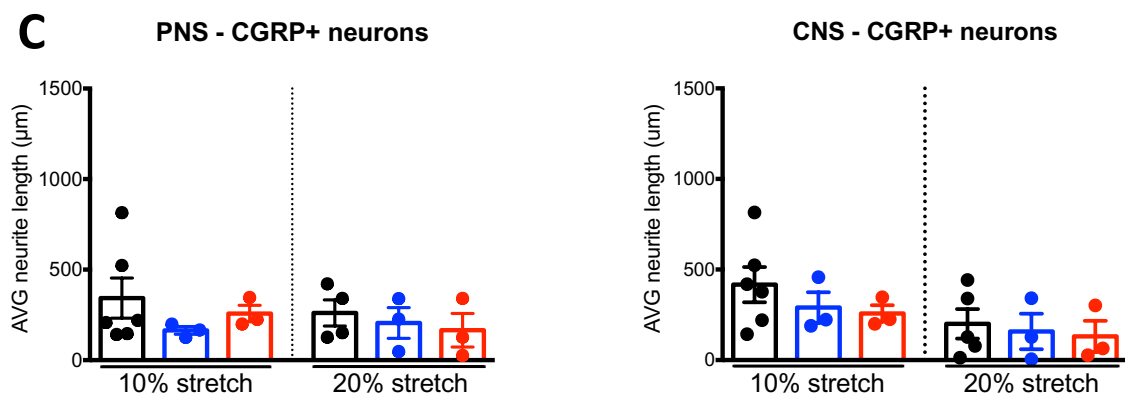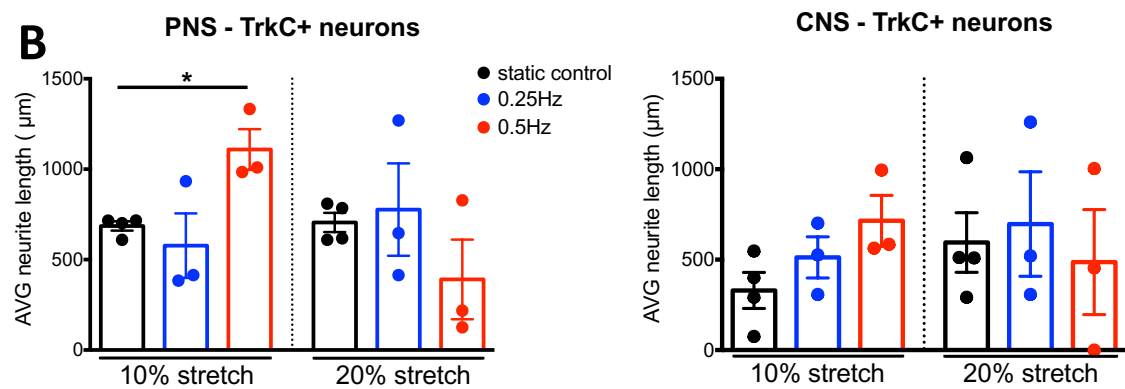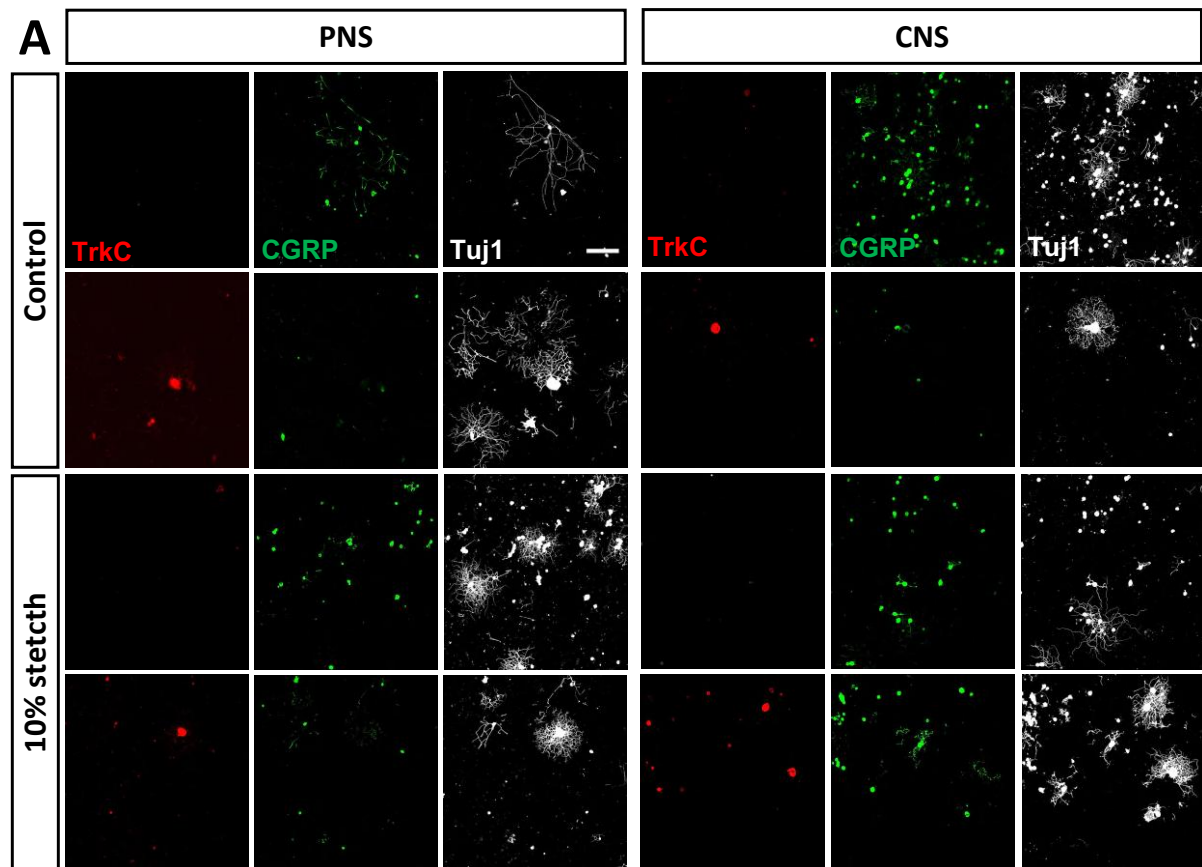
**Figure 3.26. Response of TrkC+ and CGRP+ DRG neurons to mechanical stretch. A)** Immunocytochemical analysis of DRG stained either for TrkC (green) or CGRP (red) after no stretch or mechanical stretch (10% 0.5Hz). Scale bar, 200μm, **B)** Neurite length analysis of TrkC+ DRG upon mechanical stretch with an amplitude of either 10% or 20% and frequency of 0.25Hz or 0.5Hz showed enhanced outgrowth of PNS 10% stretched TrkC+ neurons with a frequency of 0.5Hz. Two-way ANOVA, mean ± SEM, *p<0.05, **C)** Neurite length analysis of CGRP+ DRG upon mechanical stretch with an amplitude of either 10% or 20% and frequency of 0.25Hz or 0.5Hz showed no difference between stretched and the static control groups. Two-way ANOVA, mean ± SEM.
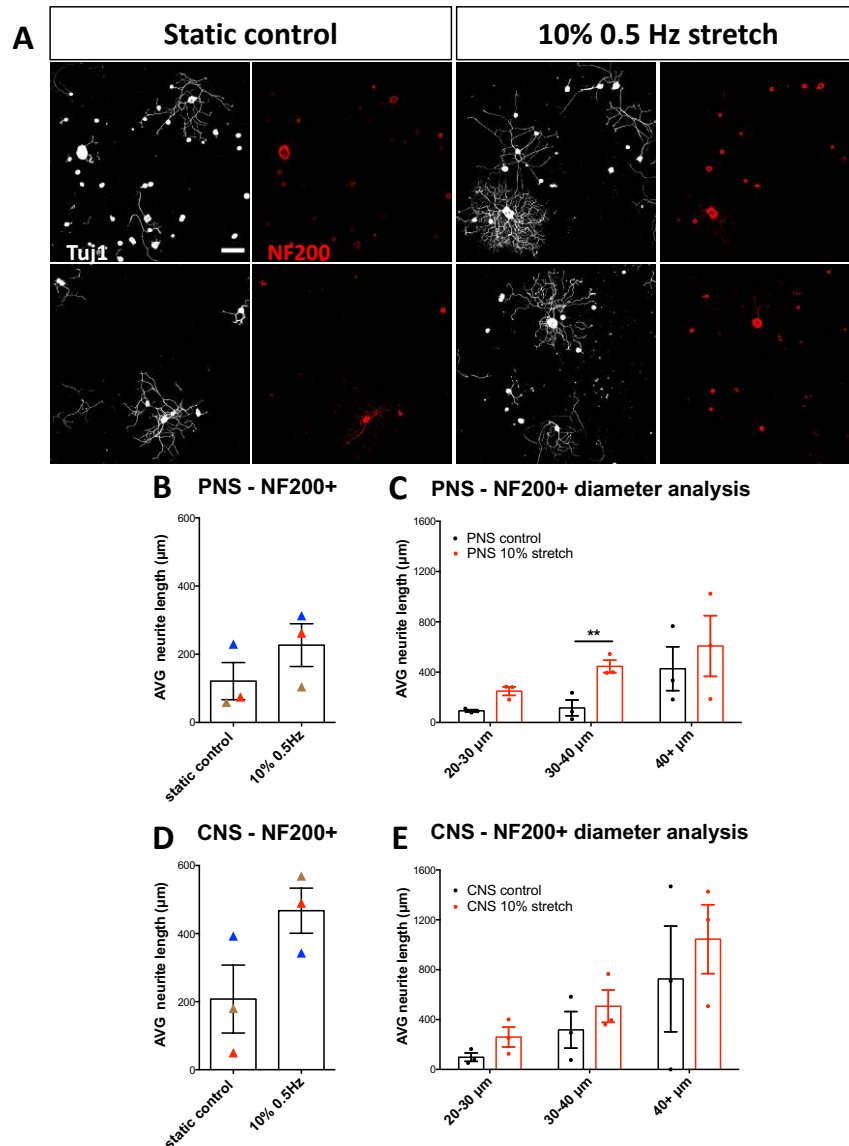


**Figure 3.27. NF200+ DRG neurons respond to mechanical stretch. A)** Immunocytochemical analysis of DRG stained for NF200 after either no stretch or mechanical stretch (10% 0.5 Hz). Scale bar, 200 μm. **B, D)** Neurite length analysis of NF200+ PNS (B) and CNS (D) DRG upon 10% 0.5 Hz mechanical stretch. Paired two-tail Student t-test, mean ± SEM, N=3. **C, E)** Diameter analysis of PNS (C) and CNS (E) DRG outgrowth comparing the static controls to the stretched explants shows that after peripheral stretch 30-40 μm-diameter neurons increase their neurite outgrowth. Two-way ANOVA with post-hoc Sidak's multiple comparison test, mean ± SEM, ** p<0.01, N=3.

### 3.2.8. ATF3 is increased by 3 hours 10% mechanical loading

Thus far, we have shown that 10% cyclic mechanical stretch of both PNS- and CNS-nerve explants managed to increase the axonal outgrowth of cultured larger diameter mechanoreceptive and proprioceptive neurons without a dramatic impact on the cytoarchitecture of the subjected nerves. However, the underlying mechanisms involved in the mechanical stimulation of axonal outgrowth remain unknown. A peripheral nerve injury induces a regenerative signal that promotes long-distance regeneration of injured neurons. A plethora of factors are involved in this signal leading to post-translational modifications of cytoplasmic proteins[193] as well as epigenetic and transcription factor changes leading to expression of RAGs[55,194,195]. An integral factor in this regenerative signal is Activating Transcription Factor 3 (ATF3)[196,197], whose nuclear levels increase after a peripheral injury and contribute to the regeneration of injured peripheral neurons[198]. In other non-neuronal models of cyclic stretch, ATF3 was found to be increased early on by gene expression and nuclear protein translocation as well as found to be integral to the beneficial effects that followed[199]. Modification of histones is an initiation signal of regenerative gene expression changes[96,200] and can be activated in animals that participate in voluntary wheel running in an enriched environment[140]. Therefore, we investigated whether 3 hours 10% 0.5 Hz mechanical stretch immediately affects ATF3 regulation or histone 3 lysine 9 lysine 14 acetylation (H3K9K14ac) by DRG sections immunohistochemistry. Remarkably, even in the short 3-hour 10% stretch period of CNS DRG-nerve explants, significant enhancement of ATF3 nuclear levels were observed (**Figure 3.28**). Further diameter analysis did not indicate significance by Two-Way ANOVA, but not specific subpopulation enhancement. Although a trend appeared, no significant changes were seen with H3K9K14ac (**Figure 3.28**). Further, there was no significance when Two-way ANOVA examined diameter analysis for H3K9K14ac.
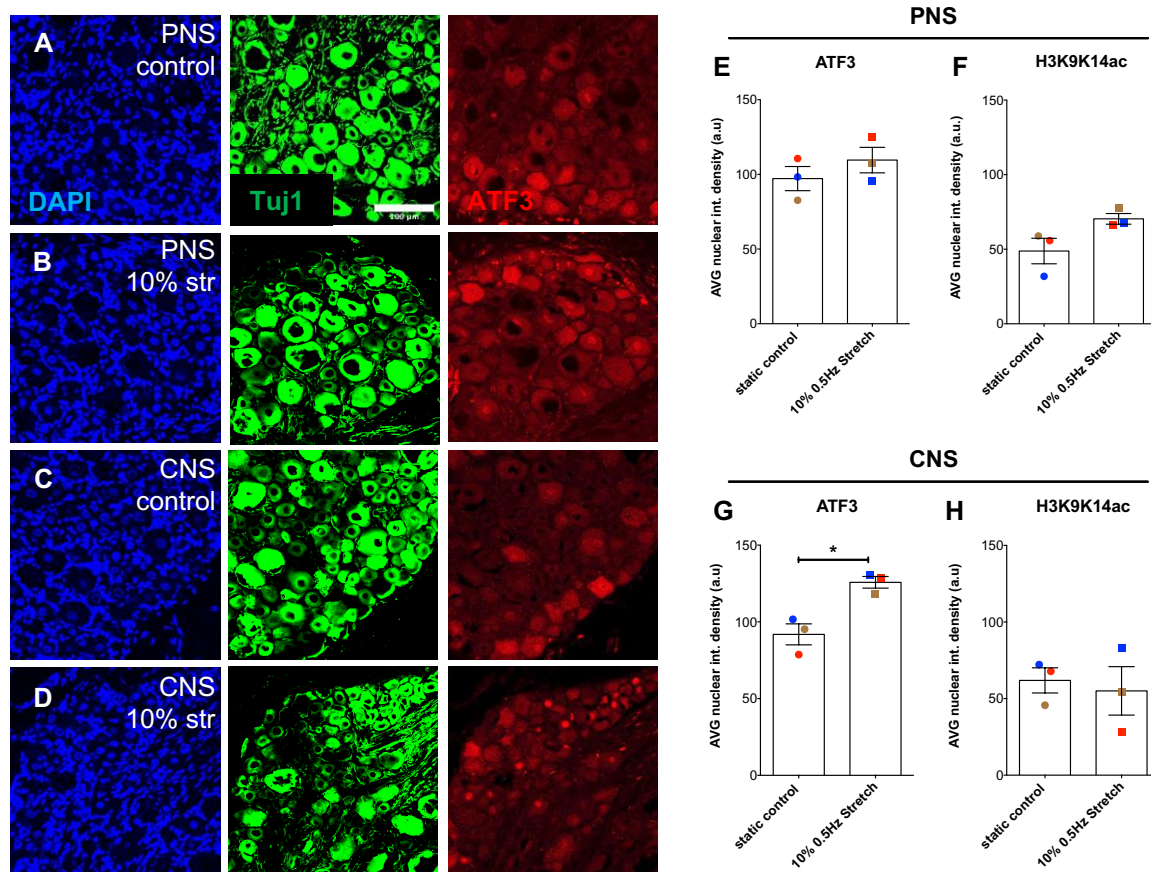
**Figure 3.28. Within 3 hours of 10% mechanical stretch, ATF3 nuclear DRG levels increased in the CNS DRG-nerve explant. A-D)** Representative immunofluorescence photomicrographs (20X) of DRG sectioned either 3 hours post- no stimulation (A) or 10% mechanical stretch (B) of PNS DRG-nerve explants and no stimulation (C) or 10% mechanical stretch (D) of CNS DRG-nerve explants. DRG were stained for DAPI (blue), βIII-tubulin (Tuj1) (green) and ATF3 (red). Scale bar, 100 μm. **E, G)** Nuclear intensity density analysis of ATF3 in DRG derived from PNS DRG-nerve explants (E) and from CNS DRG-nerve explants (G). Paired two-tailed Student t-test, mean ± SEM, *p<0.05, N=3. **F, H)** Nuclear intensity density analysis of H3K9K14ac in DRG derived from PNS DRG-nerve explants (F) and CNS DRG-nerve explants (H). Paired two-tailed Student t-test, mean ± SEM, N=3.

# Discussion

# 4.    Discussion

The present work suggests that intrinsic cell-autonomous mechanisms either initiated by a peripheral injury or by cyclical mechanical stimulation of neurons can reawaken and enhance the regenerative capacity of adult sensory neurons. The epigenetic landscape and the transcriptional status of neurons are a hub of information that can control the outcome of injured cells. Here, we identified putative RAGs regulated by PCAF and partially by Sp1 and MAZ for the first time. These TFs were also shown to regulate DRG outgrowth through PCAF. Pharmaceutical activation of PCAF by EML76 was sufficient to enhance neurite outgrowth of cultured DRG associated with increased H3K9ac, PCAF nuclear localization and partial upregulation of PCAF-RAGs. *In vivo,* sciatic nerve regeneration was enhanced by a single dose of EML76, associated with increased nuclear localization of PCAF and Sp1 and enhanced H3K9ac, when administered without any injury. Lastly, our work suggests that cyclical mechanical stimulation of peripheral or central DRG nerves with an amplitude that resembles forces physiologically existing in the PNS can induce enhanced outgrowth of large diameter DRG, partially associated with transcriptional changes.

## 4.1.    Transcriptional complex members associated with axonal regeneration: The role of Sp1 and MAZ

The manipulation of the extrinsic environment of the CNS following trauma and intrinsic mechanisms have been in the spotlight of research to enhance neuronal regeneration coupled to functional recovery[21,25,26,28,29,37,39,41,43,44]. These approaches usually aim to regulate single factors and have not been proven efficient for functional recovery. It is unlikely that single TFs are sufficient to fully promote neuronal repair, but instead, multiple functionally interacting factors will be needed. Bioinformatics analysis of regeneration-permissive neuronal populations versus non-regenerating populations provides fruitful information regarding sets of transcription factors and networks that play an important role in regeneration[111]. Our approach was to investigate transcriptional complexes that are associated with a peripheral injury-induced PCAF-driven regenerative signal. Unbiased analysis of our transcriptomics results highlighted Sp1 and MAZ as two TFs involved in the PCAF regenerative pathway.

Sp1 has not been extensively studied regarding its involvement in regenerative pathways upon peripheral lesion or spinal cord injury, and its role in neuronal damage remains unclear. Recent results have shown that upon an injury in the optic nerve, Sp1 is upregulated,

leading to the expression of the leucine-rich repeat and immunoglobin-like domain-containing protein 1 (LINGO-1), negatively affecting the survival of RGCs. Silencing of Sp1 following optic nerve crush allowed for RGC survival but did not lead to any functional recovery[201]. These results were supported by other findings showing that Sp1 is upregulated upon a neuronal injury and contributes to motor neuron degeneration in a nerve transection model, causing excitotoxic neurodegeneration[202]. Mithramycin A, an Sp1 inhibitor, used in a spinal cord contusion paradigm showed support in repair of the blood-spinal cord barrier disruption and reduced hemorrhaging, leading to functional recovery[203]. Contrastingly, Sp1 has also been associated with neuronal regeneration events. The damage-induced neuronal endopeptidase (DINE) is upregulated in the DRG after a sciatic nerve axotomy[204,205] and promotes recovery of the injured optic nerve[206]. Interestingly, it has been shown that upon a regenerative injury, DINE expression is induced by Sp1, which can recruit other regeneration-associated factors, such as ATF3, c-Jun and STAT to the promoter of DINE, leading to its expression[207]. Our results showed that Sp1 is recruited to the nucleus of injured DRG, irrespective of injury to either the peripheral or central branches. Notably, its activation by a peripheral injury is much stronger than a central lesion, although it is not clear why this is the case, it might be associated with the inadequate regenerative capacity of the CNS. Its recruitment is not in conjunction with PCAF suggesting that Sp1 might have a completely different role following a central lesion, supported by the fact that this TF, like others, can have context-dependent activator and repressor roles.

Nuclear enrichment of DRG lysates did not show increased levels of Sp1 in peripherally injured DRG. This could partially be explained by the fact that increased nuclear Sp1 localization observed through immunofluorescence derives from the analysis of the nuclei areas of only the neurons. In DRG, not only neuronal cells express Sp1, in fact, we found satellite cells heavily expressed Sp1. Therefore, neuronal Sp1 expression changes may be diluted out in the pooled DRG Western samples. Proteomics from laser captured DRG would have been an alternative to isolate the proteome of only the neurons. Although beyond the scope of this thesis, it could be exploited to identify changes in the proteome upon injury. However, the capture of only the nuclear area of DRG neurons might be challenging. On the other side, whole-cell capture would allow detection of overall proteome changes, but translocation changes would not be identified. In general, it has been shown that Sp1 is involved in injury responses following an SCI[208], and although our data showed for the first time its contribution to DRG outgrowth, its exact role in the spinal cord injury remains elusive.

Also, although not in the context of neuronal regeneration, it has been proven that Sp1 can be acetylated by PCAF and recruited to the promoters of actively expressed genes[209], but a direct interaction has not been shown in our context. Here, we aimed to analyze candidate PCAF interactors by co-immunoprecipitation coupled to mass spectrometry following a peripheral injury; however, due to the low expression levels of PCAF and the low amounts of protein yielded from DRG, this was not possible. Further optimization of the pull-down protocol is required to identify the optimal conditions to increase the amount of protein extracted from DRG. Also, we should confirm that the antibody used is optimal for Co-IP mass-spectrometry protocols. Although not a as comprehensive, an alternative option to deal with the sensitivity limit of mass-spec would be to pull down PCAF from DRG lysates following a peripheral or sham injury and stain for Sp1 and MAZ on Western blots to confirm their interaction.

MAZ's contribution to axonal regeneration is not clear, apart from its interaction with fetal Alz-50 clone 1 (FAC1) protein[210] that is increased in surviving motor neurons of amyotrophic lateral sclerosis (ALS) spinal cord[211] and its association with NGF-induced ERK signaling-mediated neurite outgrowth[212]. Given that, ERK also regulates PCAF upon a peripheral injury and our results showing that MAZ partially controls PCAF-RAGs and is important for neurite outgrowth of cultured DRG through PCAF, it would be interesting to investigate other MAZ-related pathways and find other co-regulators. Its relation to PCAF has never been cited before. We showed clear evidence that PCAF and Sp1 or MAZ are co-dependent, and next we aim to address possible mechanisms through which PCAF recruits MAZ. *In silico* analysis of MAZ's potential acetylation sites using GPS-PAIL software (http://pail.biocuckoo.org/) predicted one PCAF acetylation site in MAZ, lysine K187. Further work is required to investigate whether this site is crucial for the regenerative capacity of MAZ and if it is acetylated following a regenerative injury. In the future, we could pull down all lysine-acetylated proteins following a peripheral injury and stain for MAZ on Western blots. We could also stain for Sp1.

Lastly, MAZ was not upregulated following a central lesion, thus in the future, we could investigate if its overexpression in centrally lesioned DRG would facilitate their regeneration. For this, AVVs expressing MAZ could be used to transduce lumbar DRG prior to sciatic nerve injury and compare the regenerative potential of these neurons compared to the control group.

## 4.2. Pharmaceutical activation of PCAF may have promising results in CNS regeneration

As mentioned before, overexpression of single intrinsic factors can have a beneficial outcome on the recovery following a non-regenerative injury, but most of the time, it leads to limited regeneration and partial functional recovery. Those paradigms are based on artificial viral systems for the overexpression of the factors of interest. Many intracellular proteins, such as transcription factors and histone acetyltransferases, can work in different contexts and posttranslational modifications can regulate their function and stability in the cell[213–215]. Additionally, the translatability of overexpression approaches is not always successful as they can elicit undesirable side effects, such as an immune response[216]. In fact, overexpression might not be sufficient to activate the factor of interest and many examples show that the activation step of a TF is important for its function[215,217–219]. Intrinsic pathways can translate external stimuli into the activation of TFs and epigenetic factors to elicit an appropriate cellular response. Thus, apart from characterizing TFs that are involved in the peripheral injury-elicited PCAF-driven regenerative pathway, we took a step further to activate the regenerative program pharmaceutically. Further, we aimed to combine it the concomitant overexpression of Sp1 or MAZ in lumbar DRG, but this was not possible due to technical difficulties.

Drug screenings can have promising results when it comes to neuronal outgrowth overcoming the CNS inhibitory environment[220,221]. The roles of epigenetics in axonal regeneration have been investigated and a few studies have focused on the pharmaceutical manipulation of the epigenetic landscape upon neuronal damage to promote axonal regeneration. One approach has been the untargeted inhibition of HDACs, which set the chromatin more accessible to TFs. This inhibition can interfere with the expression of RAGs. For example, trichostatin A (TSA) or MS-275 can inhibit the function of family I and II mammalian HDACs, enhance RAG expression coupled with increased histone acetylation levels[84]. This is associated with elevated levels of axonal outgrowth of DRG *in vitro,* comparable to the regenerative effect of a conditional lesion[84]. Notably, MS-275 can enhance axonal outgrowth of centrally lesioned fibers into the lesion site but not beyond it[84], while TSA does not promote axonal regeneration of injured RGCs, although it enhances their survival[222]. Valproic acid is another HDAC inhibitor that has been demonstrated to provide neuroprotection *in vitro*, overcome the hostile environment of the CNS, and enhance functional recovery of animals subjected to a thoracic contusion injury[223]. Importantly, pan-HDAC

inhibition approaches can have serious side effects[224] due to their involvement in many cellular processes, and their exploitation needs to proceed with caution.

Apart from the inhibition of HDACs, studies have also focused on the activation of their counterparts, histone acetyltransferases. Resveratrol is a polyphenolic compound whose use upon damage in the CNS has a neuroprotective effect[225]. Interestingly, its use activates the acetyltransferase, p300, and it improves motor function upon a sciatic nerve crush[226]. It may have improved the motor function of rats in weight-drop models of SCI models but further studies are required to demonstrate the translatability of this compound[227] and whether it can proceed to the clinical trial phase. In 2019, Hutson and his colleagues used a compound called TTK21, which enhances the function of the acetyltransferase CBP, conjugated to glucose-derived carbon nanospheres (GSP). Administration of GSP-TTK21 was associated with active gene expression-related epigenetic changes and increased axonal outgrowth of cultured DRG compared to vehicle-treated DRG. Most importantly, it primed the regeneration of ascending sensory fibers beyond the lesion site following dorsal column axotomy and it led to restored electrophysiological activity across the injury site and improved locomotor performance in a moderate contusion SCI model[140]. Notably, GSP-TTK21 regenerative effect was associated with the regeneration of proprioceptive fibers and sprouting of descending reticulospinal and serotoninergic axons, while no enhanced neuropathic pain was reported[140]. The latter is a significant point regarding the treatment of peripheral and central nerve lesions, as an efficient treatment should not be correlated to increased levels of neuropathic pain.

Previous findings suggested that PCAF activation allows for increased axonal regeneration levels *in vitro* and can enhance regeneration of ascending sensory fibers almost comparably to the conditioning lesion effect[96]. That approach used an inefficient viral overexpression system to deliver and overexpress PCAF into lumbar DRG, thus here we aimed for the pharmaceutical activation of PCAF. In 2008, Sbardella and colleagues produced a chemical derivative of anarcadic acid, called pentadecylidenemalonate 1b, SPV106, which can cross the BBB and activate PCAF, but also inhibits CBP[228]. SPV106 was used in fear memory extinction behavioral tests and was found, applied intracortically or systemically, to activate PCAF in cortical neurons, facilitating the formation of fear extinction-related memories[167]. Due to this work, we used cell-based assays and showed that SPV106 could enhance neuronal outgrowth of medium to large and large diameter DRG. Nevertheless, due to SPV106's ability to block CBP and its high apoptotic potential found in U937 cells[166], we decided to test another compound called EML76. When tested on cultured DRG, EML76 increased their neurite length significantly. *In vivo*, a single dose of EML76 activated the PCAF-related signal leading to

increased levels of H3K9ac and partially upregulated PCAF-RAGs. Strikingly, a single systemic dose of EML76 was sufficient to activate PCAF within 24 hours and recruit Sp1, showing how epigenetic factors can recruit TFs. Most importantly, EML76 was used here *in vivo* for the first time to measure its efficacy in the regeneration of the sciatic nerve upon a crush injury. A single dose of EML76 is sufficient to promote a significant acceleration of sciatic nerve of 48 hours post-sciatic nerve crush. Notably, no apparent side effects could be reported 48 hours post-administration of EML76, but it would be useful to examine whether its long-term use could have possible side effects. Our *in vitro* permeability test showed that EML76 is able to cross the BBB without an adjuvant. This is a clear advantage of EML76 over TTK21, which, as mentioned above, requires a modification to cross the BBB or antibody-based approaches that need to be administered locally following SCI[229]. Interestingly, a single systemic dose of EML76 could recapitulate conditioning lesion regenerative effects, such as the nuclear recruitment of PCAF and Sp1 and H3K9ac, lasting at least 48 hours post-administration. Given the conditioning lesion data of RAG expression remaining for weeks, this is likely to occur here as well. Further, it would be useful for the administration in a spinal cord injury model to know the half-life of this compound and for how long does PCAF remain active. This is important to determine how many doses will be required to keep PCAF consistently active setting up its regenerative program upon a central lesion and whether this will allow for functional recovery.

Here, for the first time here, we characterized a panel of genes that respond to a regenerative but not to a non-regenerative injury, their expression is regulated by PCAF and can partially be upregulated by a single dose of EML76. Although the exact mechanisms of these genes in neuronal regeneration is being studied, it is clear that several have already been distinguished for their roles in neuronal survival, differentiation and repair. Indicatively, DOT1l, a histone lysine methyltransferase, has been shown to increase the proliferation and survival of neuronal stem cells and it is involved in the epigenetic regulation of neuronal stress response[230]. Adam19, a metalloprotease, is upregulated following a sciatic nerve crush and is important for neuronal remyelination[231]. Ndst1, an N-deacetylase and N-sulfotransferase, is involved in growth cone extension[232]. Interestingly, our panel includes genes, such as *shank2*[233]*, ptpn1*[234,235]*, grid2*[236]*, mylt1*[237]*, lmtk3*[238]*, stx1b*[239]*, trpm3*[240] *and syngap1*[241] that are involved in autism spectrum disorders, epilepsy, Rett syndrome and cognitive dysfunction but their role in axonal repair remains elusive. Interestingly, it is known that these disorders are characterized by aberrant neurite outgrowth[242–244], although it is unclear whether the same repertoire of genes is involved in functional outgrowth. *Crmp1* and *pfkfb3* are also upregulated

in most of our regenerative paradigms. Crpm1 is known to be involved in axonal guidance events by controlling growth cone dynamics[245] and Pfkfb3 is a metabolic regulator involved in the process of glycolysis[246], but it remains to be discovered how they specifically contribute to neuronal regeneration upon damage. Other genes from our panel that seem to have a promising role in neuronal regeneration are *ssh1* and *crtac1* (also known as *lotus*). Ssh1 is involved in the NGF-mediated neurite extension[247] and regulation of the cytoskeleton dynamics [248]. Crtac1 is an antagonist of Nogo receptor type 1, a known inhibitor of regeneration in the CNS[249]. Its overexpression has been associated with enhanced axonal regeneration following optic nerve crush or thoracic dorsal hemisection and led to functional recovery[250]. These examples indicate that axonal regeneration is a complicated process that involved many different genes and pathways. Nevertheless, they support our hypothesis that targeting a master regulator of these genes and not overexpressing them individually, might have a better outcome on the recovery upon an SCI. Further investigation of PCAF-RAGs-related pathways would shed light on alternative mechanisms related to neuronal regeneration and could be targeted in the future.

## 4.3.   Mechanical stimulation of sensory neuron growth

Mechanical forces upon and within developing neurons determine towing neurite outgrowth[251] axonal pathfinding and ultimately "stretch growth" of integrated axonal tracts[252]. Moreover, muscle contractions can guide sensory axons in zebrafish[253]. Although all neurons are constantly under tension *in vivo*, in the periphery this tension is increased by limb movement[254]. In fact, cyclic stretch produced by exercise is a common rehabilitative approach following a neuronal injury in the PNS and the CNS[255,256]. Interestingly, it has been demonstrated that treadmill training can prime dissected DRG to enhance axonal outgrowth *ex vivo* and increase regeneration of sciatic nerves upon crush[139]. Similarly, voluntary wheel running within an enriched environment led to proprioceptive growth[140]. Passive exercise and manual stimulation provide similar effects to exercise training[257–259]. Physical exercise contributes to the rate of axonal growth as well as the number of growing axons[157]. An underlying reason why exercise-trained injured animals have less misdirection of regenerating axons[157] could be that often neurite growth is found in the direction of applied stretch[260].

The beneficial effect of exercise is not limited in the recovery of the PNS, rhythmic exercise also leads to sensory[261] and motor[262] functional recovery following spinal cord injury, and is associated with upregulated levels of known neurotrophins and enhanced

sprouting[261,263]. Interestingly, Sachdeva and colleagues showed that cyclic exercise combined with peripheral grafts leads to the upregulation of RAGs (GAP-43, β-actin and neuritin) and enhanced regeneration of propriospinal, but not sensory neurons[264]. It should be noted this is likely due to non-cell autonomous mechanisms. Remarkably, when the flexibility of the vertebral column is increased as that of the lamprey (along with lack of myelin sheathing), spinal cord regeneration is observed even after multiple injuries[265], and further enhanced by swim training[266]. Swimming led to an increase of 5% strain on the spinal cord from non-stress situations[267]. Moreover, small caliber reticulospinal and propriospinal axons were the first to regrow before larger reticulospinal axons[268]. It can be postulated that smaller caliber axons may be more receptive to mechanical strain. For example, injury-inducing mechanical strain applied on DRG showed that CGRP+ neurons, which represent the majority of the thin unmyelinated C-fibers[191,269], show higher levels of Caspase-3 activation and increased levels of Caspase-3-dependent apoptosis compared to NF200+ myelinated neurons[270], which represent larger diameter A-fibers[191].

Here, for the first time, we used DRG explants attached either to their peripheral or their central branches applied with uniaxial sinusoidal mechanical stretch, imitating the cyclic nature of a limb movement and the corresponding physiological forces. Stretch parameters could be kept consistent and this allowed us to compare the responsiveness of sensory adult neurons to the same levels of mechano-stimulation of their peripheral or central branches. Our results showed for the first time that 10% stretch can promote axonal outgrowth of both PNS and CNS large diameter DRG neurons. The overall effect was clear in centrally stretched DRG neurons, but further analysis showed that NF200+ and TrkC+ peripherally stretched DRG neurons also showed significant differences. Similar to what was observed with exercise training, we found that cyclic stretch of the CNS nerve-DRG explant not only increased neurite outgrowth but also enhanced initiation of neurite outgrowth. Notably, when we applied higher amplitude stretch (20%) this did not lead to any higher regenerative effect, but instead it damaged the subjected nerves similar to that of high intensity training[191]. Possibly an intermediate level of stretch at 12% or 15% would be worth exploring further.

Physiologically, peripheral nerves may be built to resist stretch forces since they are not protected by bony structures. Interestingly, some peripheral nerves are more resistant to mechanical stretch than others[271]; with one example of peripheral nerves in the tongue of whales showing extreme elastic properties[272]. In general, it seems that peripheral nerves have been evolved to withstand forces due to their anatomy[272], since for example central nerves do not form fascicles held together by connective tissue forming the epineurium. However,

regardless of where the nerves are located, either in the PNS connected to muscle/skin or CNS behind a rigid bony structure, we observed they retain their capacity to respond to mechanical input. Although there are differences in the anatomy of the PNS and CNS nerves, it did not appear to hinder the response to stretch but may have contributed to higher levels of variability between experiments. In contrast to exercise regimes, the sciatic nerve disconnected from muscles and skin was able to sense mechanical tension. Central nerves not directly connected to either muscle or skin also responded to mechanical tension. Although this does not prove cell autonomy in response to stretch, it does narrow the possibilities to the cellular composition of the nerves themselves.

This response is limited to a subset of DRG neurons that normally code mechanical stimuli, as mechanoreceptors respond to mechanical stimuli and proprioceptors to muscular and visceral pressure. It should be noted again that these cells represent the minority of the DRG sensory neuronal pool, and this contributes to the high variability observed in results regarding these populations. Unlike previous work with exercise training, our work is unique in that we attempted to examine which population/s of sensory neurons responded to mechanical tension. After peripheral injury, neurochemical markers were found to change in the DRG[191]. It is possible in cell culture that neurochemical markers either do not work or change from standard *in vivo* conditions. It should be noted the distribution of these markers are wide in diameter analysis[273] and make it difficult for conclusive subpopulation predictions. Either dual markers to further ensure classification of neurons or single-cell transcriptomic analysis of DRG following mechanical stretch is required. This would additionally allow for better understanding of the mechanisms involved in stretch-associated regenerative pathways of each DRG subpopulation. Given that disassociation of the cells for culture did not alter the stretch-induced mechanisms, this approach should be feasible for this type of experimentation.

Although classically known as a stress-related protein, it has been shown that ATF3 mRNA levels are upregulated 6 hours upon a regenerative injury[197]. Additionally, ATF3 protein levels increase after treadmill training in rats enhancing axonal regeneration of the injured sciatic nerves[274]. We have shown that 3 hours of *ex vivo* mechanical axonal stretch was sufficient for significantly increasing nuclear localization of ATF3 in centrally stretched DRG compared to non-stretched controls. Upstream MAPK pathways were found to induce ATF3 which in turn may lead to GAP-43 expression in exercise paradigms[274]. In other cell models, cyclic stretch is known to activate mechano-signaling (channel activation and $Ca^{2+}$ influx) within a minute, then signaling cascade activation over several minutes (ROS production and MAPK signaling), followed by increased transcription factor activation from minutes to the

first hour after stretch has begun, and cytoskeletal remodeling follows up to 6 hours[275]. It would be of interest to understand if the same pathways play a role in our nerve stretch paradigm as well. To further test the requirement of *de novo* transcription to the regenerative stretch effect, we could use transcriptional inhibitors, such as actinomycin-D, during the culturing state.

Exercise induced axonal growth requires the upregulation of neurotrophins, such as BDNF[276], NT-4/5[277], NT-3[139], produced by neurons, muscles and Schwann cells. Contrastingly, paralysis leads to decreased BDNF levels[263]. As exercise-induced neurotrophin signaling was non-cell autonomous to growing axons in the CNS[264], it would be of interest to examine neurotrophin signaling in our axonal stretch model to elucidate if they are specifically responsive to axonal stretch alone or other components of exercise.

Through mechanotransduction, cells translate mechanical forces into biological responses[278]. The neuronal cytoskeleton plays a role in this process, linked to integrin-based focal adhesions[278]. Integrins have been shown to be important to the neuroregenerative process in the PNS and now also induced to allow regeneration of the CNS[279]. Further understanding the role of integrin biology in our model may allow us to unlock the mechanism underlying axonal stretch growth. For example, calcium influx from stretch-gated ion channels, such as transient receptor potential canonical 1 (TRPC1), found in the PNS and CNS, can lead to activated cleavage of talin, which links actin to integrins, important for spinal axonal growth[280]. Further, the TRP, subfamily V, member 2 (TRPV2) channel is also activated by stretch and is expressed in motor and sensory neurons during development regulating their outgrowth[281]. In adult animals, TRPV2, also known as vanilloid-receptor-like protein 1 (VRL-1), is expressed in Aδ- or Aβ-fibers in the DRG[281]. Therefore, it would be useful to examine if blockade of such channels could abolish the stretch regenerative effect and if differences in the density of such channels on the axons of central and peripheral nerves could explain their responsiveness to mechanical stimulation.

This proof-of-concept work was initiated to specifically address if cyclic stretch is directly applied to the nerve, particularly in nerves lacking this input, would this lead to enhanced neurite outgrowth. We have proven that it does and in a specific subpopulation of cells (mechano- and proprioceptors) with 10% stretch 0.5 Hz, but not greater amplitudes or lower frequencies. Although we identified a mechanism underlying axonal cyclic stretch growth (ATF3), in the future a better understanding of axonal stretch growth pathways could lead to new avenues of intervention in neuroregenerative science.

.

# Conclusions

# and

# Future Perspectives

# 5.     Conclusions and Future Perspectives

The present study has addressed further PCAF-related epigenetic/transcriptional and extrinsic mechanical loading mechanisms that can regulate neuronal regeneration. Based on our DRG bulk transcriptomics of WT and PCAF KO mice following a sham or a peripheral injury we characterized putative PCAF-RAGs, that are not upregulated upon a central lesion. Sp1 and MAZ were predicted here, *in silico,* to partially regulate PCAF-RAGs, with our Nanostring transcriptomics results supporting this prediction upon their overexpression and it was shown for the first time their importance in DRG neurite outgrowth *in vitro* and their synergy to PCAF. *In vivo*, these TFs are recruited in the nuclei of DRG following a peripheral injury but not when PCAF is missing. A CNS lesion recruited Sp1 in the DRG nuclei but failed to recruit MAZ, and PCAF. Also, we screened for the first time two chemical compounds, SPV106 and EML76, showing that they can induce the outgrowth of medium to large and large cultured DRG, respectively. We proved that EML76 works specifically through the activation of PCAF, can induce H3K9 acetylation and partially upregulates PCAF-RAGs 24 hours post-treatment of cultured DRG. *In vivo* treatment with a single dose of EML76 for 24 hours, without any previous injury, activated the PCAF regenerative signal by increasing the nuclear levels of PCAF, H3K9ac and Sp1 allowing for partial upregulation of PCAF-RAGs. Most importantly, a single systemic dose of EML76 *in vivo* in a sciatic nerve crush for 48 hours promoted increased levels of neuronal regeneration compared to the control. In the future, overexpression of Sp1 or MAZ in a peripheral lesion model could show if they can accelerate peripheral regeneration. Also, MAZ's overexpression after a central lesion could provide insight whether it can alone enhance neuronal regeneration in the CNS. Next, we could examine the efficacy of EML76 in the regeneration of ascending and descending neuronal fibers in the injured spinal cord by using a dorsal hemisection SCI model and systemic administration of EML76 for multiple days post-injury. Motor and sensory behavioral tests could determine whether pharmaceutical activation of PCAF could lead to functional recovery. Concomitant overexpression of Sp1 and MAZ would allow us to determine if there is an additive effect between the regenerative potential of EML76 and the regenerative potentials of Sp1 and MAZ overexpression found *in vitro.*

Moreover, for the first time, we addressed here whether cyclic stretch of peripherally and centrally located DRG nerves can enhance the outgrowth of cultured DRG. 10% mechanical stretch for 3 hours of central or peripheral DRG nerves was sufficient to promote enhanced outgrowth of large diameter DRG and to increase outgrowth initiation levels of

centrally stretched DRG. Higher levels of mechanical stretch (20%) failed to enhance further the outgrowth of cultured DRG, but it can cause damage to the cytoarchitecture of stretched nerves compared to non-stretched or nerves which received 10% mechanical stretch. TrkC+ neurons responded to the regenerative mechanical stretch of peripheral nerves but not the central ones. Lastly, ATF3 nuclear levels increased upon 10% stretch of peripheral nerves for 3 hours but not the central nerves but this discrepancy remains to be elucidated. Further experiments are required to determine which populations could specifically respond to regenerative mechanical stretch, by immunofluorescence or *in situ* hybridization. Transcriptomics and proteomics analyses could highlight intrinsic mechanisms that can translate external mechanical cues to a regenerative program. Ultimately, pharmaceutical targeting of pathways related to the regenerative mechanical loading could allow for the regeneration of lesioned CNS nerves which are not exposed to mechanical forces.

# **Bibliography**

# 6. Bibliography

1.  Saló, E. & Batistoni, R. *The planarian Eye: A Simple and Plastic System with Great Regenerative Capacity. P. A. Tsonis, Ed. (Elsevier, 2008)* (2008). doi:10.1016/B978-0-12-374169-1.00003-5

2.  Gentile, L., Cebrià, F. & Bartscherer, K. The planarian flatworm: An in vivo model for stem cell biology and nervous system regeneration. *DMM Disease Models and Mechanisms* **4**, 12–19 (2011).

3.  Pfefferli, C. & Jaźwińska, A. The art of fin regeneration in zebrafish. *Regeneration* **2**, 72–83 (2015).

4.  Godwin, J. W., Pinto, A. R. & Rosenthal, N. A. Macrophages are required for adult salamander limb regeneration. *Proc. Natl. Acad. Sci. U. S. A.* **110**, 9415–9420 (2013).

5.  Clark, L. D., Clark, R. K. & Heber-Katz, E. A new murine model for mammalian wound repair and regeneration. *Clin. Immunol. Immunopathol.* **88**, 35–45 (1998).

6.  Goss, R. J. & Grimes, L. N. Tissue interactions in the regeneration of rabbit ear holes. *Integr. Comp. Biol.* **12**, 151–157 (1972).

7.  Kierdorf, U., Kierdorf, H. & Szuwart, T. Deer antler regeneration: Cells, concepts, and controversies. *J. Morphol.* **268**, 726–738 (2007).

8.  Illingworth, C. M. Trapped fingers and amputated finger tips in children. *J. Pediatr. Surg.* **9**, 853–858 (1974).

9.  Lee, L. P., Lau, P. Y. & Chan, C. W. A simple and efficient treatment for fingertip injuries. *J. Hand Surg. (British Eur. Vol.* **20**, 63–71 (1995).

10. Lehoczky, J. A., Robert, B. & Tabin, C. J. Mouse digit tip regeneration is mediated by fate-restricted progenitor cells. *Proc. Natl. Acad. Sci. U. S. A.* **108**, 20609–20614 (2011).

11. Höke, A. A (heat) shock to the system promotes peripheral nerve regeneration. *Journal of Clinical Investigation* **121**, 4231–4234 (2011).

12. Hernandez-Gerez, E., Fleming, I. N. & Parson, S. H. A role for spinal cord hypoxia in neurodegeneration. *Cell Death and Disease* **10**, 1–8 (2019).

13. Liu, D., Xu, G. Y., Pan, E. & McAdoo, D. J. Neurotoxicity of glutamate at the concentration released upon spinal cord injury. *Neuroscience* **93**, 1383–1389 (1999).

14. Zipfel, G. J., Babcock, D. J., Lee, J. M. & Choi, D. W. Neuronal apoptosis after CNS injury: The roles of glutamate and calcium. *J. Neurotrauma* **17**, 857–869 (2000).

15. Yang, T., Dai, Y. J., Chen, G. & Cui, S. Sen. Dissecting the Dual Role of the Glial Scar

and Scar-Forming Astrocytes in Spinal Cord Injury. *Front. Cell. Neurosci.* **14**, 78 (2020).

16. Akbik, F., Cafferty, W. B. J. & Strittmatter, S. M. Myelin associated inhibitors: A link between injury-induced and experience-dependent plasticity. *Experimental Neurology* **235**, 43–52 (2012).

17. Bandtlow, C. E. Regeneration in the central nervous system. in *Experimental Gerontology* **38**, 79–86 (Pergamon, 2003).

18. Fujita, Y. & Yamashita, T. Axon growth inhibition by RhoA/ROCK in the central nervous system. *Frontiers in Neuroscience* **8**, (2014).

19. Gopalakrishnan, S. M. *et al.* Role of Rho kinase pathway in chondroitin sulfate proteoglycan-mediated inhibition of neurite outgrowth in PC12 cells. *J. Neurosci. Res.* **86**, 2214–2226 (2008).

20. Jerry Silver, Martin E. Schwab, and P. G. P. Central Nervous System Regenerative Failure : *Cold Spring Harb Perspect Biol* **7**, a020602 (2015).

21. Tom, V. J., Kadakia, R., Santi, L. & Houlé, J. D. Administration of chondroitinase ABC rostral or caudal to a spinal cord injury site promotes anatomical but not functional plasticity. *J. Neurotrauma* **26**, 2323–2333 (2009).

22. Bradbury, E. J. *et al.* Chondroitinase ABC promotes functional recovery after spinal cord injury. *Nature* **416**, 636–640 (2002).

23. Janzadeh, A. *et al.* The effect of chondroitinase ABC and photobiomodulation therapy on neuropathic pain after spinal cord injury in adult male rats. *Physiol. Behav.* **227**, (2020).

24. Buzoianu-Anguiano, V. *et al.* Single vs. Combined Therapeutic Approaches in Rats With Chronic Spinal Cord Injury. *Front. Neurol.* **11**, 136 (2020).

25. Fournier, A. E., GrandPre, T. & Strittmatter, S. M. Identification of a receptor mediating Nogo-66 inhibition of axonal regeneration. *Nature* **409**, 341–346 (2001).

26. Wang, K. C. *et al.* Oligodendrocyte-myelin glycoprotein is a Nogo receptor ligand that inhibits neurite outgrowth. *Nature* **417**, 941–944 (2002).

27. Liu, B. P., Fournier, A., GrandPré, T. & Strittmatter, S. M. Myelin-associated glycoprotein as a functional ligand for the Nogo-66 receptor. *Science (80-. ).* **297**, 1190–1193 (2002).

28. Domeniconi, M. *et al.* Myelin-associated glycoprotein interacts with the Nogo66 receptor to inhibit neurite outgrowth. *Neuron* **35**, 283–290 (2002).

29. Li, S. *et al.* Blockade of Nogo-66, myelin-associated glycoprotein, and oligodendrocyte

myelin glycoprotein by soluble Nogo-66 receptor promotes axonal sprouting and recovery after spinal injury. *J. Neurosci.* **24**, 10511–10520 (2004).

30. GrandPré, T., Shuxin, L. I. & Strittmatter, S. M. Nogo-66 receptor antagonist peptide promotes axonal regeneration. *Nature* **417**, 547–551 (2002).

31. Thuret, S., Thallmair, M., Horky, L. L. & Gage, F. H. Enhanced functional recovery in MRL/MpJ mice after spinal cord dorsal hemisection. *PLoS One* **7**, (2012).

32. S.K KOSTYK, P.G. POPOVICH, B.T.STOKES, P.WEI, A. L. B. J. ROBUST AXONAL GROWTH AND A BLUNTED MACROPHAGE RECOVERY AFTER SPINAL CORD INJURY IN THE MRL / MpJ MOUSE. *Neuroscience* **156**, 498–514 (2008).

33. Anderson, M. A. *et al.* Astrocyte scar formation aids central nervous system axon regeneration. *Nature* **532**, 195–200 (2016).

34. Richardson, P. M., McGuinness, U. M. & Aguayo, A. J. Axons from CNS neurones regenerate into PNS grafts. *Nature* **284**, 264–265 (1980).

35. David, S. & Aguayo, A. J. Axonal elongation into peripheral nervous system 'bridges' after central nervous system injury in adult rats. *Science (80-. ).* **214**, 931–933 (1981).

36. Canty, A. J. *et al.* In-vivo single neuron axotomy triggers axon regeneration to restore synaptic density in specific cortical circuits. *Nat. Commun.* **4**, 1–10 (2013).

37. Park, K. K. *et al.* Promoting axon regeneration in the adult CNS by modulation of the PTEN/mTOR pathway. *Science (80-. ).* **322**, 963–966 (2008).

38. Danilov, C. A. & Steward, O. Conditional genetic deletion of PTEN after a spinal cord injury enhances regenerative growth of CST axons and motor function recovery in mice. *Exp. Neurol.* **266**, 147–160 (2015).

39. Sun, F. *et al.* Sustained axon regeneration induced by co-deletion of PTEN and SOCS3. *Nature* **480**, 372–375 (2011).

40. Jin, D. *et al.* Restoration of skilled locomotion by sprouting corticospinal axons induced by co-deletion of PTEN and SOCS3. *Nat. Commun.* **6**, 1–12 (2015).

41. Gao, Y. *et al.* Activated CREB is sufficient to overcome inhibitors in myelin and promote spinal axon regeneration in vivo. *Neuron* **44**, 609–621 (2004).

42. Qiu, J., Cafferty, W. B. J., McMahon, S. B. & Thompson, S. W. N. Conditioning injury-induced spinal axon regeneration requires signal transducer and activator of transcription 3 activation. *J. Neurosci.* **25**, 1645–1653 (2005).

43. Lang, C., Bradley, P. M., Jacobi, A., Kerschensteiner, M. & Bareyre, F. M. STAT3 promotes corticospinal remodelling and functional recovery after spinal cord injury.

*EMBO Rep.* **14**, 931–937 (2013).

44. Wang, Z., Reynolds, A., Kirry, A., Nienhaus, C. & Blackmore, M. G. Overexpression of Sox11 promotes corticospinal tract regeneration after spinal injury while interfering with functional recovery. *J. Neurosci.* **35**, 3139–3145 (2015).

45. Stratton, J. & Shah, P. Macrophage polarization in nerve injury: do Schwann cells play a role? *Neural Regen. Res.* **11**, 53 (2016).

46. Lutz, A. B. *et al.* Schwann cells use TAM receptor-mediated phagocytosis in addition to autophagy to clear myelin in a mouse model of nerve injury. *Proc. Natl. Acad. Sci. U. S. A.* **114**, E8072–E8080 (2017).

47. Perry, V. H., Tsao, J. W., Feam, S. & Brown, M. C. Radiation-induced Reductions in Macrophage Recruitment Have Only Slight Effects on Myelin Degeneration in Sectioned Peripheral Nerves of Mice. *Eur. J. Neurosci.* **7**, 271–280 (1995).

48. Dailey, A. T., Avellino, A. M., Benthem, L., Silver, J. & Kliot, M. Complement depletion reduces macrophage infiltration and activation during Wallerian degeneration and axonal regeneration. *J. Neurosci.* **18**, 6713–6722 (1998).

49. Morell P & Quarles RH. *Characteristic Composition of Myelin - Basic Neurochemistry - NCBI Bookshelf.* (Lippincott-Raven, 1999).

50. David, S., Braun, P. E., Jackson, D. L., Kottis, V. & McKerracher, L. Laminin overrides the inhibitory effects of peripheral nervous system and central nervous system myelin-derived inhibitors of neurite growth. *J. Neurosci. Res.* **42**, 594–602 (1995).

51. Parrinello, S. *et al.* EphB signaling directs peripheral nerve regeneration through Sox2-dependent Schwann cell Sorting. *Cell* **143**, 145–155 (2010).

52. Clements, M. P. *et al.* The Wound Microenvironment Reprograms Schwann Cells to Invasive Mesenchymal-like Cells to Drive Peripheral Nerve Regeneration. *Neuron* **96**, 98-114.e7 (2017).

53. Min, Q., Parkinson, D. B. & Dun, X. P. Migrating Schwann cells direct axon regeneration within the peripheral nerve bridge. *Glia* 1–20 (2020). doi:10.1002/glia.23892

54. Mahar, M. & Cavalli, V. Intrinsic mechanisms of neuronal axon regeneration. *Nat. Rev. Neurosci.* **19**, 323–337 (2018).

55. Wahane, S., Halawani, D., Zhou, X. & Zou, H. Epigenetic Regulation Of Axon Regeneration and Glial Activation in Injury Responses. *Front. Genet.* **10**, 640 (2019).

56. Ma, T. C. & Willis, D. E. What makes a RAG regeneration associated? *Front. Mol. Neurosci.* **8**, (2015).

57.    Fernandes, K. J. L., Fan, D. P., Tsui, B. J., Cassar, S. L. & Tetzlaff, W. Influence of the axotomy to cell body distance in rat rubrospinal and spinal motoneurons: Differential regulation of GAP-43, tubulins, and neurofilament-M. *J. Comp. Neurol.* **414**, 495–510 (1999).

58.    Sun, F. & He, Z. Neuronal intrinsic barriers for axon regeneration in the adult CNS. *Curr. Opin. Neurobiol.* **20**, 510–518 (2010).

59.    Seijffers, R., Allchorne, A. J. & Woolf, C. J. The transcription factor ATF-3 promotes neurite outgrowth. *Mol. Cell. Neurosci.* **32**, 143–154 (2006).

60.    Raivich, G. *et al.* The AP-1 transcription factor c-Jun is required for efficient axonal regeneration. *Neuron* **43**, 57–67 (2004).

61.    Jankowski, M. P. *et al.* Sox11 transcription factor modulates peripheral nerve regeneration in adult mice. *Brain Res.* **1256**, 43–54 (2009).

62.    Bonilla, I. E., Tanabe, K. & Strittmatter, S. M. Small proline-rich repeat protein 1A is expressed by axotomized neurons and promotes axonal outgrowth. *J. Neurosci.* **22**, 1303–1315 (2002).

63.    Bomze, H. M., Bulsara, K. R., Iskandar, B. J., Caroni, P. & Pate Skene, J. H. Spinal axon regeneration evoked by replacing two growth cone proteins in adult neurons. *Nat. Neurosci.* **4**, 38–43 (2001).

64.    Shin, J. E., Geisler, S. & DiAntonio, A. Dynamic regulation of SCG10 in regenerating axons after injury. *Exp. Neurol.* **252**, 1–11 (2014).

65.    Blesch, A. *et al.* Conditioning lesions before or after spinal cord injury recruit broad genetic mechanisms that sustain axonal regeneration: Superiority to camp-mediated effects. *Exp. Neurol.* **235**, 162–173 (2012).

66.    McQuarrie, I. G., Grafstein, B. & Gershon, M. D. Axonal regeneration in the rat sciatic nerve: Effect of a conditioning lesion and of dbcAMP. *Brain Res.* **132**, 443–453 (1977).

67.    Hanz, S. *et al.* Axoplasmic importins enable retrograde injury signaling in lesioned nerve. *Neuron* **40**, 1095–1104 (2003).

68.    Yudin, D. *et al.* Localized regulation of axonal RanGTPase controls retrograde injury signaling in peripheral nerve. *Neuron* **59**, 241–252 (2008).

69.    Hanz, S. & Fainzilber, M. Retrograde signaling in injured nerve - the axon reaction revisited. *J. Neurochem.* **99**, 13–19 (2006).

70.    Neumann, S. & Woolf, C. J. Regeneration of dorsal column fibers into and beyond the lesion site following adult spinal cord injury. *Neuron* **23**, 83–91 (1999).

71.    Hannila, S. S. & Filbin, M. T. The role of cyclic AMP signaling in promoting axonal

regeneration after spinal cord injury. *Exp. Neurol.* **209**, 321–332 (2008).

72. Ramer, M. S. *et al.* Neurotrophin-3-mediated regeneration and recovery of proprioception following dorsal rhizotomy. *Mol. Cell. Neurosci.* **19**, 239–249 (2002).

73. Lu, P., Yang, H., Jones, L. L., Filbin, M. T. & Tuszynski, M. H. Combinatorial therapy with neurotrophins and cAMP promotes axonal regeneration beyond sites of spinal cord injury. *J. Neurosci.* **24**, 6402–6409 (2004).

74. Saijilafu *et al.* PI3K-GSK3 signalling regulates mammalian axon regeneration by inducing the expression of Smad1. *Nat. Commun.* **4**, 2690 (2013).

75. Liu, K. *et al.* PTEN deletion enhances the regenerative ability of adult corticospinal neurons. *Nat. Neurosci.* **13**, 1075–1081 (2010).

76. Ohtake, Y. *et al.* The effect of systemic PTEN antagonist peptides on axon growth and functional recovery after spinal cord injury. *Biomaterials* **35**, 4610–4626 (2014).

77. de Heredia, L. L. & Magoulas, C. Lack of the transcription factor C/EBPδ impairs the intrinsic capacity of peripheral neurons for regeneration. *Exp. Neurol.* **239**, 148–157 (2013).

78. Iskandar, B. J. *et al.* Folate regulation of axonal regeneration in the rodent central nervous system through DNA methylation. *J. Clin. Invest.* **120**, 1603–1616 (2010).

79. Loh, Y. H. E. *et al.* Comprehensive mapping of 5-hydroxymethylcytosine epigenetic dynamics in axon regeneration. *Epigenetics* **12**, 77–92 (2017).

80. Hong, J. Y., Davaa, G., Yoo, H., Hong, K. & Hyun, J. K. Ascorbic Acid Promotes Functional Restoration after Spinal Cord Injury Partly by Epigenetic Modulation. *Cells* **9**, 1–22 (2020).

81. Kouzarides, T. Chromatin Modifications and Their Function. *Cell* **128**, 693–705 (2007).

82. Hassan, Y. I. & Zempleni, J. A novel, enigmatic histone modification: biotinylation of histones by holocarboxylase synthetase. *Nutr. Rev.* **66**, 721–725 (2008).

83. Li, S. *et al.* The transcriptional landscape of dorsal root ganglia after sciatic nerve transection. *Sci. Rep.* **5**, 1–13 (2015).

84. Finelli, M. J., Wong, J. K. & Zou, H. Epigenetic regulation of sensory axon regeneration after spinal cord injury. *J. Neurosci.* **33**, 19664–76 (2013).

85. Cho, Y., Sloutsky, R., Naegle, K. M. & Cavalli, V. Injury-Induced HDAC5 nuclear export is essential for axon regeneration. *Cell* **155**, 894 (2013).

86. Fann, M. *et al.* Histone acetylation is associated with differential gene expression in the rapid and robust memory CD8+ T-cell response. *Blood* **108**, 3363–3370 (2006).

87. Eberharter, A. & Becker, P. B. Histone acetylation: A switch between repressive and

permissive chromatin. Second in review on chromatin dynamics. *EMBO Rep.* **3**, 224–229 (2002).

88.  Hervera, A. *et al.* PP4-dependent HDAC3 dephosphorylation discriminates between axonal regeneration and regenerative failure. *EMBO J.* **38**, 1–20 (2019).

89.  Yang, X. J., Ogryzko, V. V., Nishikawa, J. I., Howard, B. H. & Nakatani, Y. A p300/CPB-associated factor that competes with the adenoviral oncoprotein E1A. *Nature* **382**, 319–324 (1996).

90.  Roth, S. Y., Denu, J. M. & Allis, D. C. Histone Acetyltransferases. *Annu. Rev. Biochem* **70**, 81–120 (2001).

91.  Zilfou, J. T. & Lowe, S. W. Tumor suppressive functions of p53. *Cold Spring Harb. Perspect. Biol.* **1**, 1–12 (2009).

92.  Williams, A. B. & Schumacher, B. p53 in the DNA-damage-repair process. *Cold Spring Harb. Perspect. Med.* **6**, (2016).

93.  Di Giovanni, S. *et al.* The tumor suppressor protein p53 is required for neurite outgrowth and axon regeneration. *EMBO J.* **25**, 4084–4096 (2006).

94.  Liu, L. *et al.* p53 sites acetylated in vitro by PCAF and p300 are acetylated in vivo in response to DNA damage. *Mol. Cell. Biol.* **19**, 1202–9 (1999).

95.  Wang, Z. *et al.* Combinatorial patterns of histone acetylations and methylations in the human genome. *Nat. Genet.* **40**, 897–903 (2008).

96.  Puttagunta, R. *et al.* PCAF-dependent epigenetic changes promote axonal regeneration in the central nervous system. *Nat. Commun.* **5**, (2014).

97.  Ogryzko, V. V. *et al.* Histone-like TAFS within the PCAF histone acetylase complex. *Cell* **94**, 35–44 (1998).

98.  Dynan, W. S. & Tjian, R. Isolation of Transcription Factors That Discriminate between Different Promoters Recognized by RNA Polymerase II. *Cell* **32**, 669–680 (1983).

99.  Dynan, W. S. & Tjian, R. The Promoter-Specific Transcription Factor Sp 1 Binds to Upstream Sequences in the SV40 Early Promoter. *Cell* **35**, 79–87 (1983).

100. Kaczynski, J., Cook, T. & Urrutia, R. SpI- and Krueppel-like transcription factors. *Genome Biol.* **4**, (2003).

101. Mastrangelo, I. A., Coureyt, A. J., Wall, J. S., Jackson, S. P. & Hough, P. V. C. DNA looping and SpI multimer links: A mechanism for transcriptional synergism and enhancement. *Biochemistry* **88**, 5670–5674 (1991).

102. Letovsky, J. & Dynan, W. S. Measurement of the binding of transcription factor Spl to a single GC box recognition sequence. *Nucleic Acids Res.* **17**, 2639–2653 (1989).

103. Holler, M., Westin, G., Jiricny, J. & Schaffner, W. Spl transcription factor binds DNA and activates transcription even when the binding site is CpG methylated. *Genes Dev.* **2**, 1127–1135 (1988).

104. Marin, M., Karis, A., Visser, P., Grosveld, F. & Philipsen, S. Transcription Factor Sp1 Is Essential for Early Embryonic Development but Dispensable for Cell Growth and Differentiation. *Cell* **89**, 619–628 (1997).

105. Safe, S. & Abdelrahim, M. Sp transcription factor family and its role in cancer. *Eur. J. Cancer* **41**, 2438–2448 (2005).

106. Solomon, S. S., Majumdar, G., Martinez-Hernandez, A. & Raghow, R. A critical role of Sp1 transcription factor in regulating gene expression in response to insulin and other hormones. *Life Sci.* **83**, 305–312 (2008).

107. Xiao, H., Hasegawa, T. & Isobe, K.-I. p300 Collaborates with Sp1 and Sp3 in p21 waf1/cip1 Promoter Activation Induced by Histone Deacetylase Inhibitor. *J. Biol. Chem.* **275**, 1371–1376 (1999).

108. Krumm, A., Madisen, L., Yang, X.-J., Goodman, R. & Nakatani, Y. Long-distance transcriptional enhancement by the histone acetyltransferase PCAF. *Biochemistry* **95**, 13501–13506 (1998).

109. Hung, J.-J., Wang, Y.-T. & Chang, W.-C. Sp1 Deacetylation Induced by Phorbol Ester Recruits p300 To Activate 12(S)-Lipoxygenase Gene Transcription. *Mol. Cell. Biol.* **26**, 1770–1785 (2006).

110. Kiryu-Seo, S. *et al.* Neuronal injury-inducible gene is synergistically regulated by ATF3, c-Jun, and STAT3 through the interaction with Sp1 in damaged neurons. *J. Biol. Chem.* **283**, 6988–96 (2008).

111. Chandran, V. *et al.* A Systems-Level Analysis of the Peripheral Nerve Intrinsic Axonal Growth Program. *Neuron* **89**, 956–970 (2016).

112. Law, A. K. T. *et al.* TGF-I induction of the adenine nucleotide translocator I in astrocytes occurs through Smads and SpI transcriptions factors. *BMC Neurosci.* **5**, (2004).

113. Buck, C. R. *et al.* Increased adenine nucleotide translocator 1 in reactive astrocytes facilitates glutamate transport. *Exp. Neurol.* **181**, (2003).

114. Kim, K., Thu, N., Saville, B. & Safe, S. Domains of Estrogen Receptor α (ERalpha) Required for ERα/Sp1-Mediated Activation of GC-Rich Promoters by Estrogens and Antiestrogens in Breast Cancer Cells. *Mol. Endocrinol.* **17**, 804–817 (2003).

115. Stoner, M. *et al.* Estrogen regulation of vascular endothelial growth factor gene expression in ZR-75 breast cancer cells through interaction of estrogen receptor a and

SP proteins. *Oncogene* **23**, 1052–1063 (2004).

116. Chaovipoch, P. *et al.* 17beta-estradiol is protective in spinal cord injury in post- and pre-menopausal rats. *J. Neurotrauma* **23**, 830–52 (2006).

117. Vacca, V. *et al.* 17beta-estradiol counteracts neuropathic pain: a behavioural, immunohistochemical, and proteomic investigation on sex-related differences in mice. *Sci. Rep.* **6**, 18980 (2016).

118. Bossone, S. A., Asselint, C., Patelo, A. J. & Marcu, K. B. MAZ, a zinc finger protein, binds to c-MYC and C2 gene sequences regulating transcriptional initiation and termination. *Biochemistry* **89**, 7452–7456 (1992).

119. Hu, H.-M., Arcinas, M. & Boxer, L. M. A Myc-associated Zinc Finger Protein-related Factor Binding Site Is Required for the Deregulation of c-myc Expression by the Immunoglobulin Heavy Chain Gene Enhancers in Burkitt's Lymphoma*. *J. Biol. Chem.* **277**, 9819–9824 (2002).

120. Jiao, L. *et al.* The prostate cancer-up-regulated myc-associated zinc-finger protein (MAZ) modulates proliferation and metastasis through reciprocal regulation of androgen receptor. *Med. Oncol.* **30**, (2013).

121. Smits, M. *et al.* Myc-associated zinc finger protein (MAZ) is regulated by miR-125b and mediates VEGF-induced angiogenesis in glioblastoma. *FASEB J.* **26**, 2639–2647 (2012).

122. Duncan, D. D., Stupakoff, A., Hedrick, S. M., Marcu, K. B. & Siu, G. A Myc-Associated Zinc Finger Protein Binding Site Is One of Four Important Functional Regions in the CD4 Promoter. *Mol. Cell. Biol.* **15**, 3179–3186 (1995).

123. Shoemaker, J. E. *et al.* Integrated network analysis reveals a novel role for the cell cycle in 2009 pandemic influenza virus-induced inflammation in macaque lungs. *BMC Syst. Biol.* **6**, (2012).

124. Himeda, C. L., Ranish, J. A. & Hauschka, S. D. Quantitative Proteomic Identification of MAZ as a Transcriptional Regulator of Muscle-Specific Genes in Skeletal and Cardiac Myocytes. *Mol. Cell. Biol.* **28**, 6521–6535 (2008).

125. Song, J., Ugai, H., Kanazawa, I., Sun, K. & Yokoyama, K. K. Independent Repression of a GC-rich Housekeeping Gene by Sp1 and MAZ Involves the Same cis-Elements. *J. Biol. Chem.* **276**, 19897–19904 (2001).

126. Nagaoka, M., Shiraishi, Y. & Sugiura, Y. Selected base sequence outside the target binding site of zinc finger protein Sp1. *Nucleic Acids Res.* **29**, 4920–4929 (2001).

127. Song, J. *et al.* Two Consecutive Zinc Fingers in Sp1 and in MAZ Are Essential for

Interactions with cis-Elements*. *J. Biol. Chem.* **276**, 30429–30434 (2001).

128. Her, S., Bell, R. A., Bloom, A. K., Siddall, B. J. & Wong, D. L. Phenylethanolamine N-Methyltransferase Gene Expression. Sp1 and MAZ potential for tissue-specific expression. *J. Biol. Chem.* **274**, 8698–8707 (1999).

129. Parks, C. L. & Shenk, T. The Serotonin 1a Receptor Gene Contains a TATA-less Promoter that Responds to MAZ and Sp1. *J. Biol. Chem.* **271**, 4417–4430 (1995).

130. Karantzoulis-Fegaras, F. *et al.* Characterization of the Human Endothelial Nitric-oxide Synthase Promoter. *J. Biol. Chem.* **274**, 3076–3098 (1999).

131. Williams, L. J. S. & Abou-Samra, A. B. The transcription factors SP1 and MAZ regulate expression of the parathyroid hormone/parathyroid hormone-related peptide receptor gene. *J. Mol. Endocrinol.* **25**, 309–319 (2000).

132. Okamoto, S., Sherman, K., Bai, G. & Lipton, S. A. Effect of the ubiquitous transcription factors, SP1 and MAZ, on NMDA receptor subunit type 1 (NR1) expression during neuronal differentiation. *Mol. Brain Res.* **107**, 89–96 (2002).

133. Mammoto, T. & Ingber, D. E. Mechanical control of tissue and organ development. *Development* **137**, 1407–1420 (2010).

134. LeGoff, L. & Lecuit, T. Mechanical forces and growth in animal tissues. *Cold Spring Harb. Perspect. Biol.* **8**, 1–17 (2016).

135. Geffeney, S. L. & Goodman, M. B. How We Feel: Ion Channel Partnerships that Detect Mechanical Inputs and Give Rise to Touch and Pain Perception. *Neuron* **74**, 609–619 (2012).

136. Proske, U. & Gandevia, S. C. The proprioceptive senses: Their roles in signaling body shape, body position and movement, and muscle force. *Physiol. Rev.* **92**, 1651–1697 (2012).

137. Smith, D. H. Stretch growth of integrated axon tracts: Extremes and exploitations. *Prog. Neurobiol.* **89**, 231–239 (2009).

138. Suter, D. M. & Miller, K. E. The emerging role of forces in axonal elongation. *Prog. Neurobiol.* **94**, 91–101 (2011).

139. Molteni, R., Zheng, J. Q., Ying, Z., Gómez-Pinilla, F. & Twiss, J. L. Voluntary exercise increases axonal regeneration from sensory neurons. *Proc. Natl. Acad. Sci. U. S. A.* **101**, 8473–8478 (2004).

140. Hutson, T. H. *et al.* Cbp-dependent histone acetylation mediates axon regeneration induced by environmental enrichment in rodent spinal cord injury models. *Sci. Transl. Med.* **11**, eaaw2064 (2019).

141. Lamoureux, P., Ruthel, G., Buxbaum, R. E. & Heidemann, S. R. Mechanical tension can specify axonal fate in hippocampal neurons. *J. Cell Biol.* **159**, 499–508 (2002).

142. Loverde, J. R. & Pfister, B. J. Developmental axon stretch stimulates neuron growth while maintaining normal electrical activity, intracellular calcium flux, and somatic morphology. *Front. Cell. Neurosci.* **9**, 308 (2015).

143. Loverde, J. R., Ozoka, V. C., Aquino, R., Lin, L. & Pfister, B. J. Live imaging of axon stretch growth in embryonic and adult neurons. *J. Neurotrauma* **28**, 2389–2403 (2011).

144. Pfister, B. J., Iwata, A., Meaney, D. F. & Smith, D. H. Extreme stretch growth of integrated axons. *J. Neurosci.* **24**, 7978–7983 (2004).

145. Szikszay, T., Hall, T. & Von Piekartz, H. In vivo effects of limb movement on nerve stretch, strain, and tension: A systematic review. *J. Back Musculoskelet. Rehabil.* **30**, 1171–1186 (2017).

146. Collier, A. & Burge, P. Ulnar Nerve At the Elbow. *Curr. Orthop.* **15**, 256d263-256d263 (2001).

147. Hicks, D. & Toby, E. B. Ulnar nerve strains at the elbow: The effect of in Situ decompression and medial epicondylectomy. *J. Hand Surg. Am.* **27**, 1026–1031 (2002).

148. Byl, C., Puttlitz, C., Byl, N., Lotz, J. & Topp, K. Strain in the median and ulnar nerves during upper-extremity positioning. *J. Hand Surg. Am.* **27**, 1032–1040 (2002).

149. Lewis, J., Ramot, R. & Green, A. Changes in mechanical tension in the median nerve: Possible implications for the upper limb tension test. *Physiotherapy* **84**, 254–261 (1998).

150. Manvell, N., Manvell, J. J., Snodgrass, S. J. & Reid, S. A. Tension of the Ulnar, Median, and Radial Nerves During Ulnar Nerve Neurodynamic Testing: Observational Cadaveric Study. *Phys. Ther.* **95**, 891–900 (2015).

151. Alshami, A. M., Babri, A. S., Souvlis, T. & Coppieters, M. W. Strain in the tibial and plantar nerves with foot and ankle movements and the influence of adjacent joint positions. *J. Appl. Biomech.* **24**, 368–376 (2008).

152. Kleinrensink, G J, Stoeckart R, Vleeming A, Snijders CJ, M. P. Mechanical tension in the median nerve. *Clin Biomech.* **10**, 240–244 (1995).

153. Sunderland, S. & Bradley, K. C. Stress-strain phenomena in human peripheral nerve trunks. *Brain* **84**, 102–119 (1961).

154. Babbage, C. S., Coppieters, M. W. & McGowan, C. M. Strain and excursion of the sciatic nerve in the dog: Biomechanical considerations in the development of a clinical test for increased neural mechanosensitivity. *Vet. J.* **174**, 330–336 (2007).

155. Coppieters, M. W. *et al.* Strain and Excursion of the Sciatic, Tibial, and Plantar Nerves

during a Modified Straight Leg Raising Test. *J. Orthop. Res. Sept.* **25**, 1121–1127 (2007).

156. Higgins, S., Lee, J. S., Ha, L. & Lim, J. Y. Inducing neurite outgrowth by mechanical cell stretch. *Biores. Open Access* **2**, 212–216 (2013).

157. English, A. W., Wilhelm, J. C. & Sabatier, M. J. Enhancing recovery from peripheral nerve injury using treadmill training. *Ann. Anat.* **193**, 354–361 (2011).

158. Jung, S.-Y., Seo, T.-B. & Kim, D.-Y. Treadmill exercise facilitates recovery of locomotor function through axonal regeneration following spinal cord injury in rats. *J. Exerc. Rehabil.* **12**, 284–292 (2016).

159. Yamauchi, T. *et al.* Distinct but overlapping roles of histone acetylase PCAF and of the closely related PCAF-B/GCN5 in mouse embryogenesis. *Proc. Natl. Acad. Sci. U. S. A.* **97**, 11303–11306 (2000).

160. Xia, P. *et al.* EB1 acetylation by P300/CBP-associated factor (PCAF) ensures accurate kinetochore-microtubule interactions in mitosis. *Proc. Natl. Acad. Sci. U. S. A.* **109**, 16564–16569 (2012).

161. Gai, X. *et al.* Histone acetyltransferase PCAF accelerates apoptosis by repressing a GLI1/BCL2/BAX axis in hepatocellular carcinoma. *Cell Death Dis.* **6**, e1712–e1712 (2015).

162. Jin, Q. *et al.* Distinct roles of GCN5/PCAF-mediated H3K9ac and CBP/p300-mediated H3K18/27ac in nuclear receptor transactivation. *EMBO J.* **30**, 249–262 (2011).

163. Wallberg, A. E., Pedersen, K., Lendahl, U. & Roeder, R. G. p300 and PCAF Act Cooperatively To Mediate Transcriptional Activation from Chromatin Templates by Notch Intracellular Domains In Vitro. *Mol. Cell. Biol.* **22**, 7812–7819 (2002).

164. Nagy, Z. & Tora, L. Distinct GCN5/PCAF-containing complexes function as co-activators and are involved in transcription factor and global histone acetylation. *Oncogene* **26**, 5341–5357 (2007).

165. Wang, Y. L., Faiola, F., Xu, M., Pan, S. & Martinez, E. Human ATAC is a GCN5/PCAF-containing acetylase complex with a novel NC2-like histone fold module that interacts with the TATA-binding protein. *J. Biol. Chem.* **283**, 33808–33815 (2008).

166. Milite, C. *et al.* Modulation of the activity of histone acetyltransferases by long chain alkylidenemalonates (LoCAMs). *Bioorg. Med. Chem.* **19**, 3690–3701 (2011).

167. Wei, W. *et al.* p300/CBP-associated factor selectively regulates the extinction of conditioned fear. *J. Neurosci.* **32**, 11930–11941 (2012).

168. Stemkowski, P. L., Noh, M. C., Chen, Y. & Smith, P. A. Increased excitability of

medium-sized dorsal root ganglion neurons by prolonged interleukin-1β exposure is K+ channel dependent and reversible. *J. Physiol.* **593**, 3739–3755 (2015).

169. Sliwinski, C., Nees, T. A., Puttagunta, R., Weidner, N. & Blesch, A. Sensorimotor activity partially ameliorates pain and reduces nociceptive fiber density in the chronically injured spinal cord. *J. Neurotrauma* **35**, 2222–2238 (2018).

170. Adams, C. E., Awad, G. A., Rathbone, J., Thornley, B. & Soares-Weiser, K. Chlorpromazine versus placebo for schizophrenia. *Cochrane Database Syst. Rev.* **2014**, (2014).

171. Bunney, B. S. & Aghajanian, G. K. A comparison of the effects of chlorpromazine, 7-hydroxychlorpromazine and chlorpromazine sulfoxide on the activity of central dopaminergic neurons. *Life Sci.* **15**, 309–318 (1974).

172. Obara, K. *et al.* Characterization of binding of antipsychotics to muscarinic receptors using mouse cerebral cortex. *J. Pharmacol. Sci.* **140**, 197–200 (2019).

173. Wallace, T. L. & Bertrand, D. Alpha7 neuronal nicotinic receptors as a drug target in schizophrenia. *Expert Opin. Ther. Targets* **17**, 139–155 (2013).

174. Park, J.-S. *et al.* Cottonseed Oil Protects Against Intestinal Inflammation in Dextran Sodium Sulfate-Induced Inflammatory Bowel Disease. *J. Med. Food* **22**, 672–679 (2019).

175. Jain, P., Satapathy, T. & Pandey, R. K. Rhipicephalus microplus (acari: Ixodidae): Clinical safety and potential control by topical application of cottonseed oil (Gossypium sp.) on cattle. *Exp. Parasitol.* **219**, 108017 (2020).

176. Ramaiya, A., Li, G., M. Petiwala, S. & J. Johnson, J. Single Dose Oral Pharmacokinetic Profile of α-Mangostin in Mice. *Curr. Drug Targets* **13**, 1698–1704 (2012).

177. Mason, M. R. J., Lieberman, A. R., Grenningloh, G. & Anderson, P. N. Transcriptional Upregulation of SCG10 and CAP-23 Is Correlated with Regeneration of the Axons of Peripheral and Central Neurons in Vivo. (2002). doi:10.1006/mcne.2002.1140

178. Shin, J. E., Geisler, S. & DiAntonio, A. Dynamic regulation of SCG10 in regenerating axons after injury. *Exp. Neurol.* **252**, 1–11 (2014).

179. Cho, Y. *et al.* Activating injury-response genes with hypoxia enhances axon regeneration through neuronal HIF-1α. *Neuron* **88**, 720–734 (2015).

180. Kurtz, S. M. & Devine, J. N. PEEK biomaterials in trauma, orthopedic, and spinal implants. *Biomaterials* **28**, 4845–4869 (2007).

181. Panayotov, I. V., Orti, V., Cuisinier, F. & Yachouh, J. Polyetheretherketone (PEEK) for medical applications. *J. Mater. Sci. Mater. Med.* **27**, 1–11 (2016).

182. Brown, M. J., Pleasure, D. E. & Asbury, A. K. Microdissection of peripheral nerve. Collagen and lipid distribution with morphological correlation. *J. Neurol. Sci.* **29**, 361–369 (1976).

183. Machado, J. A. *et al.* Stretch-induced nerve injury: A proposed technique for the study of nerve regeneration and evaluation of the influence of gabapentin on this model. *Brazilian J. Med. Biol. Res.* **46**, 929–935 (2013).

184. Marmigère, F. & Ernfors, P. Specification and connectivity of neuronal subtypes in the sensory lineage. *Nat. Rev. Neurosci.* **8**, 114–127 (2007).

185. de Moraes, E. R., Kushmerick, C. & Naves, L. A. Morphological and functional diversity of first-order somatosensory neurons. *Biophys. Rev.* **9**, 847–856 (2017).

186. Olson, W., Dong, P., Fleming, M. & Luo, W. The specification and wiring of mammalian cutaneous low-threshold mechanoreceptors. *Rev. Dev. Biol.* **5**, 389–404 (2016).

187. Lefcort, F., Clary, D. O., Rusoff, A. C. & Reichardt, L. F. Inhibition of the NT-3 receptor trkC, early in chick embryogenesis, results in severe reductions in multiple neuronal subpopulations in the dorsal root ganglia. *J. Neurosci.* **16**, 3704–3713 (1996).

188. Usoskin, D. *et al.* Unbiased classification of sensory neuron types by large-scale single-cell RNA sequencing. *Nat. Neurosci.* **18**, 145–153 (2015).

189. Keller, A. V. *et al.* Nociceptor-dependent locomotor dysfunction after clinically-modeled hindlimb muscle stretching in adult rats with spinal cord injury. *Exp. Neurol.* **318**, 267–276 (2019).

190. Lechner, S. G., Frenzel, H., Wang, R. & Lewin, G. R. Developmental waves of mechanosensitivity acquisition in sensory neuron subtypes during embryonic development. *EMBO J.* **28**, 1479–1491 (2009).

191. Ruscheweyh, R., Forsthuber, L., Schoffnegger, D. & Sandkühler, J. Modification of classical neurochemical markers in identified primary afferent neurons with Aβ-, Aδ-, and C-fibers after chronic constriction injury in mice. *J. Comp. Neurol.* **502**, 325–336 (2007).

192. Lawson, B. Y. S. N. & Waddell, P. J. Soma neurofillament immunoreactivity is related to cell size and fibre conduction velocity in rat primary sensory neurons. *J. Physiol.* **435**, 41–63 (1991).

193. Luo, D., Chakraborty, G. & Ingoglia, N. A. Post-translational modification of proteins by arginine and lysine following crush injury and during regeneration of rat sciatic nerves. *Restor. Neurol. Neurosci.* **2**, 53–61 (1990).

194. Patodia, S. & Raivich, G. Role of transcription factors in peripheral nerve regeneration. *Front. Mol. Neurosci.* **5**, 1–15 (2012).

195. van Kesteren, R. E., Mason, M. R. J., MacGillavry, H. D., Smit, A. B. & Verhaagen, J. A Gene Network Perspective on Axonal Regeneration. *Front. Mol. Neurosci.* **4**, 1–6 (2011).

196. Gey, M. *et al.* Atf3 mutant mice show reduced axon regeneration and impaired regeneration-associated gene induction after peripheral nerve injury. *Open Biol.* **6**, (2016).

197. Tsujino, H. *et al.* Activating transcription factor 3 (ATF3) induction by axotomy in sensory and motoneurons: A novel neuronal marker of nerve injury. *Mol. Cell. Neurosci.* **15**, 170–182 (2000).

198. Seijffers, R., Mills, C. D. & Woolf, C. J. ATF3 increases the intrinsic growth state of DRG neurons to enhance peripheral nerve regeneration. *J. Neurosci.* **27**, 7911–7920 (2007).

199. Koivisto, E. *et al.* Characterization of the regulatory mechanisms of activating transcription factor 3 by hypertrophic stimuli in rat cardiomyocytes. *PLoS One* **9**, (2014).

200. Palmisano, I. *et al.* Epigenomic signatures underpin the axonal regenerative ability of dorsal root ganglia sensory neurons. *Nat. Neurosci.* **22**, 1913–1924 (2019).

201. Wu, Y. *et al.* SP1-mediated upregulation of LINGO-1 promotes degeneration of retinal ganglion cells in optic nerve injury. *CNS Neurosci. Ther.* **26**, 1010–1020 (2020).

202. García-Morales, V. *et al.* Sp1-regulated expression of p11 contributes to motor neuron degeneration by membrane insertion of TASK1. *Nat. Commun.* **10**, 1–23 (2019).

203. Lee, J. Y., Choi, H. Y., Park, C. S., Ju, B. G. & Yune, T. Y. Mithramycin A Improves Functional Recovery by Inhibiting BSCB Disruption and Hemorrhage after Spinal Cord Injury. *J. Neurotrauma* **35**, 508–520 (2018).

204. Kiryu-Seo, S. *et al.* Damage-induced neuronal endopeptidase (DINE) is a unique metallopeptidase expressed in response to neuronal damage and activates superoxide scavengers. *Proc. Natl. Acad. Sci. U. S. A.* **97**, 4345–4350 (2000).

205. Kato, R., Kiryu-Seo, S. & Kiyama, H. Damage-induced neuronal endopeptidase (DINE/ECEL) expression is regulated by leukemia inhibitory factor and deprivation of nerve growth factor in rat sensory ganglia after nerve injury. *J. Neurosci.* **22**, 9410–9418 (2002).

206. Kaneko, A., Kiryu-Seo, S., Matsumoto, S. & Kiyama, H. Damage-induced neuronal

endopeptidase (DINE) enhances axonal regeneration potential of retinal ganglion cells after optic nerve injury. *Cell Death Dis.* **8**, e2847 (2017).

207. Kiryu-Seo, S. *et al.* Neuronal injury-inducible gene is synergistically regulated by ATF3, c-Jun, and STAT3 through the interaction with Sp1 in damaged neurons. *J. Biol. Chem.* **283**, 6988–6996 (2008).

208. Chen, G., Fang, X. & Yu, M. Regulation of gene expression in rats with spinal cord injury based on microarray data. *Mol. Med. Rep.* **12**, 2465–2472 (2015).

209. Huang, W. *et al.* Trichostatin A induces transforming growth factor β type II receptor promoter activity and acetylation of Sp1 by recruitment of PCAF/p300 to a Sp1·NF-Y complex. *J. Biol. Chem.* **280**, 10047–10054 (2005).

210. Jordan-Sciutto, K. L., Dragich, J. M., Caltagarone, J., Hall, D. J. & Bowser, R. Fetal Alz-50 clone 1 (FAC1) protein interacts with the myc-associated zinc finger protein (ZF87/MAZ) and alters its transcriptional activity. *Biochemistry* **39**, 3206–3215 (2000).

211. Mu, X., Springer, J. E. & Bowser, R. FAC1 expression and localization in motor neurons of developing, adult, and amyotrophic lateral sclerosis spinal cord. *Exp. Neurol.* **146**, 17–24 (1997).

212. Rhodes, J., Lutka, F., Jordan-Sciutto, K. & Bowser, R. Altered expression and distribution of FACI during NGF-induced neurite outgrowth of PC12 cells. *Neuroreport (Oxford)* **14**, 449–452 (2003).

213. Benayoun, B. A. & Veitia, R. A. A post-translational modification code for transcription factors: sorting through a sea of signals. *Trends Cell Biol.* **19**, 189–197 (2009).

214. Filtz, T. M., Vogel, W. K. & Leid, M. Regulation of transcription factor activity by interconnected post-translational modifications. *Trends in Pharmacological Sciences* **35**, 76–85 (2014).

215. Legube, G. & Trouche, D. Regulating histone acetyltransferases and deacetylases. *EMBO Rep.* **4**, 944–947 (2003).

216. Liu, Y. *et al.* Application of recombinant adenovirus for in vivo gene delivery to spinal cord. *Brain Res.* **768**, 19–29 (1997).

217. Herdegen, T. *et al.* Lasting N-terminal phosphorylation of c-Jun and activation of c-Jun N- terminal kinases after neuronal injury. *J. Neurosci.* **18**, 5124–5135 (1998).

218. Tedeschi, A., Nguyen, T., Puttagunta, R., Gaub, P. & Di Giovanni, S. A p53-CBP/p300 transcription module is required for GAP-43 expression, axon outgrowth, and regeneration. *Cell Death Differ.* **16**, 543–554 (2009).

219. Shankaranarayanan, P., Chaitidis, P., Kühn, H. & Nigam, S. Acetylation by Histone

Acetyltransferase CREB-binding Protein/p300 of STAT6 Is Required for Transcriptional Activation of the 15-Lipoxygenase-1 Gene. *J. Biol. Chem.* **276**, 42753–42760 (2001).

220. Usher, L. C. *et al.* A chemical screen identifies novel compounds that overcome glial-mediated inhibition of neuronal regeneration. *J. Neurosci.* **30**, 4693–4706 (2010).

221. Sherman, S. P. & Bang, A. G. High-throughput screen for compounds that modulate neurite growth of human induced pluripotent stem cell-derived neurons. *DMM Dis. Model. Mech.* **11**, (2018).

222. Gaub, P. *et al.* The histone acetyltransferase p300 promotes intrinsic axonal regeneration. *Brain* **134**, 2134–2148 (2011).

223. Lv, L., Han, X., Sun, Y., Wang, X. & Dong, Q. Valproic acid improves locomotion in vivo after SCI and axonal growth of neurons in vitro. *Exp. Neurol.* **233**, 783–790 (2012).

224. Shah, R. R. Safety and Tolerability of Histone Deacetylase (HDAC) Inhibitors in Oncology. *Drug Saf.* **42**, 235–245 (2019).

225. Singleton, R. H., Yan, H. Q., Fellows-Mayle, W. & Dixon, C. E. Resveratrol attenuates behavioral impairments and reduces cortical and hippocampal loss in a rat controlled cortical impact model of traumatic brain injury. *J. Neurotrauma* **27**, 1091–1099 (2010).

226. Ding, Z. *et al.* Resveratrol Promotes Nerve Regeneration via Activation of p300 Acetyltransferase-Mediated VEGF Signaling in a Rat Model of Sciatic Nerve Crush Injury. *Front. Neurosci.* **12**, 341 (2018).

227. Xu, B. P. *et al.* Neurological recovery and antioxidant effects of resveratrol in rats with spinal cord injury: A meta-Analysis. *Neural Regen. Res.* **15**, 482–490 (2020).

228. Sbardella, G. *et al.* Identification of long chain alkylidenemalonates as novel small molecule modulators of histone acetyltransferases. *Bioorganic Med. Chem. Lett.* **18**, 2788–2792 (2008).

229. Kucher, K. *et al.* First-in-man intrathecal application of neurite growth-promoting anti-nogo- a antibodies in acute spinal cord injury. *Neurorehabil. Neural Repair* **32**, 578–589 (2018).

230. Roidl, D. *et al.* DOT1L Activity Promotes Proliferation and Protects Cortical Neural Stem Cells from Activation of ATF4-DDIT3-Mediated ER Stress In Vitro. *Stem Cells* **34**, 233–245 (2016).

231. Wakatsuki, S., Yumoto, N., Komatsu, K., Araki, T. & Sehara-Fujisawa, A. Roles of meltrin-β/ADAM19 in progression of schwann cell differentiation and myelination during sciatic nerve regeneration. *J. Biol. Chem.* **284**, 2957–2966 (2009).

232. Dumoulin, A., Dagane, A., Dittmar, G. & Rathjen, F. G. S-palmitoylation Is Required for the Control of Growth Cone Morphology of DRG Neurons by CNP-Induced cGMP Signaling. *Front. Mol. Neurosci.* **11**, 345 (2018).

233. Berkel, S. *et al.* Mutations in the SHANK2 synaptic scaffolding gene in autism spectrum disorder and mental retardation. *Nat. Genet.* **42**, 489–491 (2010).

234. Zhang, L. *et al.* Hyperactivated PTP1B phosphatase in parvalbumin neurons alters anterior cingulate inhibitory circuits and induces autism-like behaviors. *Nat. Commun.* **11**, 1–15 (2020).

235. Tautz, L. PTP1B: A new therapeutic target for Rett syndrome. *J. Clin. Invest.* **125**, 2931–2934 (2015).

236. Kalkan, Z., Durasi, I. M., Sezerman, U. & Atasever-Arslan, B. Potential of GRID2 receptor gene for preventing TNF-induced neurodegeneration in autism. *Neurosci. Lett.* **620**, 62–69 (2016).

237. Mansfield, P., Constantino, J. N. & Baldridge, D. MYT1L: A systematic review of genetic variation encompassing schizophrenia and autism. *Am. J. Med. Genet. Part B Neuropsychiatr. Genet.* **183**, 227–233 (2020).

238. Montrose, K., Kobayashi, S., Manabe, T. & Yamamoto, T. Lmtk3-KO Mice Display a Range of Behavioral Abnormalities and Have an Impairment in GluA1 Trafficking. *Neuroscience* **414**, 154–167 (2019).

239. Wolking, S. *et al.* Clinical spectrum of STX1B -related epileptic disorders. *Neurology* **92**, E1238–E1249 (2019).

240. Dyment, D. A. *et al.* De novo substitutions of TRPM3 cause intellectual disability and epilepsy. *Eur. J. Hum. Genet.* **27**, 1611–1618 (2019).

241. Berryer, M. H. *et al.* Mutations in SYNGAP1 Cause Intellectual Disability, Autism, and a Specific Form of Epilepsy by Inducing Haploinsufficiency. *Hum. Mutat.* **34**, 385–394 (2013).

242. Sampathkumar, C. *et al.* Loss of MeCP2 disrupts cell autonomous and autocrine BDNF signaling in mouse glutamatergic neurons. *Elife* **5**, 1–23 (2016).

243. Bakos, J., Bacova, Z., Grant, S. G., Castejon, A. M. & Ostatnikova, D. Are Molecules Involved in Neuritogenesis and Axon Guidance Related to Autism Pathogenesis? *NeuroMolecular Med.* **17**, 297–304 (2015).

244. Larner, A. J. Axonal sprouting and synaptogenesis in temporal lobe epilepsy: Possible pathogenetic and therapeutic roles of neurite growth inhibitory factors. *Seizure Eur. J. Epilepsy* **4**, 249–258 (1995).

245. Higurashi, M. *et al.* Localized role of CRMP1 and CRMP2 in neurite outgrowth and growth cone steering. *Dev. Neurobiol.* **72**, 1528–1540 (2012).

246. Lv, Y. *et al.* PFKFB3-mediated glycolysis is involved in reactive astrocyte proliferation after oxygen-glucose deprivation/reperfusion and is regulated by Cdh1. *Neurochem. Int.* **91**, 26–33 (2015).

247. Endo, M., Ohashi, K. & Mizuno, K. LIM kinase and slingshot are critical for neurite extension. *J. Biol. Chem.* **282**, 13692–13702 (2007).

248. Tedeschi, A. *et al.* ADF/Cofilin-Mediated Actin Turnover Promotes Axon Regeneration in the Adult CNS. *Neuron* **103**, 1073-1085.e6 (2019).

249. Kawakami, Y. *et al.* The soluble form of LOTUS inhibits nogo receptor-mediated signaling by interfering with the interaction between Nogo receptor type 1 and p75 neurotrophin receptor. *J. Neurosci.* **38**, 2589–2604 (2018).

250. Hirokawa, T. *et al.* Regulation of axonal regeneration by the level of function of the endogenous Nogo receptor antagonist LOTUS. *Sci. Rep.* **7**, 1–9 (2017).

251. Gilmour, D., Knaut, H., Maischein, H. M. & Nüsslein-Volhard, C. Towing of sensory axons by their migrating target cells in vivo. *Nat. Neurosci.* **7**, 491–492 (2004).

252. Pfister, B. J., Iwata, A., Meaney, D. F. & Smith, D. H. Extreme Stretch Growth of Integrated Axons. *J. Neurosci.* **24**, 7978–7983 (2004).

253. Paulus, J. D., Willer, G. B., Willer, J. R., Gregg, R. G. & Halloran, M. C. Muscle contractions guide Rohon-Beard peripheral sensory axons. *J. Neurosci.* **29**, 13190–13201 (2009).

254. Siechen, S., Yang, S., Chiba, A. & Saif, T. Mechanical tension contributes to clustering of neurotransmitter vesicles at presynaptic terminals. *Proc. Natl. Acad. Sci. U. S. A.* **106**, 12611–6 (2009).

255. Sandrow-Feinberg, H. R. & Houlé, J. D. Exercise after spinal cord injury as an agent for neuroprotection, regeneration and rehabilitation. *Brain Res.* **1619**, 12–21 (2015).

256. Armada-da-silva, P. A. S., Pereira, C. & Amado, S. Role of Physical Exercise for Improving Posttraumatic Nerve Regeneration. **109**, (2013).

257. Udina, E., Puigdemasa, A. & Navarro, X. Passive and active exercise improve regeneration and muscle reinnervation after peripheral nerve injury in the rat. *Muscle and Nerve* **43**, 500–509 (2011).

258. Pachter, B. R. & Eberstein, A. Passive exercise and reinnervation of the rat denervated extensor digitorum longus muscle after nerve crush. *Am. J. Phys. Med. Rehabil.* **68**, 179–182 (1989).

259. Bendella, H. *et al.* Non-invasive stimulation of the vibrissal pad improves recovery of whisking function after simultaneous lesion of the facial and infraorbital nerves in rats. *Exp. Brain Res.* **212**, 65–79 (2011).

260. Chang, Y. J., Tsai, C. J., Tseng, F. G., Chen, T. J. & Wang, T. W. Micropatterned stretching system for the investigation of mechanical tension on neural stem cells behavior. *Nanomedicine Nanotechnology, Biol. Med.* **9**, 345–355 (2013).

261. Hutchinson, K. J., Gómez-Pinilla, F., Crowe, M. J., Ying, Z. & Basso, D. M. Three exercise paradigms differentially improve sensory recovery after spinal cord contusion in rats. *Brain* **127**, 1403–1414 (2004).

262. Goldshmit, Y., Lythgo, N., Galea, M. P. & Turnley, A. M. Treadmill training after spinal cord hemisection in mice promotes axonal sprouting and synapse formation and improves motor recovery. *J. Neurotrauma* **25**, 449–465 (2008).

263. Gómez-Pinilla, F., Ying, Z., Roy, R. R., Molteni, R. & Reggie Edgerton, V. Voluntary exercise induces a BDNF-mediated mechanism that promotes neuroplasticity. *J. Neurophysiol.* **88**, 2187–2195 (2002).

264. Sachdeva, R., Theisen, C. C., Ninan, V., Twiss, J. L. & Houlé, J. D. Exercise dependent increase in axon regeneration into peripheral nerve grafts by propriospinal but not sensory neurons after spinal cord injury is associated with modulation of regeneration-associated genes. *Exp. Neurol.* **276**, 72–82 (2016).

265. Hanslik, K. L. *et al.* Regenerative capacity in the lamprey spinal cord is not altered after a repeated transection. *PLoS One* **14**, e0204193 (2019).

266. Doyle, L. M. F. & Roberts, B. L. Exercise enhances axonal growth and functional recovery in the regenerating spinal cord. *Neuroscience* **141**, 321–327 (2006).

267. Luna, C., Detrick, L., Shah, S. B., Cohen, A. H. & Aranda-espinoza, H. Mechanical properties of the lamprey spinal cord : Uniaxial loading and physiological strain. *J. Biomech.* **46**, 2194–2200 (2013).

268. Zhang, G., Rodemer, W., Sinitsa, I., Hu, J. & Selzer, M. E. Source of Early Regenerating Axons in Lamprey Spinal Cord Revealed by Wholemount Optical Clearing with BABB. *Cells* **9**, 2427 (2020).

269. Assas, B. M., Pennock, J. I. & Miyan, J. A. Calcitonin gene-related peptide is a key neurotransmitter in the neuro-immune axis. *Frontiers in Neuroscience* **8**, 23 (2014).

270. Gladman, S. J., Ward, R. E. & Michael-titus, A. T. The effect of mechanical strain or hypoxia on cell death in subpopulations of rat dorsal root ganglion neurons in vitro. *Neuroscience* **171**, 577–587 (2010).

271. Kerns, J. *et al.* Mechanical Properties of the Human Tibial and Peroneal Nerves Following Stretch With Histological Correlations. *Anat. Rec.* **302**, 2030–2039 (2019).

272. Vogl, A. W. *et al.* Stretchy nerves are an essential component of the extreme feeding mechanism of rorqual whales. *Curr. Biol.* **25**, R360–R361 (2015).

273. Perry, M. J., Lawson, S. N. & Robertson, J. Neurofilament immunoreactivity in populations of rat primary afferent neurons: A quantitative study of phosphorylated and non-phosphorylated subunits. *J. Neurocytol.* **20**, 746–758 (1991).

274. Kim, J. E., Cho, Y. H. & Seo, T. B. Treadmill exercise activates ATF3 and ERK1/2 downstream molecules to facilitate axonal regrowth after sciatic nerve injury. *J. Exerc. Rehabil.* **16**, 141–147 (2020).

275. Birukov, K. G. Cyclic stretch, reactive oxygen species, and vascular remodeling. *Antioxidants Redox Signal.* **11**, 1651–1667 (2009).

276. Udina, E., Cobianchi, S., Allodi, I. & Navarro, X. Effects of activity-dependent strategies on regeneration and plasticity after peripheral nerve injuries. *Ann. Anat.* **193**, 347–353 (2011).

277. English, A. W., Meador, W. & Carrasco, D. I. Neurotrophin-4/5 is required for the early growth of regenerating axons in peripheral nerves. *Eur. J. Neurosci.* **21**, 2624–2634 (2005).

278. Martino, F., Perestrelo, A. R., Vinarský, V., Pagliari, S. & Forte, G. Cellular mechanotransduction: From tension to function. *Front. Physiol.* **9**, 1–21 (2018).

279. Nieuwenhuis, B., Haenzi, B., Andrews, M. R., Verhaagen, J. & Fawcett, J. W. Integrins promote axonal regeneration after injury of the nervous system. *Biol. Rev.* **93**, 1339–1362 (2018).

280. Kerstein, P. C. *et al.* Mechanosensitive TRPC1 channels promote calpain proteolysis of talin to regulate spinal axon outgrowth. *J. Neurosci.* **33**, 273–285 (2013).

281. Shibasaki, K., Murayama, N., Ono, K., Ishizaki, Y. & Tominaga, M. TRPV2 enhances axon outgrowth through its activation by membrane stretch in developing sensory and motor neurons. *J. Neurosci.* **30**, 4601–4612 (2010).